INFORMATION TO USERS

This manuscript has been reproduced from the microfilm master. UMI films the text directly from the original or copy submitted. Thus, some thesis and dissertation copies are in typewriter face, while others may be from any type of computer printer.

The quality of this reproduction is dependent upon the quality of the copy submitted. Broken or indistinct print, colored or poor quality illustrations and photographs, print bleedthrough, substandard margins, and improper alignment can adversely affect reproduction.

In the unlikely event that the author did not send UMI a complete manuscript and there are missing pages, these will be noted. Also, if unauthorized copyright material had to be removed, a note will indicate the deletion.

Oversize materials (e.g., maps, drawings, charts) are reproduced by sectioning the original, beginning at the upper left-hand corner and continuing from left to right in equal sections with small overlaps.

ProQuest Information and Learning
300 North Zeeb Road, Ann Arbor, MI 48106-1346 USA
800-521-0600

Two Degree-of-Freedom Modeling and Robust Control of Chatter in Metal Cutting by Using Piezoactuators

Jian Wang

A Thesis
in
The Department
of
Mechanical and Industrial Engineering

Presented in Partial Fulfillment of the Requirement
For the Degree of Master of Applied Science at
Concordia University
Montreal, Quebec, Canada

January 2003

© Jian Wang, 2003

National Library of Canada
Acquisitions and Bibliographic Services
395 Wellington Street
Ottawa ON K1A 0N4
Canada

Bibliothèque nationale du Canada
Acquisitions et services bibliographiques
395, rue Wellington
Ottawa ON K1A 0N4
Canada

Your file Votre référence

Our file Notre référence

The author has granted a non-exclusive licence allowing the National Library of Canada to reproduce, loan, distribute or sell copies of this thesis in microform, paper or electronic formats.

The author retains ownership of the copyright in this thesis. Neither the thesis nor substantial extracts from it may be printed or otherwise reproduced without the author's permission.

L'auteur a accordé une licence non exclusive permettant à la Bibliothèque nationale du Canada de reproduire, prêter, distribuer ou vendre des copies de cette thèse sous la forme de microfiche/film, de reproduction sur papier ou sur format électronique.

L'auteur conserve la propriété du droit d'auteur qui protège cette thèse. Ni la thèse ni des extraits substantiels de celle-ci ne doivent être imprimés ou autrement reproduits sans son autorisation.

0-612-77996-3

Canada

Two Degree-of-Freedom Modeling and Robust Control of Chatter in Metal Cutting by Using Piezoactuators

Jian Wang

Abstract

Self-excited vibrations, also called chatter, are known to cause detrimental effects on the machined surface finish while decreasing the machining efficiency and productivity. Chatter is small-amplitude and high-frequency vibration, and an active vibration control providing a force to the cutting system is necessary to overcome the chatter effect. To provide such a force, piezoelectric actuators have been introduced into the metal cutting systems.

In this thesis, the metal cutting processes are described as two degree-of-freedom systems with two-dimensional or three-dimensional forces. One of the main contributions in this thesis work is that the hysteretic characteristic models are incorporated into the chatter suppression control in metal cutting systems. It should be noted that this incorporation severely complicates the tasks of control law designs and analyses. In order to overcome the chatter effect, several robust adaptive control schemes are proposed for different scenarios in this thesis. The simulation results show significant reduction of chatter by using the proposed adaptive control laws in all the cases.

Acknowledgments

I wish to express my indebtedness to my supervisor, Dr. Chun-Yi Su, for his invaluable academic guidance, encouragement and financial support throughout the development of this thesis and all the papers we have published.

I would also like to thank my wife, Mrs. Xiaohua Wang, for her emotional encouragement and understanding by her long hours dedicated work.

I would like to thank my parents for their understanding and support.

Finally, I would like to thank everyone who have selflessly assisted my research and discussed my thesis with me within the past two years.

Contents

List of Figures ---------- ix

List of Tables ---------- xiii

Nomenclature ---------- xiv

Chapter 1 Introduction ---------- 1

1.1 Main Objective of the Thesis ---------- 1

1.2 An Industrial Problem in Metal Cutting – Chatter Vibration ---------- 1

1.3 Overview of Research on Chatter Vibration ---------- 6

1.3.1 Structure Dynamics in Machine Tools ---------- 7

1.3.2 Cutting Dynamics in Machine Tools ---------- 7

1.3.3 Feedback of the Closed-Loop Dynamic System of Machine Tools--- 8

1.3.4 Comprehensive Overview on Machine Tool Chatter ---------- 8

1.4 Basic Theory of Chatter Vibration ---------- 13

1.5 Main Characteristics of Turning ---------- 24

1.6 Contributions of This Thesis Work ---------- 26

1.7 Organization of This Thesis ---------- 28

Chapter 2 Modeling of Machine Structure and Cutting Process ---------- 29

2.1 The Machine Operation as a Closed-Loop System ---------- 29

2.2 Modeling of Machine Structure ---------- 31

2.3 Modeling of Cutting Process ---------- 40

2.3.1 Hysteresis – A Cause of Chatter Occurrence ---------- 40

2.3.2 Mathematical Hysteresis Models of Dynamic Cutting Process ------ 44

2.4 Modeling of Uncut Chip Thickness ---------- 46

2.5 The Closed Loop of Metal Cutting System ---------- 49

2.6 Simulation Results ---------- 51

2.6.1 Simulations of the Dynamic System Responses without Forces ----- 51

2.6.2 Simulations of the Dynamic System Responses with Hysteresis Effect ---------- 52

2.7 Summary ---------- 54

Chapter 3 Applications of Piezoactuators in the Suppression of Chatter ---------- 55

3.1 Surveys on Control Schemes on Chatter Suppression in Turning ------- 55

3.2 Main Characteristics of Applications of Piezoelectricity ---------- 56

3.3 Dynamic Behavior and Mathematical Modeling of Piezoactuators ------- 58

3.3.1 Hysteretic Characteristics of Piezoactuators ---------- 59

3.3.2 Mathematical Model of Piezoactuators ---------- 60

3.4 Applications of Piezoactuators in Turning ---------- 62

3.5 Structure of the Dependent Piezoactuator on Tool Holder ---------- 63

3.6 Structure of the Independent Piezoactuators from Tool Holder ---------- 64

3.7 Summary ---------- 65

Chapter 4 Chatter Suppression for the Controlled System with 2-D Model and Dependent Piezoactuator ---------- 66

4.1 Dynamic Model of Turning Process ---------- 66

4.2 Adaptive Controller Design ---------- 68

4.2.1 Designed Control Law ---------- 71

4.2.2 Stability Analysis of the System ---------- 73

4.3 Simulation Results ---------- 75

4.4 Summary ---------- 76

Chapter 5 Chatter Suppression for the Controlled System with 3-D Model and Dependent Piezoactuators ---------- 77

5.1 Dynamic Model of Turning Process ---------- 78

5.2 Adaptive Controller Design ---------- 80

5.2.1 Design Control Law ---------- 83

5.2.2 Stability Analysis of the System ---------- 87

5.3 Simulation Results ---------- 88

5.4 Summary ---------- 90

Chapter 6 Chatter Suppression for the Controlled System with 2-D Model and Independent Piezoactuator ---------- 91

6.1 Dynamic Model of Turning Process ---------- 91

6.2 Adaptive Controller Design ---------- 94

6.2.1 Dynamic Estimate of $z(t, y_p^{(4)}, y_p^{(3)}, y_p^{(2)})$ ---------- 96

6.2.2 Design Control Law ---------- 97

6.2.3 Stability Analysis of the System ---------- 99

6.3 Simulation Results ----------100

6.4 Summary ----------102

Chapter 7 Chatter Suppression for the Controlled System with 3-D Model and Independent Piezoactuators ---------- 103

7.1 Dynamic Model of Turning Process ---------- 103

7.2 Adaptive Controller Design ---------- 107

7.2.1 Dynamic Estimate of $z(t, y_p^{(4)}, y_p^{(3)}, y_p^{(2)})$ ---------- 110

7.2.2 Design Control Law ---------- 110

7.2.3 Stability Analysis of the System ---------- 114

7.3 Simulation Results ---------- 116

7.4 Summary ---------- 118

Chapter 8 Conclusions and Future Work ---------- 119

8.1 Conclusions ---------- 119

8.2 Future Work ---------- 120

8.2.1 Phase Difference Effect on Chatter ---------- 120

8.2.2 Damping Forces Acting on the Workpiece ---------- 121

8.2.3 Type *B* of Chatter ---------- 123

Appendix A: The Estimate of Disturbance $z(t, y_p^{(4)}, y_p^{(3)}, y_p^{(2)})$ (scalar) ---------- 124

Appendix B: The Estimate of Disturbance $z(t, y_p^{(4)}, y_p^{(3)}, y_p^{(2)})$ (vector) ---------- 127

Appendix C: Sliding Surface Design for the Dynamic System with Two-Dimensional Forces ---------- 130

Appendix D: Sliding Surface Design for the Dynamic System with Three-Dimensional Forces ---------- 132

References ---------- 142

List of Figures

Figure 1.1 Undulations on the machined surface caused by chatter ---------- 2

Figure 1.2 An example of primary chatter on the surface of a square thread -------- 4

Figure 1.3 An example of regenerative chatter in the turning process ---------- 4

Figure 1.4 Mode coupling chatter in a system with two degrees-of-freedom -------- 5

Figure 1.5 Chatter of type *A* and type *B* in turning process ---------- 6

Figure 1.6 Basic closed-loop diagram of chatter occurrence ---------- 7

Figure 1.7 Basic diagram of the chatter loop ---------- 13

Figure 1.8 Depth *t* expressing chip width *b* in turning ---------- 14

Figure 1.9 Vibration in the direction *Y* produces changes in chip thickness ------- 15

Figure 1.10 The "normal to the cut " direction *Y* ---------- 17

Figure 1.11 Cutting an undulated surface ---------- 18

Figure 1.12 A system with two degrees-of-freedom ---------- 20

Figure 1.13 A system with multi-degrees-of-freedom ---------- 22

Figure 1.14 The schematic of a turning system ---------- 25

Figure 1.15 General-purpose applications in turning ---------- 25

Figure 1.16 Typical operations in turning ---------- 26

Figure 2.1 Block diagram representation of the metal cutting dynamics ---------- 30

Figure 2.2 Block diagram of chatter loop ---------- 30

Figure 2.3 The scheme of the machine system with two degrees-of-freedom ------- 32

Figure 2.4 Machine structure with two degrees-of-freedom ---------- 33

Figure 2.5 The schematic of turning operation with two-dimensional forces ------- 35

Figure 2.6 The schematic of turning operation with three-dimensional forces ------- 37

Figure 2.7 Workpiece and cutting edge ---------- 40

Figure 2.8 Waveform of the displacement and cutting forces fluctuating ---------- 41

Figure 2.9 (a) Cutting force-uncut chip thickness relationship ---------- 41

Figure 2.9 (b) Thrust force-uncut chip thickness ---------- 41

Figure 2.9 (c) Resultant force-uncut chip thickness ---------- 41

Figure 2.10 Vibratory deflection of turning tool and cutting force fluctuation (M.S) --- 43

Figure 2.11 Vibratory deflection of turning tool and cutting force fluctuation (C.I) --- 43

Figure 2.12 Relationship between cutting force and vibratory deflection (M.S) ------- 43

Figure 2.13 Relationship between cutting force and vibratory deflection (C.I) ------- 43

Figure 2.14 Chatter mark configuration ---------- 44

Figure 2.15 Backlash of hysteresis model ---------- 44

Figure 2.16 The scheme of the cutting tool in a turning ---------- 47

Figure 2.17 Vibratory system of the workpiece ---------- 47

Figure 2.18 Block diagram of chatter loop with two-dimensional forces ---------- 50

Figure 2.19 Block diagram of chatter loop with three-dimensional forces ---------- 50

Figure 2.20 The dynamic response of metal cutting system without
2-dimensional or 3-dimensional forces ---------- 51

Figure 2.21 Response of the system with active hysteresis, primary chatter,
2-dimensional forces ---------- 52

Figure 2.22 Response of the system with active hysteresis, regenerative chatter,
2-dimensional forces ---------- 52

Figure 2.23 Response of the system with active hysteresis, primary chatter,
3-dimensional forces ---------- 53

Figure 2.24 Response of the system with active hysteresis, regenerative chatter,
3-dimensional forces ---------- 53

Figure 3.1 Hysteretic characteristics between the voltage and deflection of piezo ------- 60

Figure 3.2 Hysteresis response given by Eq. 3.2 ---------- 61

Figure 3.3 The schematic of turning with a piezoactuator ---------- 62

Figure 3.4 The section view of piezoactuator structure ---------- 63

Figure 3.5 Dynamic model of dependent piezoactuator on tool holder ---------- 64

Figure 3.6 Dynamic model of independent piezoactuator from tool holder ---------- 65

Figure 4.1 Schematic model of turning system with dependent piezoactuator and 2-D force models ---------- 67

Figure 4.2 Block diagram of turning system with piezoactuator and controller ------- 68

Figure 4.3 Response y(t) of dynamic system with the control law ---------- 75

Figure 4.4 Response of main cutting force $F_c(t)$ during cutting process ---------- 75

Figure 4.5 Response of thrust force $F_t(t)$ during cutting process ---------- 76

Figure 5.1 Schematic model of turning system with dependent piezoactuators and 3-D force models ---------- 78

Figure 5.2 Block diagram of turning system with piezoactuators and controllers ------- 79

Figure 5.3 Response of dynamic system with the control law ---------- 89

Figure 5.4 Response of main cutting force $F_c(t)$ during cutting process ---------- 89

Figure 5.5 Response of thrust force $F_t(t)$ during cutting process ---------- 89

Figure 5.6 Response of thrust force $F_f(t)$ during cutting process ---------- 90

Figure 6.1 Schematic model of turning system with independent piezoactuator and 2-D force models ---------- 92

Figure 6.2 Block diagram of turning system with piezoactuator and controller ------- 93

Figure 6.3 Response y(t) of dynamic system with the control law ----------101

Figure 6.4 Steady-state error of the dynamic system with the control law ----------101

Figure 6.5 Response of main cutting force $F_c(t)$ during cutting process ---------- 101

Figure 6.6 Response of thrust force $F_t(t)$ during cutting process ---------- 101

Figure 6.7 Displacement of the controlled piezoactuator during cutting process ------ 102

Figure 7.1 Schematic model of turning system with independent piezoactuators and 3-D force models ---------- 104

Figure 7.2 Block diagram of turning system with the piezoactuators and controllers --- 106

Figure 7.3 Response of dynamic system with the control law ---------- 116

Figure 7.4 Steady-state error of the dynamic system with the control law ---------- 116

Figure 7.5 Response of main cutting force $F_c(t)$ during cutting process ---------- 116

Figure 7.6 Response of thrust force $F_t(t)$ during cutting process ---------- 117

Figure 7.7 Response of thrust force $F_f(t)$ during cutting process ---------- 117

Figure 7.8 Displacement of the controlled piezoactuator in the thrust-direction ------ 117

Figure 7.9 Displacement of the controlled piezoactuator in feeding direction ------ 118

Figure 8.1 Variation of clearance angle b in cutting process ---------- 122

List of Tables

Table A: Parameters of the Controlled System with 2-Dimensional Forces and Dependent Piezoactuator ---------- 134

Table B: Parameters of the Controlled System with 3-Dimensional Forces and Dependent Piezoactuators ---------- 136

Table C: Parameters of the Controlled System with 2-Dimensional Forces and Independent Piezoactuator ---------- 138

Table D: Parameters of The Controlled System with 3-Dimensional Forces and Independent Piezoactuators ---------- 140

Nomenclature

$y_i(t)$	The displacements between the cutting tool and workpiece along the direction normal to the machined surface due to each freedom-directions ($i = 1, 2$)
$y_p(t)$	The displacement between cutting tool and independent tool holder
m	The equivalent mass of the machine structure
m_p	The equivalent mass of the piezoactuator
c_i	The damping ratios of the mass-spring structure ($i = 1, 2$)
k_i	The spring factors of the mass-spring structure ($i = 1, 2$)
$F_c(t)$	The main cutting force
$F_t(t)$	The thrust force
$F_f(t)$	The feed force
$F_v(t)$	The blocked-force of piezoactuator due to the applied voltage
$F_{pt}(t)$	The reaction force between the piezoactuator and workpiece in the direction of the thrust force
$F_{pf}(t)$	The reaction force between the piezoactuator and workpiece in the direction of the feed force
$u(t)$	The uncut (or undeformed) chip thickness of workpiece (shown in Fig. 2.16 or in p 448 referred to [3])
$u_o(t)$	The desired uncut (or undeformed) chip thickness of the workpiece
τ	The time delay
μ	The cutting overlap factor, $0 \le \mu \le 1$
α_i	The angles between the direction normal to the machined surface and each freedom-direction ($i = 1, 2$)
β	The angle between the feed force-direction and direction $y(t)$
b	The clearance angle between the tool flank and the cut surface of part
K_r	The major cutting edge angle
γ_i	The coefficient of adaptive functions ($i = 1, 2, 3, 4, 5, 6, 7$)

A_i	The hysteresis slope ($i = c,\ t,\ f$) associated with the cutting force, thrust force and feed force respectively in the system models
B_i	The hysteresis distance ($i = c,\ t,\ f$) associated with the cutting force, thrust force and feed force respectively in the system models
K_p	The stiffness of the piezoactuator
v(t)	The applied voltage in the piezoactuator
$\rho(t)$	The boundedness of the variable parameter $e(t, \cdot, \cdot,)$
H	Time lead associated with the chip thickness oscillations at the free end of the shear plane relative to the chip thickness oscillations at the tool tip shown
ΔL_o	The maximum value of nominal displacement without external force or restraint
L(t)	The deflection of piezoactuators
$\sigma(t)$	The sliding surface
σ_t	A tuning error in the controlled system
S	The sliding matrix
ε	The desired error of the systems
$x_i(t)$	The state variables of the systems (i = 1, 2, 3, 4)
$q_1,\ q_2,\ q_3$	Exist positive scalars
p	The positive constant in the equation about the piezoactuator
$g(v(t))$	The item in the equation about the piezoactuator
ρ_a	The boundedness of the variable parameter $g(v(t))$
$V(t)$	The Lyapunov function candidate
$\theta_i(t)$	Coefficients in the system (i = 1, 2, 3, 4, 5, 6, 7)
$\hat{\theta}_i(t)$	The adaptive estimates of coefficients $\theta_i(t)$ (i = 1, 2, 3, 4, 5, 6, 7)
∂	The differential operator
ψ	A positive constant
$\bar{C}_i(t)$	The small positive constants (i = 1, 2)
χ_i	The positive constants (i = 1, 2)

Chapter 1

Introduction

Introduction - the general theories of the chatter vibration control in the metal cutting processes and the literature surveys are given in this chapter. The contributions and organization of this thesis are also outlined.

1.1 Main Objective of the Thesis

The main objective of this thesis work is to suppress the chatter vibrations during turning processeses, the mathematical models of which is described as two degree-of-freedom of the dynamic systems. By the aid of piezoelectric actuators, the study designs corresponding adaptive control laws for both two-dimensional and three-dimensional cutting force models in this systems.

1.2 An Industrial Problem in Metal Cutting – Chatter Vibration

In metal cutting, such as turning, energetic vibrations are often encountered. These vibrations give rise to undulations on the machined surface and excessive variations of the cutting forces, which jeopardize the life of the cutting tool and the machine. Characteristic surface patterns caused by these vibrations in turning are shown in Fig. 1.1 [1]. in Fig. 1.1, points *A*, *B*, and *C* indicate one cycle of vibration, *A-B* and *B-C* represent the stroke of the workpiece approaching the cutting edge and the recess stroke, respectively. It is seen that because of the phase lag of undulation, the area

being cut in an approaching stroke is less than that being cut in a recess stroke, and therefore the cutting force in recess stroke is larger than in approaching stroke.

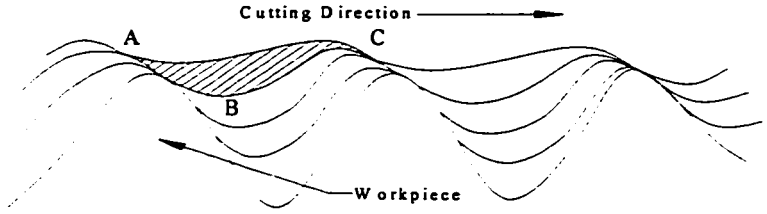

Figure 1.1 Undulations on the machined surface caused by chatter

Under some cutting conditions, mainly for cuts with a small chip width, vibrations do not occur, and the cutting process is stable. However, under some other conditions, vibrations occur due to the increasing forces, the cutting process becomes unstable. It will be mentioned that it is always possible to reach instability by increasing the width of chip. These vibrations belong to the class of self-excited vibrations, and the source of the self-excited energy is the cutting process itself. In metal cutting, such self-excited vibrations are referred to as chatter in [2].

Because of the above-mentioned effects, it is generally considered that cutting conditions must be selected so as to avoid chatter. As a result, the choices for cutting conditions (i.e., speed, feed rate, depth of cut, type of cutter, material, and so on) for a particular machining operation is often limited to realize the optimal conditions with respect to surface finish, tool life and machining output.

The phenomenon of chatter has been studied with the aim of creating rules by means of which the choice of cutting conditions can be made and, the design of machine tools with higher stability can be realized. The latter issue is the predominant one in the present study.

"Chatter is a nuisance to metal cutting and can be demonstrated on any chip-producing machine tool. The effects of chatter are adverse and affect surface finish, dimensional accuracy, tool life

and machine life. Undulations in the surface finish are commonly referred to as chatter or chatter marks. A great many factors contribute to chatter marks. In the case of turning, the basic mechanics of the cutting process itself results in slide motion, perhaps caused by unbalance in the drive system, servo instability, or stick-slip friction, can result in periodic variations in the finish. However, forced and self-excited vibrations are the major sources of the problems about the finish of workpieces referred to as chatter." [3]

Chatter, in metal cutting processes, is the self-ecxited vibration caused by the lag of fluctuation in the horizontal cutting force behind the horizontal vibrational of the workpiece [9].

The properties of chatter, as self-excited vibration, are 1) small amplitude and high frequency; 2) the forces that sustain the vibration are created and controlled by the vibration itself.

As an introduction to the chatter theory presented in the following chapters, the basic principles of self-excited vibrations in metal cutting will first be explained. Three principles will be presented, each of which in itself may be a sufficient and independent source of vibration energy. Although they will be discussed separately, it will be mentioned that in practice they all act simultaneously. The explanations will be given for the simplest possible cases of vibratory systems. These principles are:

(1) The first principle is called as "*the primary chatter*" principle. It accounts for the fact that the cutting tool is cutting on a "fresh" surface of the workpiece, i.e., the successive passes of cutting tool do not overlap any previous ones on the workpiece. For turning, this principle can dominate in the first cutting revolution, and it strongly depends on the pre-condition that the workpiece has a smooth surface when it is "fresh". An example to primary chatter is shown in Fig. 1.2.

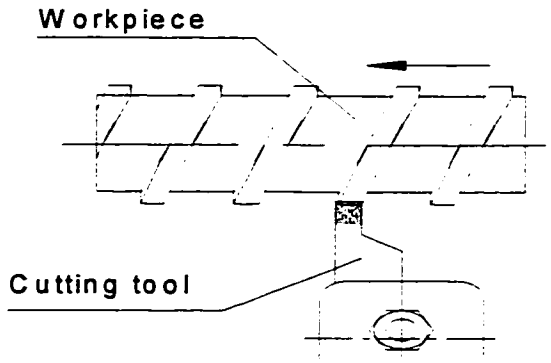

Figure 1.2 An example of primary chatter on the surface of a square thread

(2) The second principle is usually called "*the regenerative chatter*" principle. The simplest system to which it can be applied is a single degree-of-freedom system. With the exception of artificially arranged special cases, the tool always subsequently cuts the part of a surface, which it has already been cut during the previous revolution (in turning). Therefore, as shown in Fig. 1.3, if there was a vibration between the cutting tool and the workpiece during the *ith* cut and the produced surface has become undulated, the chip of the *(i+1)th* cut is removed from that undulated surface. If the amplitudes of the vibration in the direction of the normal to the cut surface in the *ith* cut and the *(i+1)th* cut are denoted by Y_0 and Y, then the amplitude of chip thickness variation is $(Y\text{-}Y_0)$. Here, both of Y and Y_0 are time vectors, so that $Y(t) = qY_0e^{-j\phi}$ where ϕ is the phase shift angle between the two subsequent undulations.

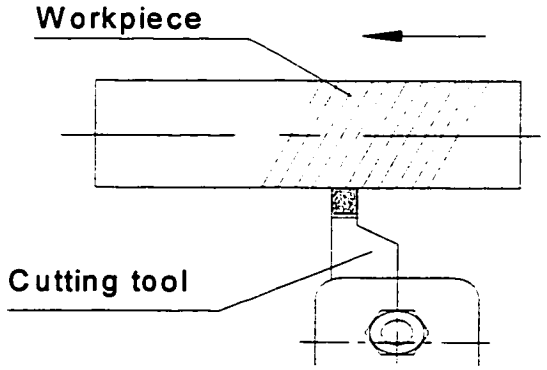

Figure 1.3 An example of regenerative chatter in the turning process

(3) The third principle of self-excited vibrations in metal cutting, "*the mode coupling*" principle, can take place with at least two degree-of-freedom (i.e., two modes). An example of the simplest form of such a system is illustrated in Fig. 1.4. It consists of a mass m attached to two springs of different stiffness acting in two directions X_1 and X_2 which are mutually perpendicular in the simplest case. If vibration occurs with a frequency ω in Fig. 1.4, the mass vibrates simultaneously in both directions X_1 and X_2 with different amplitudes and with a difference in phase. Thus, its resulting motion is an elliptical one.

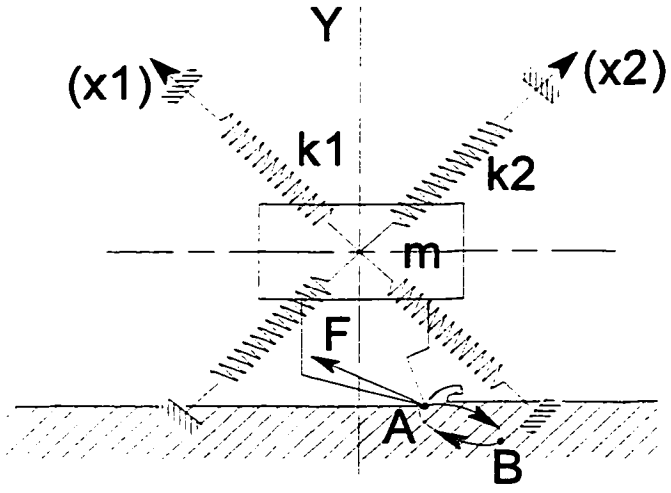

Figure 1.4 Mode coupling chatter in a system with two degree-of-freedom

The primary chatter is generally called as "wave producing" chatter while the regenerative chatter is referred to "wave removing" chatter.

Focusing on the chatter directions, Tobias and Fishwick [4] distinguish that there are two types of chatter, Type *A* and Type *B*, based on different chatter directions. This is shown in Fig. 1.5.

(1) Type *A* chatter occurs when the amplitudes lie in the plane perpendicular to the cutting direction.

(2) Type *B* chatter occurs when the chatter amplitudes have a component co-directional with the cutting speed regardless whether the amplitudes are co-directional with the feed or perpendicular to it. Furthermore, it is shown in [4] that type *A* chatter is a special case of type *B* chatter.

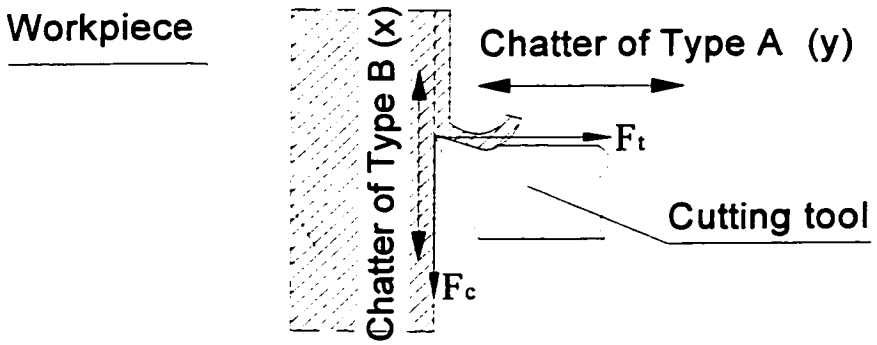

Figure 1.5 Chatter of type A and type B in turning process

It will be assumed [4][5] that chatter can exist in either the direction *A* or *B* shown in Fig. 1.5, but not both at once. When the relative stiffness in one direction, supposed to be *A*, is small but in the other direction, supposed to be *B*, is large. In that case, type *A* could occur. In the thesis, the study will concentrate on the type A of chatter suppression.

1.3 Overview of Research on Chatter Vibration

The metal cutting systems may be represented by using a closed-loop model from Merritt [3] shown in Fig. 1.6. This model consists of a flexible machine structure, a metal cutting process, which requires a force varying with the tool position and perhaps with its time derivatives, and feedback paths. In this closed-loop model, the machine deflections alter the cutting tool positions, which in turn alter the cutting forces. An additional feedback path accounts for the regenerative effect defined by Hanna and Tobias [6].

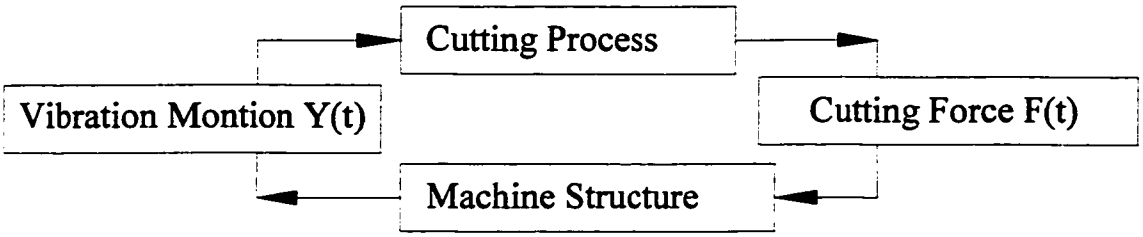

Figure 1.6 Basic closed-loop diagram of chatter occrence

1.3.1 Structure Dynamics in Machine Tools

Long and Lemon [7] initiated the self-excited vibration analyses of the mechanical systems by lumping the masses at points and connecting these points with elastic and dissipative elements. After choosing reference systems and sign conventions, the differential equations of motion are derived and solved under prescribed boundary conditions. In this method, the dynamic response to any input can be obtained on any form required by the particular stability theory.

Modern operational techniques of the vibration analyses, such as the mobility and impedance concepts, greatly facilitate the foregoing approachs. These techniques introduce the idea of the "transfer function" and the associated frequency response with the resulting data presented in the form required for stability analysis [8].

1.3.2 Cutting Dynamics in Machine Tools

Doi and Kato [9] and Tobias [4] have observed that there is a phase difference between the main cutting force and thrust force components of the resulting force vector. As well, they observed that the phase increases with the frequencies of the vibrations. The fact that a phase exists limits the validity of the simple model of the metal cutting process.

Nachtigal and Cook [10] visualize two distinct models for phase behavior between the cutting forces and uncut chip thicknesses. The first of these is concerned with the fact that the cutting forces are determined by the instantaneous lengths of the shear planes. The second model is based upon the effect discussed by Minis and Tembo [11] wherein the shear angle is a function of the inclination of the uncut work surface. Thus, with a wavy surface, the shear angle fluctuates around an average value. This will introduce the nonlinearity into the relationships between the oscillating uncut chip thicknesses and the oscillating forces.

1.3.3 Feedback of the Closed-Loop Dynamic System of Machine Tools

The paper by Merritt [3] shows that self-excited chatter can be represented by a feedback loop. The analysis of this loop by using feedback control theory yields a straightforward method of calculating the asymptotic and lobed borderline of stability for a machine tool system with a structure having n degrees of freedom and assuming negligible cutting process dynamics.

1.3.4 Comprehensive Overview on Machine Tool Chatter

The first comprehensive treatise about self-excited machine tool vibrations was written by Cumming and Kobayashi [12] who gave a theoretical explanation of their test results obtained for a one degree-of-freedom system. Further papers about vibrations with one degree-of-freedom were published by Sarnicola and Boothroyd [13]. The self-excited vibrations of the systems with two degree-of-freedom were investigated by Hanna and Tobias [6]. A mathematical analysis of the systems having two degrees of freedom has been made by Aslie and Achen [14]. They considered the variations of cutting forces F_1 and F_2 due to the depth of cut (i.e., the feeds in the orthogonal

cutting processes) and the velocities at the cutting tool-workpiece interface and discussed the criterion of stability by means of the Hurwitz determinant.

A number of investigations on self-excited chatter of machine tools have been made with the objectives that the limit of the stability would be identified as the machine tool performance, that potential cutting conditions for stable machining would be investigated, and that an effective method to prevent occurrence of chatter would be developed. The role of the cutting mechanism, the regenerative effect, and the structural dynamics of a machine tool, will be made obvious to identify the stability limit for the chatter. A stability chart is presented on the basis of methods developed by Tlusty [15], Taylor and Tobias [16] and Merritt [3].

Ota and Kono [17] and others pointed out the existence of a new phenomenon and named it the "multi-regenerative effect": the chip cut by the present tool motion has the trace of the tool motion not only one turn before, but two or more turns before. The effect plays an important role in the continuation of the vibration with finite amplitude. Their papers showed how it works for a basic system where a single degree-of-freedom system was assumed.

In the paper by Kaneko and Sato [18], the investigation simulating the behavior of the workpiece in turning was performed by assuming a two degree-of-freedom system and taking the multiple regenerative effects into account.

The existing experimental results, usually obtained from frequency response by moving the tool sinusoidal by external means, point out the differences between the steady state and dynamic cutting processes. The dynamic cutting forces are generally lower than the static ones for the same value of the undeformed chip thickness as shown by Albrecht [19].

Taylor and Tobias [16] covered a wide range of frequencies (0-400 cps) and showed that above 100 cps, the oscillations in the thrust force lead the oscillation in the tool displacement. Kegg [20] observed that the phase lead angles are different for the two components (cutting and thrust forces) of the resultant cutting force and that within a band of scatter both phase lead angles increased with the exciting frequency.

Marui and Kato [21] have experimentally determined the values of the phase lead in cutting of aluminum alloy with 20 degrees rake angle tool. The experimental results of Marui and Ema [22] by employing a high-speed camera have shown a phase lead between the measured shear angle and the uncut chip thickness for different amplitudes of the depth of cut and cutting speeds. They assumed that the cutting force is a linear function of the shear angle, and hence it follows that the oscillations of the cutting force lead those of the uncut chip thickness.

In most published studies, the actual waveforms of the dynamically varying cutting forces obtained from experimental frequency response are unfortunately not presented. Kegg [20], Doi and Kato [9] remarked that they observed that the force waveform was not purely sinusoidal, but they filtered out the high frequency components and recorded only the fundamental sine wave. An exception is the study of Albrecht [19] who clearly shows the resulting non-sinusoidal waveforms of the cutting and thrust forces when the tool is displaced sinusoidally.

The theories of dynamic cutting, far from being complete, mostly consider the influence of the geometrical changes in the cutting conditions, and by doing so considerably simplify the actual physical situation. Some theories, such as those of Albrecht [19], have succeeded to some extent in explaining the phase difference between the oscillations in the uncut chip thickness and the cutting forces. For example, Lauderbaugh and Ulsoy [23], by introducing some simplifications, arrived at

an expression for the phase angle by which the resulting oscillations in the force lead the oscillations in the undeformed chip thickness depending upon the cutting conditions and frequency of the oscillations for both "wave producing" and "wave removing" cutting mechanisms.

For the case of wave removing, Doi [24] obtained a numerical solution for the cutting force as a function of the undeformed chip thickness at the outer edge of the shear zone and plotted this relationship. The successful plot has the character of an active hysteresis.

The existing theories on dynamic cutting mostly assume that the shear angle remain constant and neglect the influence of the changes in the cutting speed, rake angle and friction on the rake face. Also, fluctuations in the rubbing force on the clearance face are likely to play a more important role than they are recognized in the existing theories.

Thompson [25] has pointed out that the flank-face interference will introduce a strong nonlinear component in the cutting forces. He has suggested that this limits effectively the amplitude of vibrations to the point where plastic deformation occurs on the clearance face. Kegg [20] postulated that an elastic deformation on the clearance face gives rise to a fluctuating friction force leading the undeformed chip thickness by a phase angle of 90 degrees.

Although the dynamic cutting forces are obviously complicated functions of the time dependent variables such as chip thickness, rake angle, shear angle, cutting speed, rubbing force on the tool nose or clearance force, and friction force on the rake face, the existing stability analysis assume the simplest linear relationship between the cutting force and uncut chip thickness.

Merrit [3] employed the proportional relationships between the cutting forces and variations of chip thicknesses and suggested the evaluation of the constant of proportionality from the material properties and steady state cutting geometry.

Hanna and Tobias [6] suggested a linear relationship between the dynamic cutting force, uncut chip thickness, speed and feed rate, but in their stability analysis they neglected the influence of speed of the spindle. They considered the coupling between the cutting process and structural dynamics and obtained the relationship between the width of cut and spindle speed on the borderline of stability for structures with one to n degrees of freedom.

Nair and Danai [26] introduced the overlapping factor μ, which accounts for the part of previous cut that is overlapped with the succeeding cut. Merrit [3] has expressed the cutting process and structural dynamics in the form of a block diagram that gives a good overview of the whole system. The proportional relationship between the uncut chip thickness and cutting force cannot cause any phase difference between them. In linear causal systems, the output cannot lead the input for sufficiently high frequencies. Hence, there is a strong indication that any linear relationship between the uncut chip thickness and the cutting force cannot satisfactorily express the dynamics of the cutting process.

Saravanja and Dsouza [27] pointed out that the stability of self-excited and regenerative chatter will be investigated with a nonlinear relationship between the cutting force and uncut chip thickness. This nonlinear relationship exhibited active hysteresis and was obtained from Albrecht's experimental results [19]. The nonlinear active hysteresis relationship explains the observed phase lead as well as the decrease in the dynamic cutting stiffness (ratio between the cutting force and uncut chip thickness) and the nonsinusoidal waveform of the cutting force better as reported by

Ablrecht [19] and Kegg [20]. The stability of the chatter loop is investigated here by employing the describing function approach for structure dynamics with two degree-of-freedom.

As stated earlier, the non-linear relationship between the uncut chip thickness and forces in cutting under dynamic conditions is obtained from the experimental results of Albert [28].

1.4 Basic Theory of Chatter Vibration

In metal cutting processes, where substantial energy is being transmitted and mechanical damping ratio is low, a very small portion of that energy is sufficient to maintain large amplitude vibrations. The mechanisms, which cause chatter, are invariably second-order effects, which do not appear in the simple theory and hence are difficult to investigate directly.

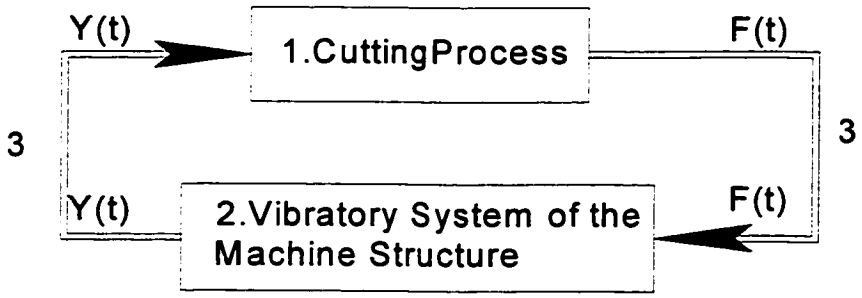

Figure 1.7 Basic diagram of the chatter loop

The basic diagram of the closed-loop process of self-excited vibrations in metal cutting is presented in Fig. 1.7. It is a closed-loop system including two fundamental parts, namely the cutting process and the vibratory system of the machine structure, as well as the mutual directional orientation of the two parts [29].

It indicates that the vibration *Y(t)* between the tool and workpiece influences the cutting process so as to cause a variation *F(t)* of the cutting forces which are acting on the vibratory system of the

machine, and generating again vibration $Y(t)$. The mutual orientation 3 of the two fundamental parts, incorporated in the links between block 1 and block 2, occurs because the machined surface has a definite location in space, the cutting force has a definite direction, and also the vibratory system of the machine has a definite location in space, with definite directions of vibration in its individual modes. By changing the mutual directional orientation of both basic parts, the mutual influence is changed and the limit condition for stable machining is changed too.

Thus, three groups of the parameters influencing the occurrence of chatter may be considered:

a. Those of the cutting process

b. Those of the vibratory system of the machine structure

c. Those of the orientation of the cutting process with respect to the vibratory system of the machine.

The influence of the cutting conditions, i.e., block 2 in Fig. 1.7, upon chatter is not dealt with in great detail in this thesis. These influences will be assumed as a standard, constant set throughout the work. The parameters, which will be considered, are the chip width b, or some other parameters related to the chip width, for example, the depth of cut t in turning shown in Fig. 1.8.

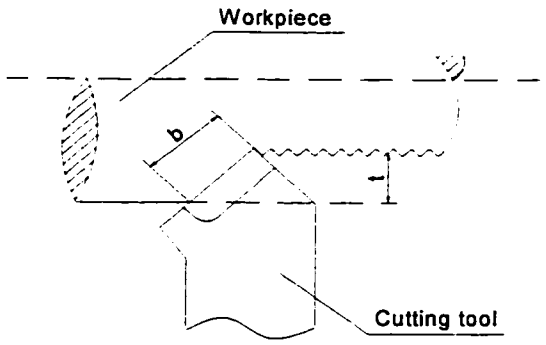

Figure 1.8 Depth t expressing chip width b in turning

The stability of different types of machines can then be measured by performing a cutting test under a standard set of cutting conditions starting with a small chip width b and increasing it until the cut with a "limit chip width b_{lim}" is attained, when the chatter starts to occur. The value b_{lim} can be used as a criterion of stability for individual cases (specified by machine type, arrangement and orientation).

The cutting process is represented by the transfer function relating vibration *Y(t)* and force *F(t)* in the closed-loop system in Fig. 1.7. Throughout this study, two simplified assumptions will be made for the transfer function [29]:

a. The variation of the force acting on the workpiece is caused only by the effect of the change of chip cross-section.

b. The direction of the variable component of the cutting force is the same as the direction of the cutting force in a stable process.

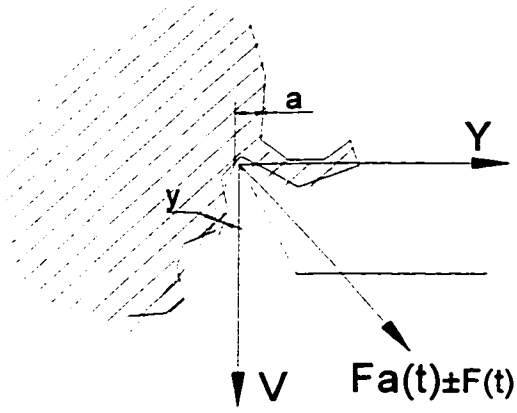

Figure 1.9 Vibration in the direction *Y* produces changes in chip thickness

The basics of the cutting process transfer function, i.e., block 1 in Fig. 1.7, are illustrated in Fig. 1.9. Only the component of vibration falling into the plane perpendicular to the direction of the

cutting velocity $v(t)$ influences the chip cross-section. That is, the vibration in the direction by Y. During the vibration with an amplitude Y, the average chip thickness a, corresponding to a stable process, varies between $(a-Y)$ and $(a+Y)$. The variation Y of the chip thickness causes a variation with an amplitude $F(t)$ of the average force $F_a(t)$ (corresponding to a stable process). Then the average values of the chip thickness and of the force do not influence the vibratory process, an expression [29] of the relationship between the variable components of the chip thickness and the force will be:

$$F(t) = -kY(t) \tag{1.1}$$

The minus sign on the right-hand side of Eq. 1.1 corresponds to the chosen senses of $F(t)$ and $Y(t)$ indicated in Fig. 1.9 if k is positive. The coefficient k expresses either the intensity of the coupling between the vibration and cutting force or the gain in this part of the loop.

Fig. 1.10 illustrates the conditions in the plane perpendicular to the cutting velocity. If there is a vibration X in the direction X inclined at an angle ε to the cutting edge, it must follow that the change in the chip cross-section parameters and the change in the cutting force, caused by the deviation X, will be changed according to value of ε. It also follows that a direction Y may be found in which the deviation causes the maximum change in the cutting force; it is the direction of the maximum gradient of the force with respect to the vibration. A deviation in the direction perpendicular to the direction Y will not cause any change in the force. Readers can refer to [16].

Therefore, vibration X in the direction X will influence the cutting force only by its projection Y onto the direction Y. Usually, the chip width b is far greater than the chip thickness a, and therefore the direction Y is almost perpendicular to the main cutting edge. The direction Y, which is also perpendicular to the cutting velocity, will be called "the normal to the cut surface".

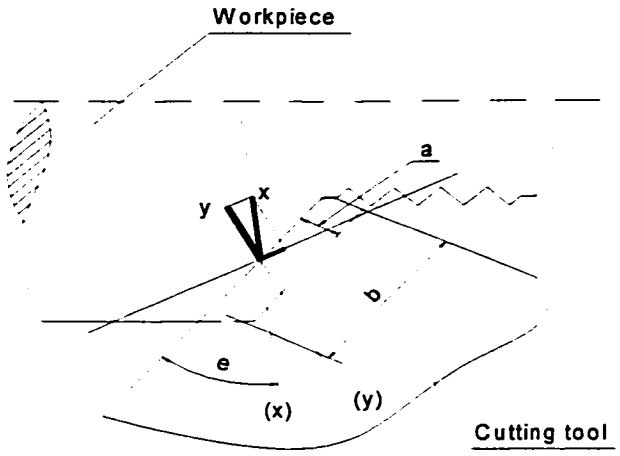

Figure 1.10 The "normal to the cut " direction Y

The system is excited by the force acting between the cutting tool and workpiece in the direction of the cutting force, and the vibration in the direction of the normal to the cutting surface is measured relatively between the cutting tool and workpiece.

For usual thin chips, the direction Y is normal to the main cutting edge to a good approximation and the coupling between the force and the vibration expressed by Eq. 1.1 is proportional to the chip width b. Accordingly, Eq. 1.1 may be rewritten as:

$$F(t) = -brY(t) \tag{1.2}$$

where r is a coefficient, depending on all other cutting conditions except for b.

With respect to "*the regenerative chatter*" principle, the simplest system to which it can be applied is a single degree-of-freedom system. It will be recognized that the diagram given in Fig. 1.9 does not correspond to the actual machining operations. In Fig. 1.11, if there is the vibration between the tool and workpiece during the ith cut and the produced surface has become undulated, the chip of the $(i+1)$th cut is removed from that undulated surface. If the amplitude of the vibration in the

direction of the normal to the cut surface in the ith cut is Y_0 and in the $(i+1)$th cut it is Y, then the amplitude of chip thickness variation is $(Y-Y_0)$. So that $Y(t) = qe^{-j\psi}Y_0(t)$ where ψ is the phase shift angle between the two subsequent undulations. Consequently, instead of Eq. 1.2, Eq. 1.3 must be used for actual metal-cutting operation:

$$F(t) = -k(Y(t) - Y_0(t)) \tag{1.3}$$

It may be understood, on the basis of Fig. 1.11, that because of the undulation Y_0, the cutting force contains a variable component, which excites vibration X of the vibratory system with the normal component Y. The vibration Y creates again an undulated surface on the workpiece and the regeneration of the undulation proceeds in the subsequent cuts. The frequency ω of the vibration and the phase shift ψ between undulations in subsequent cuts will adjust themselves so that maximum energy is delivered to the vibration of the system.

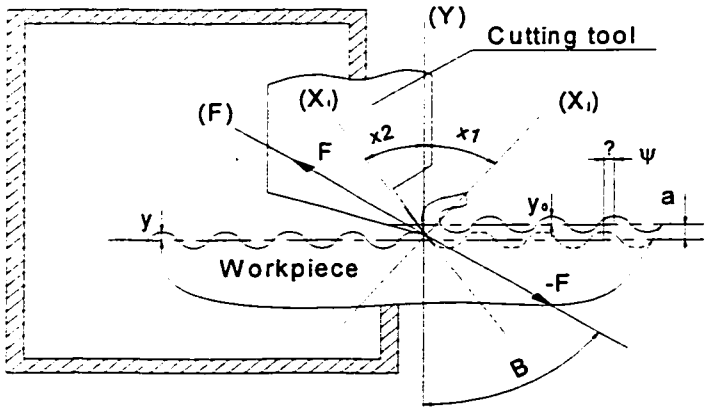

Figure 1.11 Cutting an undulated surface

This energy will be sufficient to cover the losses of the energy caused by the damping in the vibratory system so that vibration in subsequent cuts do not diminish but increase. Thus, a special case of dynamic instability, the regenerative chatter, occurs. As will be shown later, it is the

intensity of the coupling between the variation of chip thickness and that of cutting force, given by the value $(b \cdot r)$, which determines whether instability will arise. In practice, regenerative chatter always occurs when the chip width b is sufficiently large. The limiting case of stability is one in which undulations in subsequent cuts neither decress nor increase.

For "*the mode coupling*" principle with two degree-of-freedom, if in the case depicted in Fig. 1.4 vibration occurs with a frequency ω, then the mass vibrates in both directions X_1 and X_2 simultaneously with different amplitudes and different phase. Thus, its resulting motion is an elliptise. Assuming that the tool moves in the direction of the arrow in Fig. 1.4, then, during the half-period of the motion from A to B, the cutting force acts in the direction of the velocity of the motion. In the first half-period, therefore, energy is dissipated by the system, whereas in the second half-period energy is delivered to the vibratory system by the cutting force. Because the second half-period of the movement is performed with a greater average depth of cut, the average force in this half-period is greater than the average force in the first half-period. Consequently, in one cycle, the energy delivered to the system is greater than the energy dissipated by the system. The surplus of energy may be able to cover damping losses. It has been shown that with suitable arrangements of the system, the procedure described actually occurs and self-excited vibration is developed. Among various interesting properties of the arrangements shown in Fig. 1.4, if the direction X_1 falls between directions Y and F, and the direction X_2 is perpendicular to direction X_1, instability based on "mode coupling" can occur only if the stiffnesses of the two springs satisfy $k_1<k_2$. Inversely, if $k_1>k_2$, the cutting process is stable at all cutting conditions.

In all actual cases, undulations of subsequent cuts overlap, and the vibratory system has more than one degree of freedom. Therefore, all principles always appear simultaneously. It is necessary to

describe which was expressed in Fig. 1.7, by a corresponding mathematical expression, so as to include the principles and find the limiting equation of stability.

For further discussion on the cutting process, we assume a very simple system with two degree-of-freedom where the directions of the two modes are different.

The system is shown in Fig. 1.12. A mass m (common for both modes) is attached to two springs, acting in directions X_1 and X_2. For simplicity it is assumed that direction X_1 and X_2 are perpendicular to each other. The springs in the direction X_1 and X_2 have stiffnesses k_1 and k_2.

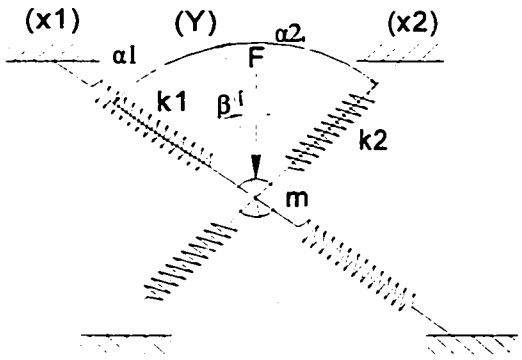

Figure 1.12 A system with two degree-of-freedom

The two modes of the system may be well separated and represented by the vibrations in the directions X_1 and X_2. It is obvious that the stiffness k_1 and k_2 are stiffness of the individual modes. Natural vibrations of the system are described in Eq. 1.4

$$x = X_1 e^{(-\delta_1 + j\nu_1)t} + X_2 e^{(-\delta_2 + j\nu_2)t} \tag{1.4}$$

where the values δ_1, ν_1 and δ_2, ν_2 are simply determined by k_1, c_1 m and k_2, c_2 m, respectively; the values x, X_1, X_2 are in this case not only time vectors but also space vectors; the resulting motion is performed in the plane (X_1, X_2) and its path has the form of the well-known Lissajous

curves (damped); the values X_1 and X_2 depend on the initial conditions; the vibration in only one of the two modes can be achieved, if either $X_1 = 0$, *or* $X_2 = 0$ (and also the initial velocities are zero).

If a force $f = Fe^{j\omega t}$ acts on the mass m in the direction F, with angles α_1 and α_2 between directions F and X_1 and F and X_2 respectively, it excites vibration simultaneously in both modes with the same frequency. The resulting vibration is again a time and space vector:

$x = Xe^{j\omega t}$

$$X = X_1 + X_2 = \frac{F\cos\alpha_1}{k_1}\frac{\Omega_1^2}{\Omega_1^2 + (j\omega)^2 + 2\delta_1(j\omega)} + \frac{F\cos\alpha_2}{k_2}\frac{\Omega_2^2}{\Omega_2^2 + (j\omega)^2 + 2\delta_2(j\omega)} \qquad (1.5)$$

where $\delta = \frac{c}{2m}$, $\Omega = \sqrt{\frac{k}{m}}$ is the natural frequency of the undamped system, and $\nu = \sqrt{\Omega^2 - \delta^2}$.

The path of x is an ellipse in the plane (X_1, X_2). Its form depends on the parameters of the system and on the frequency ω of the exciting force. Eq. 1.5 implies that the vibration in each of the modes is excited by the projection of the force in their directions.

If only the component of the resulting vibration in a direction Y is of interest, it may be realized that it is a sum of the projection of directions X_1 and X_2 into direction Y:

$$Y = F\left(\frac{\cos(\alpha_1 - \beta)\cos\alpha_1\Omega_1^2}{k_1(\Omega_1^2 + (j\omega)^2 + 2\delta_1(j\omega))} + \frac{\cos(\alpha_2 - \beta)\cos\alpha_2\Omega_2^2}{k_2(\Omega_2^2 + (j\omega)^2 + 2\delta_2(j\omega))}\right) \qquad (1.6)$$

In an similar way to the two preceding systems, systems with many masses, located quite generally in the three dimensional space and partly interconnected with many springs may be

assumed. A two-dimensional schematic representation of such a system is depicted in Fig. 1.13. If the discussion given in the preceding cases are extended and generalized, it may be understood that these systems will have many degrees of freedom with many natural frequencies Ω_i, damping constants δ_i and corresponding modal shapes. For every modal shape there exists a particular direction X_i in which a particular point, such as point 2 in Fig. 1.13, of the system vibrates in the given modes. (Several modes can eventually have one common direction).

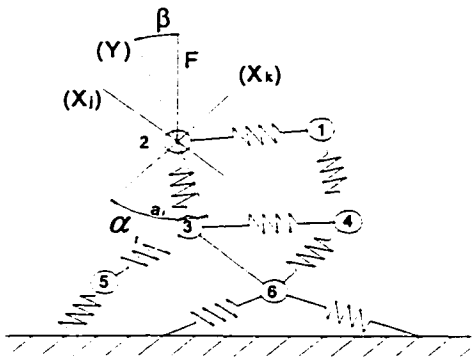

Figure 1.13 A system with multi degree-of-freedom

If a variable force $f = Fe^{j\omega t}$ acts on the point 2 shown in Fig. 1.13, and if a particular direction Y is chosen, the angle between directions Y and F being β and the angles between direction Y and individual modal directions X_i being α_i, then vibration of the point 2 in the direction Y will be:

$$y = Ye^{j\omega t}$$

$$\text{where } Y = F\sum_{i=1}^{n}\left(\frac{u_i}{k_i}\frac{\Omega_i^2}{\Omega_i^2 - \omega^2 + 2\delta_i(j\omega)}\right) \tag{1.7}$$

The "directional factors u_i" are defined as:

$$u_i = \cos\alpha_i \cos(\alpha_i - \beta) \tag{1.8}$$

where k_i is stiffness corresponding to the individual modes.

A machine tool structure is a vibratory system with an infinite number of degrees of freedom. It is remembered that systems with an infinite number of degrees of freedom possess an infinite number of modes with corresponding natural frequencies. However, the frequencies are distinct representing separated values in the range from $\Omega = 0$ up to $\Omega = \infty$. For forced vibrations, with the force acting at a particular point in the system or between two particular points and vibration measured at a particular point or between two particular points, a particular stiffness k_l corresponds to every one of the infinite number of modes. The higher the natural frequency of the mode is, the higher the value of its stiffness is. Observations also show that the value of damping is usually higher in higher modes. Therefore, the higher the mode, the smaller its participation in the resulting vibration. It follows that for a particular required accuracy of calculation, all but several lower modes of the system can be neglected. Thus the actual structure of the machine can in practice be considered as a system with a small number (usually less than ten) of degrees of freedom.

Following the preceding discussions to describe self-excited vibrations in metal cutting, it is now necessary to express the closed-loop system of Fig. 1.7 mathematically. Transfer functions for both parts have already been derived in the preceding sections. They are expressed for the part relating to the cutting process by Eq. 1.3 and for the part relating to the machine tool, including the mutual orientation of both parts by Eq. 1.7.

As a basic theory, some assumptions will now be established which contains several simplifications. By special experiments and observations, the simplifications that are introduced have been shown significantly the practical application of the theory to the analysis of the stability of machine tool structures. The simplifications enable the procedures of stability analysis to be

carried out with a reasonable amount of work. The methods of the analyses are based on this simplified theory. It will, therefore, be referred to as the *basic theory* in the sense of its significance for practical use.

The assumptions made for simplification are [29]:

(a) The vibratory system of the machine is linear.

(b) The direction of the variying component of the cutting force is constant.

(c) The variable component of the cutting force depends only on vibration in the direction Y (t) of the normal to the cut surface.

(d) The value of the variable component of the cutting force varies proportionately and instantaneously with the vibration displacement y.

This basic theory and method of the stability analyses, proposed by Srinivasan and Nachtigal [30] differ from the methods used by Thompson [31], Tobias and Ismail [5] in that the graphical solution of the limit of stability is performed not in the complex plane of the receptance curve of the machine but in the real plane. This permits an understanding of how the limit of stability depends on the individual mode of the structure and leads to the suggestion of adequate changes of the structures.

1.5 Main Characteristics of Turning

The turning tool is used for external and internal cylindrical machining processes. The basic external operations include: facing, straight turning, taper turning, shoulder turning, turning grooves, knurling, cutting off and threading. The basic internal operations are: drilling, boring, turning internal straight, tapering, and undercut surface, countersinking, counter boring, reaming, tapping and threading. A simple turning is shown in Fig. 1.14.

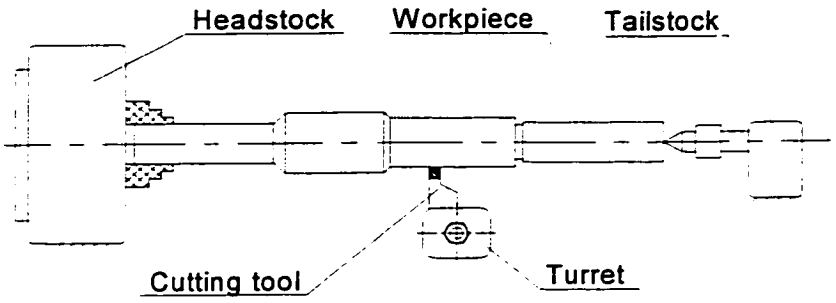

Figure 1.14 The schematic of a turning system

The case 1 and case 2, given in Fig. 1.15, will be regarded as the main turning operations, on which the machine structure will be discussed.

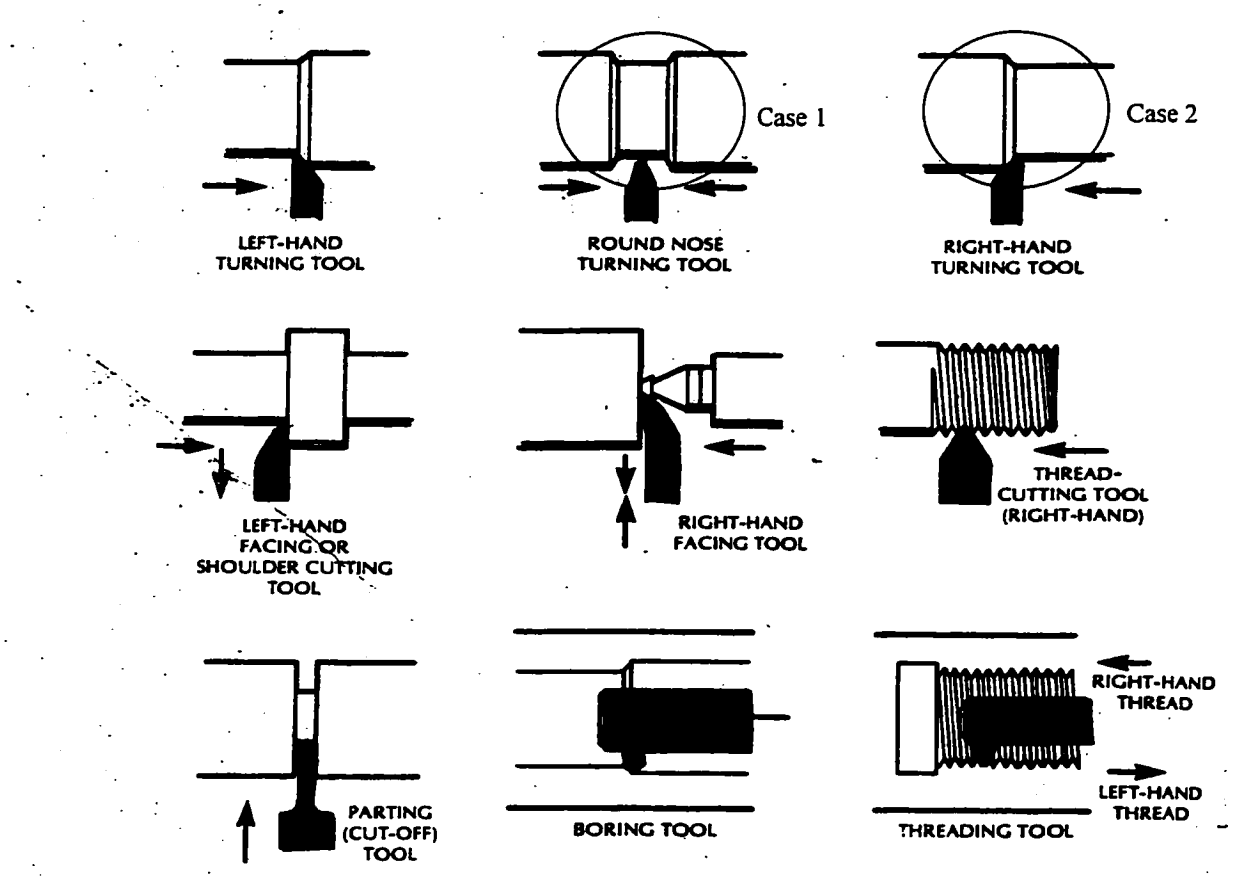

Figure 1.15 General-purpose applications in turning [32]

In case 1, the forces between the workpiece and tool appear in two-dimensional space. It means that the only two forces including main cutting force and thrust force exist during the turning operation. In case 2, the forces between the workpiece and tool appear in three-dimensional space. It means that not only the main cutting force and thrust force but also the feed force exists during the turning operation. The forces are shown in Fig. 1.16.

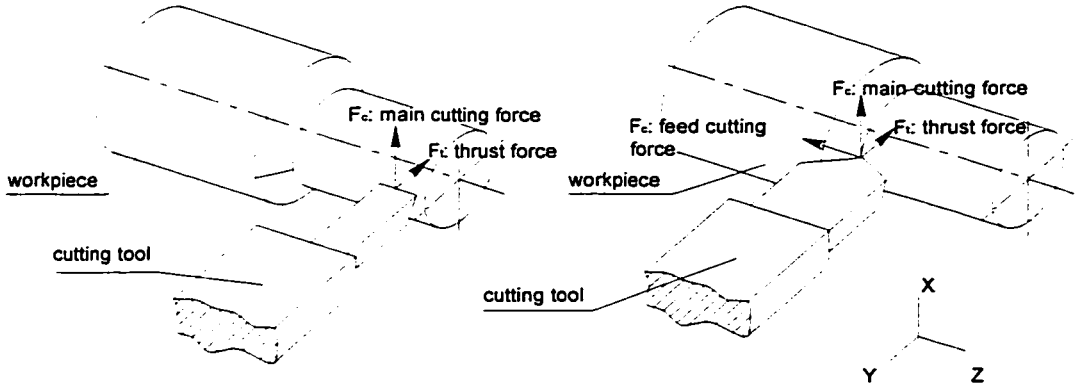

Case 1:forces acting on the workpiece in 2D orthogonal cutting

Case 2:forces acting on the workpiece in 3D orthogonal cutting

Figure 1.16 Typical operations in turning

1.6Contributions of This Thesis Work

The work presented here was motivated by the industrial problem of metal cutting in turning operation. In turning, the occurrence of self-excited vibrations, so called chatter, is undesirable as it gives rise to production problems, causes detrimental effects on the machined surface finish, decreases the machining efficiency, causes tool wear and decreases the tool life. Because of the small amplitude (as small as several microns) and high frequency properties of chatter, an active vibration control, providing forces acting on the cutting system, is required to overcome the adverse effects of chatter.

In this thesis, the vibratory system, i.e., the machine structure based on turning process, with two degree-of-freedom has been investigated. Meanwhile, the orthogonal cutting processes with two-dimensional and three-dimensional force models shown in Fig. 1.16 will be discussed in detail.

There are strong indications that the relationship between the cutting forces and uncut chip thickness displays hysteretic behavior in cutting processes. The mechanism of energy excitation for chatter is given in [27]. It is concluded that chatter is the self-excited vibration caused by the hysteresis relationships between forces and deflection of the workpiece. In this thesis, work will focus on the relationships between cutting forces and variation of chip thickness as a hysteresis model where nonlinearity dominates. In addition, work in this thesis will take into account the unavoidable effect of time delay in metal cutting process.

To rapidly adjust the displacement between the workpiece and cutting tool during the cutting process, the piezoelectric actuators, as high-precision positioning elements in the metal cutting process, are introduced into the design of the chatter supression. Nevertheless, piezoactuators also display hysteretic behavior between the deflection of piezoactuators and the voltage applied to the piezoactuators. With respect to different mechanical structures of piezactuators in metal cutting processes, in this thesis, the mathematical models of piezoactuators will be implemented under two structures, i.e., dependent and independent from the cutting tool holders

In this thesis, robust controllers are developed to deal with unknown hysteretic characteristic combined with time delay in metal cutting processes. The proposed robust adaptive controllers ensure the suppression of chatter and global stability in the metal cutting system. The simulations of outputs of the controlled systems will be givens graphically.

1.7 Organization of This Thesis

The present chapter provides a brief introduction and a literature reviewed on chatter vibrations in metal cutting, specifically, in turning. In chapter 2, the mathematical models of machine structure and hysteretic characteristics of dynamic cutting process are presented. Active hysteresis is provided to be one of the causes of chatter occurrence as it provides the energy for chatter excitation and maintenance. The simulations based on these models demonstrate the behaviors of hysteresis behaviors. In chapter 3, main characteristics and applications of piezoactuators are described. The hysteretic characteristics of the relationships between the applied voltage and deflection of piezoactuator are demonstrated as well. Mathematical model for this hysteresis is provided.

From chapter 4 through chapter 7, piezoactuators are introduced for the adjustments of the machine tool displacements. Based on different turning models, different adaptive control laws are proposed for eliminating the chatter. In chapter 4, dynamic system with two-dimensional forces and model of piezoactuator that is dependent on the tool holder are treated; in chapter 5, dynamic system with three-dimensional forces and models of piezoactuators that are dependent on the tool holder are treated; in chapter 6, dynamic system with two-dimensional forces and model of piezoactuator that is independent from the tool holder are treated; In chapter 7, dynamic system with three-dimensional forces and models of piezoactuators that are independent from the tool holder are treated.

In chapter 8, the conclusions of the thesis and some recommendations for the future work in this field will be outlined.

Chapter 2

Modeling of Machine Structure and Cutting Process

Introduction – based on theoretical analyses and experiments by precedents, the paper presents the models of machine structure, hysteretic characteristics of cutting process and output feedback in turning. Meanwhile, it proves that active hysteretic characteristic relationship between cutting forces and uncut chip thickness of the workpiece in cutting process is the main cause of chatter occurrence. Taking into account several situations in metal cutting process, the simulations of the response of dynamic metal cutting systems are conducted.

2.1 The Machine Operation as a Closed-Loop System

In continuous machining processes, the structures are often excited by abrupt changes in the cutting forces due to hard spots in the workpiece, material cleared from a built-up edge on the cutting tool, or a chip breaking. The structures respond to the change in the applied force $F(t)$ with a relative displacement $Y(t)$ between the tool and the workpiece. This displacement $Y(t)$ affects the values of the parameters of the cutting processes, such as chip thickness, effective cutting angle, etc., which in turn result in further variations of the cutting forces.

The interactions between the machine structures and the cutting processes are described by a closed-loop system that incorporates two fundamental blocks as shown in Fig. 2.1. The machine

structures block describe the relationships between the cutting forces F(t), which are applied on the structures, and the displacements Y(t) of the machine structures

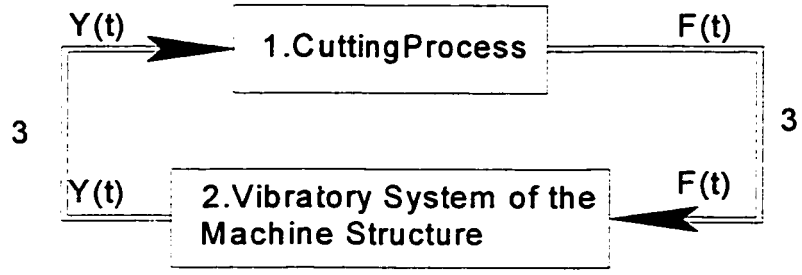

Figure 2.1 Block diagram representation of the metal cutting dynamics

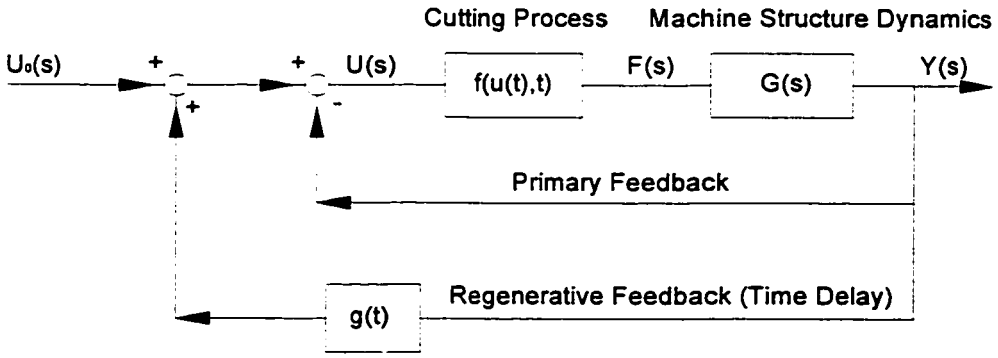

Figure 2.2 Block diagram of chatter loop

The effects of the relative displacements $Y(t)$ on the variations of the cutting forces F, which can be described by "cutting equations", are represented in the cutting process block in Fig. 2.1. The intrinsic coupling of the machining operation suggests the treatment of the chatter problem as a closed loop system stability problem. However, complete analyses and experimental investigations of the dynamics of both major system components in Fig. 2.1 is required prior to the development of a stability criterion for the coupled machining system. These analyses have already been dealt with in [29].

As a summary, the machine structures and cutting processes can be presented by a closed-loop diagram as shown in Fig. 2.2. In Fig. 2.2, the block G(s) represents the dynamics of the machine structure; the block f(u(t),t) describes the relationship between the cutting force and the displacement $Y(t)$ between the cutting tool and the workpiece; the block g(t) indicated the feedback of the displacement $Y(t)$ in the previous revolution; the "Primary Feedback" is the feedback of the displacement $Y(t)$ in the current revolution.

2.2 Modeling of Machine Structure

To predict the onset of chatter, namely, self-excited vibration in turning, it is necessary to obtain the representation of the dynamics of the machine structure, and the representation of relative motion of the machine structure as a function of oscillatory force applying to the cutting tool. Therefore these representations are the steady state solutions of the partial differential equations defining the motions of the structures as various forcing functions. The solutions would be extremely difficult to obtain in closed form, therefore approximate techniques are investigated.

The mathematical analyses of the systems with two degree-of-freedom have been made by Saravanja-fabris and D'souza [27]. They considered that the variations of cutting forces F_1 due to depth of cuts (i.e. the feed in the orthogonal cutting processes) and relative velocity between the cutting tool and workpiece; discussed the criterion of stability by means of the Hurwitz determinant.

A dynamic cutting system can be considered as a spring-mass-damper system with two degree-of-freedom. The forces may be conveniently divided into three components: the main cutting force, thrust force and feed force [32].

A schematic representation of the system with two degree-of-freedom considered in this thesis is described in the Fig. 2.3. One dynamic system to be considered is the cutting tool shown in Fig. 2.3(a), the other is the workpiece and the spindle in Fig. 2.3(b). It will be noted that the schemes are not affected the research on the dynamic performance. Generally, in this thesis, the dynamic systems of machine structures with two degree-of-freedom based on the Fig. 2.3 (b) will be taken into consideration for deriving the mathematical models.

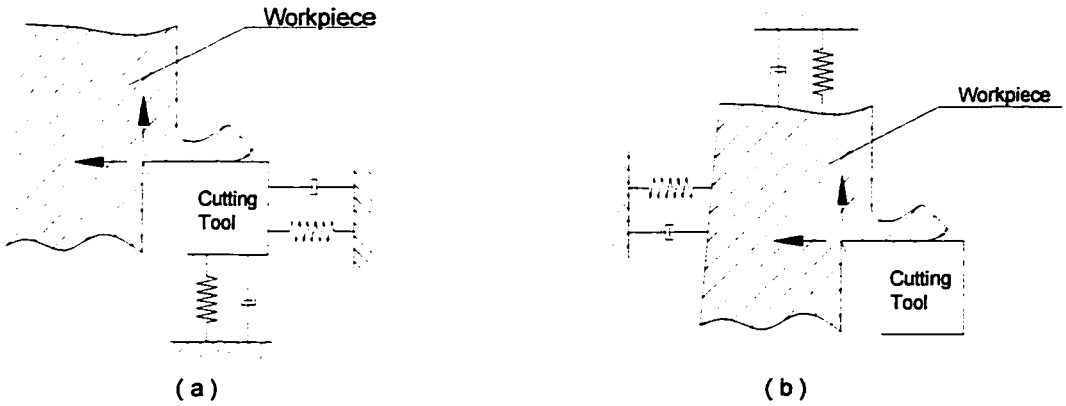

Figure 2.3 The scheme of the machine system with two degree-of-freedom

In this thesis, the schematic diagram of the dynamic system of turning tool structure with two degree-of-freedom is described in Fig. 2.4. A mass (namely a combination of workpiece and spindle) is attached to the rigid support S_1 and S_2 through the springs k_1 and k_2, dampers c_1 and c_2. The damping ratios and the spring constants for both directions S_1 and S_2 are taken differently. For simplicity, it is assumed that directions S_1 and S_2 are perpendicular to each other.

In the situation of two-dimensional orthogonal cutting operations, main cutting force and thrust force act onto the workpiece due to the fixed cutting tool, both of the directions of two forces are shown in Fig 2.4. The displacement y between the cutting tool and workpiece is made positive for the direction that the workpiece leaves from the cutting tool.

The chip-formation mechanism will to be controlled by instant cutting conditions, including feed, speed, and depth of cut, etc. Any change in these conditions during the cutting processes will instantaneously change the values of the normal forces $F(t)$ and the relative speed v of the chip to the tool, even affect the dynamic behavior of the systems. Under conditions of small vibrations, it is reasonable to assume that the relationships between forces F and speed v remain the same as those under steady state cutting conditions. In other words, the physical relationships established in steady state cutting can be applied to dynamic cutting processes as well, if the amplitudes of vibrations are relatively small. This argument will be carried throughout this thesis in the developments of the mathematical models governing the system behavior.

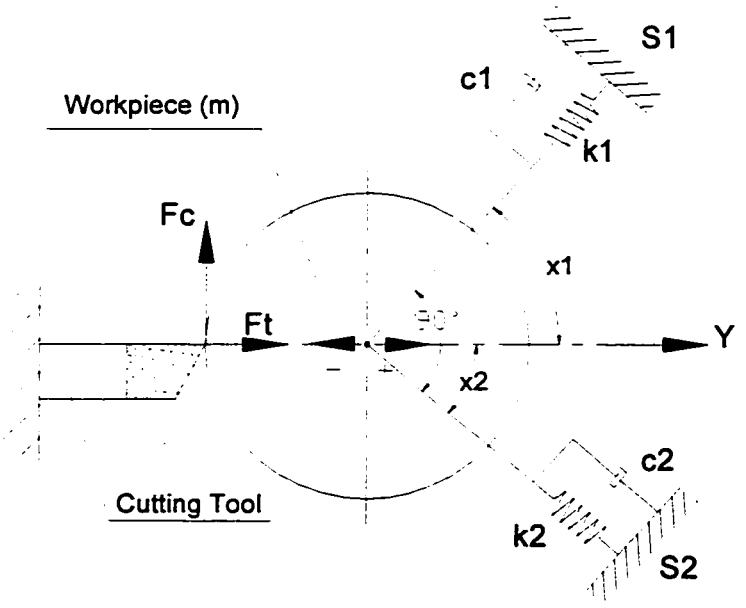

Figure 2.4 Machine structure with two degree-of-freedom

The conventional vibration analyses of mechanical systems precede by lumping masses at points and connect this mass-point to elastic and dissipative elements. After choosing reference systems and sign conventions, the differential equations of motions are derived and solved under desirable

boundary conditions. In this method, the dynamic responses to any inputs can be obtained on any form required by the particular stability theories.

Modern operational techniques of vibration analyses, such as the mobility and impedance concepts, greatly facilitate the foregoing approachs. These techniques introduce the idea of the transfer functions, and the associated frequency responses, with the resulting data presented in precisely the form required for stability analyses. However, these techniques no way reduce the complexity of obtaining solutions for the equations of motions for the systems. Each degree of freedom adds to the analytical complexity of the vibration analyses, and even with large digital computers, their capacities are taxed and the costs become prohibitive when studying complex structures.

However, some continuous structures with certain symmetrical properties can be analyzed accurately, using a digital computer. These programs obtain undamped natural frequencies and corresponding mode shapes. Highly accurate results often can be obtained with these programs owing to the methods, which allow nearly unlimited degrees of freedom to be input to the computer programs. Computer costs are kept relatively low because no attempt is made at obtaining all natural frequencies. Instead, only those frequencies in a specified range of interest, say 0-1500 cps (i.e., cycle per second), are sought out by the computer programs.

As mentioned earlier, natural frequencies and mode shapes are not sufficient for stability analyses for chatter. Knowing these values for a particular structure, it is possible to approximate accurately those transfer functions of interest in the frequency ranges of computed critical frequencies. This is done under the assumptions that internal structural damping is small which experience indicates to

be true. Thus, if large external damping mechanism can be treated as boundary conditions, the foregoing approximate techniques seem appealing.

The cutting forces displace the workpiece and the structure of the machine. Therefore, the dynamic compliance characteristic of the structure is of interest from the viewpoint of chatter. Machine structures are continuous systems, and are described by partial differential equations. These are formidable equations with complex boundary conditions and constraints. In most cases, the dynamic systems may be approximated adequately using lumped-parameter analyses.

Since it is not presently possible to compute all the quantities required to define modes of vibrations, the dynamic compliance of a structure must be obtained experimentally for each possible machining operation. The relative displacement y(t) is measured normal to the instantaneous cut surface because the chatter, namely Type A, in this direction affects the uncut chip thickness very much.

Case 1: the structure of turning with 2-dimensional forces in Fig. 2.5

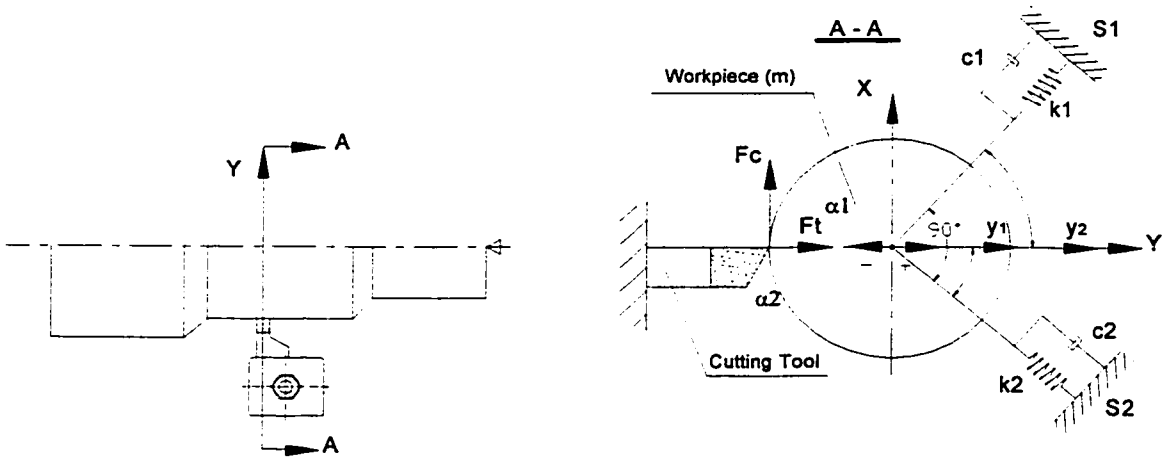

Figure 2. 5 The schematic of turning operation with two-dimensional forces

1. Mode in direction S1 in Fig. 2.5, the dynamic equation of the system in this mode is:

$$\frac{m}{\cos\alpha_1}\frac{d^2y_1(t)}{dt^2}+\frac{c_1}{\cos\alpha_1}\frac{d\ y_1(t)}{dt}+\frac{k_1}{\cos\alpha_1}y_1(t)=F_1(t) \tag{2.1}$$

After Laplace transformation, the dynamic compliance:

$$\frac{y_1(s)}{F_1(s)}=\frac{1}{\frac{m}{\cos\alpha_1}s^2+\frac{c_1}{\cos\alpha_1}s+\frac{k_1}{\cos\alpha_1}} \tag{2.2}$$

where $F_1(t)$ is the resulting cutting force between the cutting tool and workpiece in mode S1, $F_1(t)=\cos\alpha_1 F_t(t)+\sin\alpha_1 F_c(t)$, $F_t(t)$ is main cutting force, $F_c(t)$ is thrust force, α_1 is the angle between the mode S1 and the direction Y; y(t) is defined the relative displacement between the cutting tool and workpiece along the direction Y; m denotes to equivalent mass of the metal cutting system; k_1 is represented as the spring factor in mode S1; c_1 is represented as the damping ratio in mode S1.

2. Mode in direction S2 in Fig. 2.5, the dynamic equation of the system in this mode is:

$$\frac{m}{\cos\alpha_2}\frac{d^2y_2(t)}{dt^2}+\frac{c_2}{\cos\alpha_2}\frac{d\ y_2(t)}{dt}+\frac{k_2}{\cos\alpha_2}y_2(t)=F_2(t) \tag{2.3}$$

Which may be Laplace transformed to give the following dynamic compliance:

$$\frac{y_2(s)}{F_2(s)}=\frac{1}{\frac{m}{\cos\alpha_2}s^2+\frac{c_2}{\cos\alpha_2}s+\frac{k_2}{\cos\alpha_2}} \tag{2.4}$$

where $F_2(t)$ is the resulting cutting force between the cutting tool and workpiece in mode S2, $F_2(t)=\cos\alpha_2 F_t(t)-\sin\alpha_2 F_c(t)$, $F_t(t)$ is main cutting force, $F_c(t)$ is thrust force, α_2 is the angle between the mode S2 and the direction Y; y(t) is defined the relative displacement between the cutting tool and workpiece along the direction Y; m denotes to equivalent mass of the metal cutting system; k_2 is represented as the spring factor in mode S1; c_2 is represented as the damping ratio in mode S2.

3. The dynamic equation of complete vibratory system

For the complete vibratory system in Fig. 2.5, the combination of Eq. 2.1 and Eq. 2.3 can be rewritten as matrix formula as following:

$$\begin{pmatrix} \frac{m}{\cos\alpha_1} & 0 \\ 0 & \frac{m}{\cos\alpha_2} \end{pmatrix}\begin{pmatrix} \frac{d^2y_1(t)}{dt^2} \\ \frac{d^2y_2(t)}{dt^2} \end{pmatrix}+\begin{pmatrix} \frac{c_1}{\cos\alpha_1} & 0 \\ 0 & \frac{c_2}{\cos\alpha_2} \end{pmatrix}\begin{pmatrix} \frac{dy_1(t)}{dt} \\ \frac{dy_2(t)}{dt} \end{pmatrix}+\begin{pmatrix} \frac{k_1}{\cos\alpha_1} & 0 \\ 0 & \frac{k_2}{\cos\alpha_2} \end{pmatrix}\begin{pmatrix} y_1(t) \\ y_2(t) \end{pmatrix}$$
$$=\begin{pmatrix} 1 & 0 \\ 0 & 1 \end{pmatrix}\begin{pmatrix} F_1(t) \\ F_2(t) \end{pmatrix}=\begin{pmatrix} \cos\alpha_1 & \sin\alpha_1 \\ \cos\alpha_2 & -\sin\alpha_2 \end{pmatrix}\begin{pmatrix} F_t(t) \\ F_c(t) \end{pmatrix} \qquad (2.5)$$

In terms of the Eq. 1.7, the dynamic compliance of a lumped-parameter model with two degree-of-freedom can be shown:

$$y(s)=y_1(s)+y_2(s)=\frac{F_1(s)}{\frac{m}{\cos\alpha_1}s^2+\frac{c_1}{\cos\alpha_1}s+\frac{k_1}{\cos\alpha_1}}+\frac{F_2(s)}{\frac{m}{\cos\alpha_2}s^2+\frac{c_2}{\cos\alpha_2}s+\frac{k_2}{\cos\alpha_2}} \qquad (2.6)$$

where $F_1(s)=\cos\alpha_1 F_t(s)+\sin\alpha_1 F_c(s)$, $F_2(s)=\cos\alpha_2 F_t(s)-\sin\alpha_2 F_c(s)$; the other parameters are defined above.

Case 2: the structure of turning with 3-dimensionai forces in Fig. 2.6

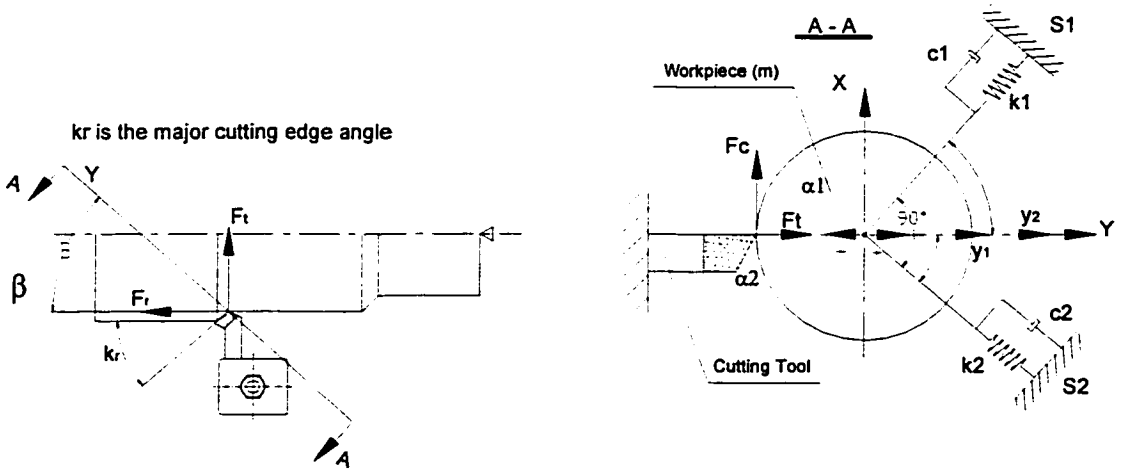

Figure 2. 6 The schematic of turning with three-dimensional forces

1. Mode in direction S1 in Fig. 2.6, the dynamic equation of the system in this mode is

$$\frac{m}{\cos\alpha_1}\frac{d^2y_1(t)}{dt^2}+\frac{c_1}{\cos\alpha_1}\frac{d\ y_1(t)}{dt}+\frac{k_1}{\cos\alpha_1}y_1(t)=F_1(t) \tag{2.7}$$

After Laplace transformation, the dynamic compliance:

$$\frac{y_1(s)}{F_1(s)}=\frac{1}{\frac{m}{\cos\alpha_1}s^2+\frac{c_1}{\cos\alpha_1}s+\frac{k_1}{\cos\alpha_1}} \tag{2.8}$$

where $F_1(t)$ is the resulting cutting force between the cutting tool and workpiece in mode S1, $F_1(t)=\cos\alpha_1\sin\beta\cdot F_t(t)+\sin\alpha_1F_c(t)+\cos\alpha_1\cos\beta\cdot F_f(t)$, $F_f(t)$ is defined as the feed force between the cutting tool and workpiece, the other parameters are defined in case 1; the definition of β is shown in Fig. 2.6.

2. Mode in direction S1 in Fig. 2.5, the dynamic equation of the system in this mode is

$$\frac{m}{\cos\alpha_2}\frac{d^2y_2(t)}{dt^2}+\frac{c_2}{\cos\alpha_2}\frac{d\ y_2(t)}{dt}+\frac{k_2}{\cos\alpha_2}y_2(t)=F_2(t) \tag{2.9}$$

Which may be Laplace transformed to give the following dynamic compliance:

$$\frac{y_2(s)}{F_2(s)}=\frac{1}{\frac{m}{\cos\alpha_2}s^2+\frac{c_2}{\cos\alpha_2}s+\frac{k_2}{\cos\alpha_2}} \tag{2.10}$$

where $F_2(t)$ is the resulting cutting force between the cutting tool and workpiece in mode S2, $F_2(t)=\cos\alpha_2\sin\beta\cdot F_t(t)-\sin\alpha_2F_c(t)+\cos\alpha_2\cos\beta\cdot F_f(t)$, $F_f(t)$ is defined as the feed force between the cutting tool and workpiece, the other parameters are defined in case 1; the definition of β is shown in Fig. 2.6.

3. The dynamic equation of complete vibratory system

For the complete vibratory system, the combination of Eq. 2.7 and Eq. 2.9 can be rewritten as:

$$\begin{pmatrix} \frac{m}{\cos\alpha_1} & 0 \\ 0 & \frac{m}{\cos\alpha_2} \end{pmatrix}\begin{pmatrix} \frac{d^2y_1(t)}{dt^2} \\ \frac{d^2y_2(t)}{dt^2} \end{pmatrix}+\begin{pmatrix} \frac{c_1}{\cos\alpha_1} & 0 \\ 0 & \frac{c_2}{\cos\alpha_2} \end{pmatrix}\begin{pmatrix} \frac{dy_1(t)}{dt} \\ \frac{dy_2(t)}{dt} \end{pmatrix}+\begin{pmatrix} \frac{k_1}{\cos\alpha_1} & 0 \\ 0 & \frac{k_1}{\cos\alpha_1} \end{pmatrix}\begin{pmatrix} y_1(t) \\ y_2(t) \end{pmatrix}$$

$$=\begin{pmatrix} 1 & 0 \\ 0 & 1 \end{pmatrix}\begin{pmatrix} F_1(t) \\ F_2(t) \end{pmatrix}=\begin{pmatrix} \cos\alpha_1\sin\beta & \sin\alpha_1 & \cos\alpha_1\cos\beta \\ \cos\alpha_2\sin\beta & -\sin\alpha_2 & \cos\alpha_2\cos\beta \end{pmatrix}\begin{pmatrix} F_t(t) \\ F_c(t) \\ F_f(t) \end{pmatrix} \qquad (2.11)$$

In terms of the Eq. 1.7, the dynamic compliance of a lumped-parameter model with two degree-of-freedom can be shown:

$$y(s)=y_1(s)+y_2(s)=\frac{F_1(s)}{\frac{m}{\cos\alpha_1}s^2+\frac{c_1}{\cos\alpha_1}s+\frac{k_1}{\cos\alpha_1}}+\frac{F_2(s)}{\frac{m}{\cos\alpha_2}s^2+\frac{c_2}{\cos\alpha_2}s+\frac{k_2}{\cos\alpha_2}} \qquad (2.12)$$

where $F_1(t)=\cos\alpha_1\sin\beta\cdot F_t(t)+\sin\alpha_1 F_c(t)+\cos\alpha_1\cos\beta\cdot F_f(t)$, and $F_2(t)=\cos\alpha_2\sin\beta\cdot F_t(t)-\sin\alpha_2 F_c(t)+\cos\alpha_2\cos\beta\cdot F_f(t)$; the other parameters are defined in preceding sections.

It will be noted again that the relative displacement y(t) is measured normal to the instantaneous cut surface because variations (chatter) in this direction affect the uncut chip thickness very much.

In the dynamic equations of machine structure, each of forces, including main cutting force, thrust force, and feeding force, has been applied to the different dynamic compliance, instead of the resultant forces. Therefore the orientation of the resultant cutting forces as space vector will not affect the applications of the dynamic equations, i.e., the applications of the dynamic equations above will not be limited by the constraint of the orientations of the resultant forces during metal cutting processes, which is the assumption (b) in the chapter 1.

2.3 Modeling of Cutting Process

2.3.1 Hysteresis – A Cause of Chatter Occurrence

A large number of investigations on chatter on turning processes have been performed to study the mechanisms of chatter vibrations in order to suppress chatter. One of the proposed mechanisms is the active hysteretic behavior appearing in the dynamic cutting processes.

Because chatter is caused in the horizontal vibration of workpiece, we treat the problem based upon that direction only. In Fig. 2.7 referred to [9], let point C denote the center of the workpiece before cutting. If a cut is operated on the workpiece, the center C displaces to the point O and this displacement is denoted as a. We can define point O as the point of origin and indicate displacement of workpiece by $y(t)$. When the motion is in the direction away from the cutting tool edge, $y(t)$ is considered positive.

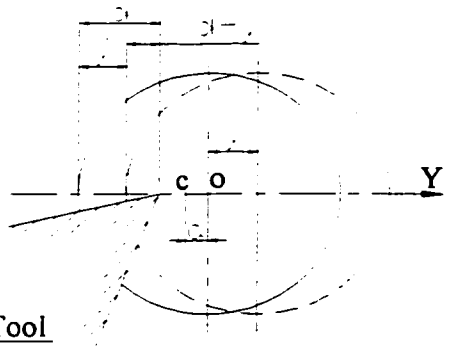

Figure 2.7 Workpiece and cutting edge

As stated earlier, the nonlinear relationship between the uncut chip thickness and forces in cutting dynamic conditions is obtained from the experimental results of Albercht [19]. In his experiments, the end of a tubular workpiece was machined orthogonal with a cutting tool mounted on a special two-component tool dynamometer and activated in the direction of feed by a hydraulic actuator. The sinusoidal motion imparted to the tool causes cyclic change in the uncut chip thickness during cutting, resulting in the dynamic response of the cutting forces, including the main cutting force,

thrust force and the resultant force. Albercht has presented oscilloscope traces of the oscillations in tool displacement, main cutting force, and thrust force. We amplified the oscilloscope traces of Albercht and used the values of amplitudes for their scaling. The waveforms for one cycle are shown in Fig. 2.8.

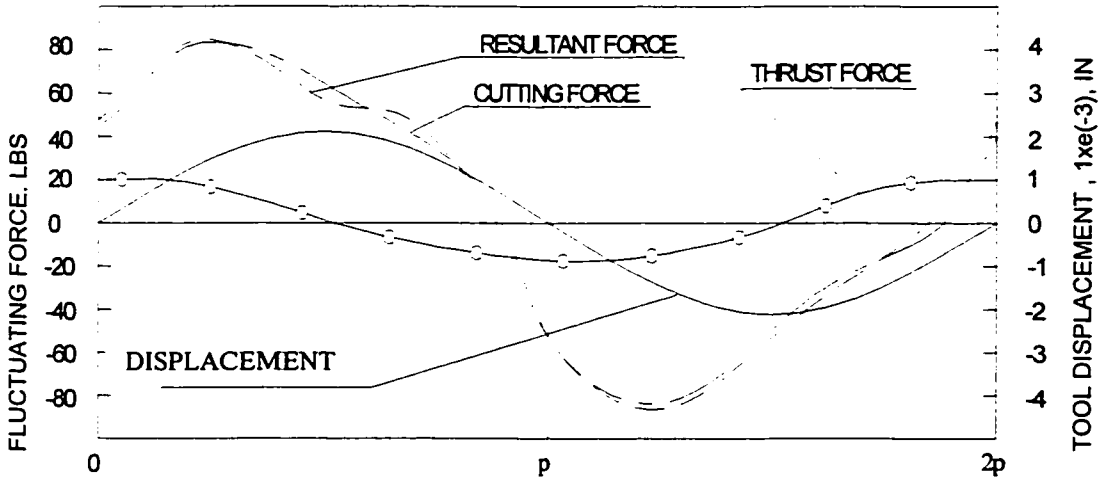

Figure 2.8 Waveform of the displacement and cutting forces fluctuating (Computered from data of [27])

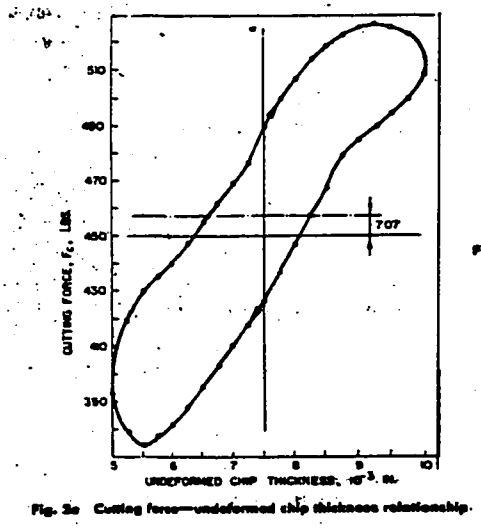

Figure 2.9 (a) Cutting force-uncut chip thickness relationship

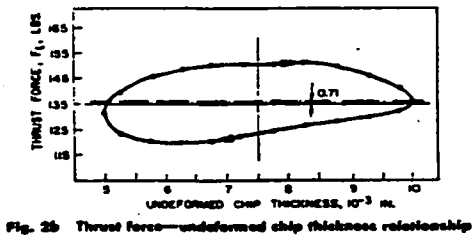

Figure 2.9 (b) Thrust force-uncut chip thickness

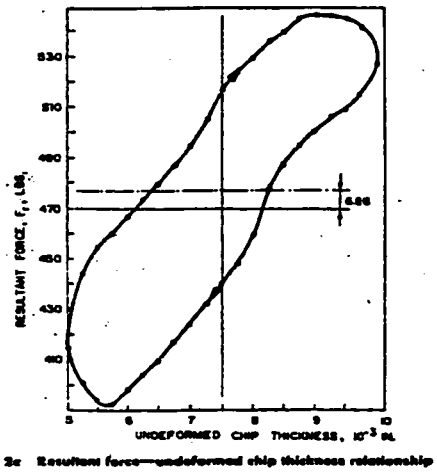

Figure 2.9 (c) Resultant force-uncut chip thickness

It may be observed from Fig. 2.8 that the tool motion closely resembles a sine wave but the waveform of the main cutting and thrust forces have skewed shapes and they both lead the input wave (tool motion). The frequency in Fig. 2.8 is 400 cps and Albercht [19] has presented a frequency response chart that shows that the effect of frequency upon the amplitudes is negligible. Now, it is possible to obtain the relationships between the dynamically varying forces and uncut chip thickness by plotting the amplitude of the forces versus that of the chip thickness at the same instant in Fig. 2.8. These relationships are shown in Fig. 2.9(a), (b) and (c) [27]. It can be seen from these figures that the dynamic cutting processes exhibit active hysteresis that always give rise to a leading phase shift.

In Marui and Ema's experiment [33], for the mechanism of chatter vibration, with respect to different metal cutting conditions for one cycle of the chatter vibration, the relationships between the cutting forces F_t (t) and the horizontal displacement y(t) are shown in Fig. 2.10, 2.11, 2.12 and 2.13 [33]. Based on the research to the above experimental results, hysteretic characteristic is clearly noticed for the cutting forces in both conditions, so the cutting forces acting against the turning tool when the tool deflects downward is lager than when it deflects upward. Since this cutting forces act downward against the turning tool, vibratory energy can be supplied to the vibratory system by this cutting forces during the downward deflection phase. On the other hand, the turning tool dissipates energy in the next half-cycle phase in which the turning tool vibrates upward, contrary to the cutting forces. Accordingly, the energy is supplied in the vibratory system during one vibration cycle, and the chatter vibration thus continues. This supplied energy is, of course, consumed by the positive damping of the system.

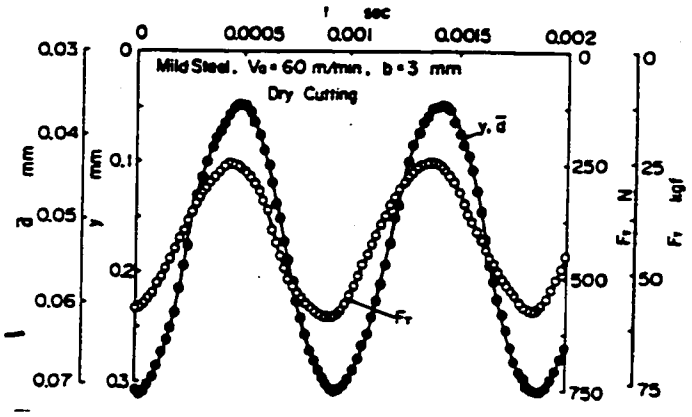

Figure 2.10 Vibratory deflection of turning tool and cutting force fluctuation (M.S)

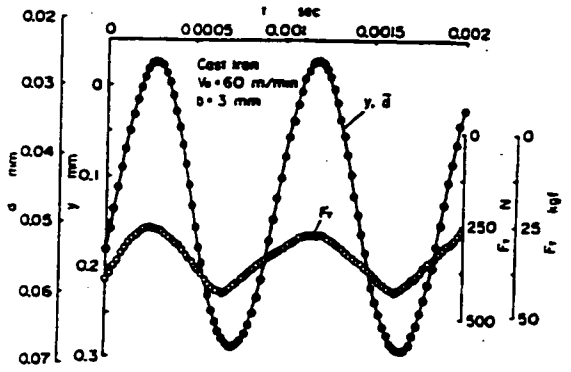

Figure 2.11 Vibratory deflection of turning tool and cutting force fluctuation (C.I)

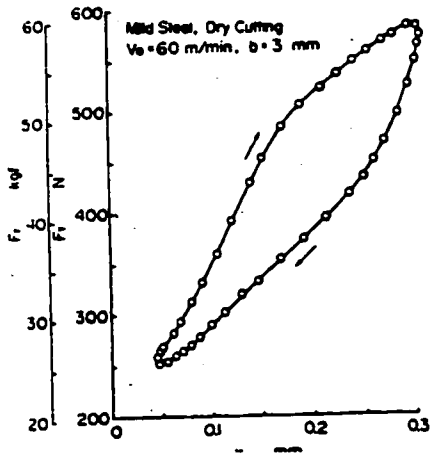

Figure 2.12 Relationship between cutting force and vibratory deflection (M.S)

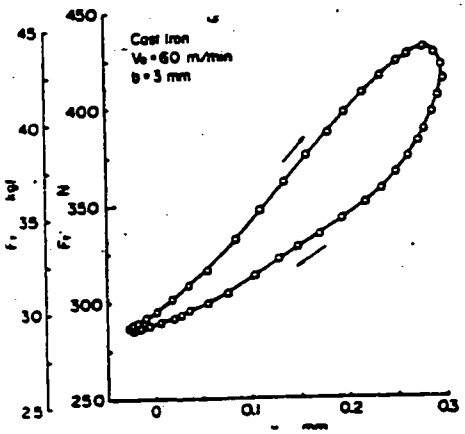

Figure 2.13 Relationship between cutting force and vibratory deflection (C.I)

Subsequently, in order to determine the reason for these hysteretic characteristics of the cutting forces, the chatter mark is investigated. Fig. 2.14 from [33] shows an example of the chatter marks (included by black dots) measured by a surface profile tracer. The solid line in Fig. 2.14 represents the configuration of chatter marks plotted by combining the revolution of the workpiece, where the cutting distance is taken as $e = V_0 t - a\sin(2\pi ft)$, ($V_0$ is nominal cutting speed, e is cutting distance). Both the measured and calculated results of the chatter marks agree with each other. The chatter marks also become jagged as shown in Fig. 2.14, in the case of the cutoff type, which is

used in this experiment. Accordingly, it is clear in Fig. 2.14 that the flank surface will come into contact with the workpiece material, that extremely violent interference will thereby result, because the chatter marks show a steep slope when the uncut chip thickness increase with downward deflection of the turning tool.

2.3.2 Mathematical Hysteresis Models of Dynamic Cutting Process

For the designs of the control laws in metal cutting systems, some simplifications are required for the hysteresis models of the cutting forces and cutting tool motions.

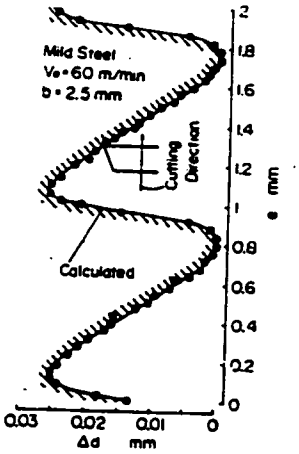

Figure 2.14 Chatter mark configuration

In this thesis, we will treat the hysteretic characteristics of the relationships between the cutting forces and uncut chip thickness as backlash hysteresis due to their resemblance in profile in the metal cutting systems, in Fig. 2.15. The reasons will be demonstrated in the following figures.

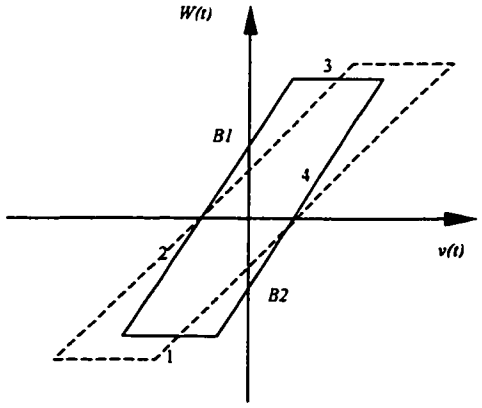

Figure 2.15 Backlash of hysteresis model

Traditionally, a backlash hysteresis nonlinearity can be described as following [34]:

$$w(t) = P(v(t)) = P(k,B) = \begin{cases} Av(t) + B_1 & if \quad \dot{v}(t) > 0 \\ Av(t) + B_2 & if \quad \dot{v}(t) < 0 \\ w(t_-) & if \quad \dot{v}(t) = 0 \end{cases} \tag{2.13}$$

where $P(.)$ is hysteretic functions; $A > 0$ is the slope of the lines in Fig. 2.15, $B_1 = -B_2 = B > 0$ is backlash distance.

According to the preceding analyses, due to the different descriptions of hysteresis models for the main cutting force and thrust force, the following functions will be used to describe the hysteretic characteristics of the main cutting force $F_c(t)$, thrust force $F_t(t)$ and feed force $F_f(t)$ in terms of the uncut chip thickness $v(t)$ in metal cutting processes,

$$F_c(t) = P_c(v(t)) = P(k_c, B_c) = \begin{cases} A_c v(t) + B_c & if \quad \dot{v}(t) > 0 \\ A_c v(t) - B_c & if \quad \dot{v}(t) < 0 \\ F_c(t_-) & if \quad \dot{v}(t) = 0 \end{cases} \tag{2.14}$$

$$F_t(t) = P_t(v(t)) = P(k_t, B_t) = \begin{cases} A_t v(t) + B_t & if \quad \dot{v}(t) > 0 \\ A_t v(t) - B_t & if \quad \dot{v}(t) < 0 \\ F_t(t_-) & if \quad \dot{v}(t) = 0 \end{cases} \tag{2.15}$$

$$F_f(t) = P_f(v(t)) = P(k_f, B_f) = \begin{cases} A_f v(t) + B_f & if \quad \dot{v}(t) > 0 \\ A_f v(t) - B_f & if \quad \dot{v}(t) < 0 \\ F_f(t_-) & if \quad \dot{v}(t) = 0 \end{cases} \tag{2.16}$$

where A_t, A_c, A_f are the slopes of the lines, B_t, B_c, B_f are backlash distance responding to main cutting, thrust and feed forces respectively, these parameters can be assumed positive.

A widely held opinion is that the cutting forces always decrease with increasing cutting speed. But if these velocities are low, an increase of the cutting forces with the velocity can be observed in many cases. The slopes of the cutting forces versus speed curves can vary from positive to negative and need not be the same for the forces F_c and F_t.

The cutting forces always increase with the depth of cut. The slopes of the cutting forces versus depth-of-cut curves depend upon the workpiece material and the depth of cut itself. The slopes increase with increasing depth of cut. The slopes of F_c and F_t may also differ from each other. Further, the slopes of these curves include the effect of cold-working of the work surface, which has an appreciable influence on the excitation of vibrations.

2.4 Modeling of Uncut Chip Thickness

In machining work as shown in Fig. 2.16 and 2.17, the horizontal rigidity of the tool is usually much greater than that of the workpiece, so Type *A* of chatter is considered only. The vibratory system of the machine tool shown in Fig. 2.17 is entirely similar to that of the workpiece shown in Fig. 2.16 as to dynamic effects. The results obtained on the horizontal vibration of the workpiece are also directly applicable to the vertical vibration of the cutting tool where the vibration of the workpiece may be considered negligible.

A main cutting force or thrust force in Fig. 2.17 removing a wave generated by a previous cut is affected by the waving surface $y(t-T+H)$ which is antecedent to the present vibration $y(t)$ by a time value *T-H*, and precedes the cutting edge nearly by a certain distance *e* in Fig. 2.17, where *T* is time interval of one revolution of workpiece and *H* is time lead associated with the chip thickness oscillations at the free end of the shear plane relative to the chip thickness oscillations at the tool tip shown in Fig. 2.17.

While the cutting speed is defined as *v*, the depth of cut is denotes as *d*, the value of the shearing angle during wave removing is presented as *A*, then the geometrical relation in Fig. 2.17 yields the time lead *H*:

$$H = d\cos(A/v) \tag{2.17}$$

For orthogonal cutting process, the chip thickness $u(t)$ in the case of the primary effect can be described as

$$u(t) = y(t) - y(t-T) \tag{2.18}$$

where $y(t)$ is the displacement between the cutting tool and workpiece along Y-axis and T is the time interval during one revolution of workpiece.

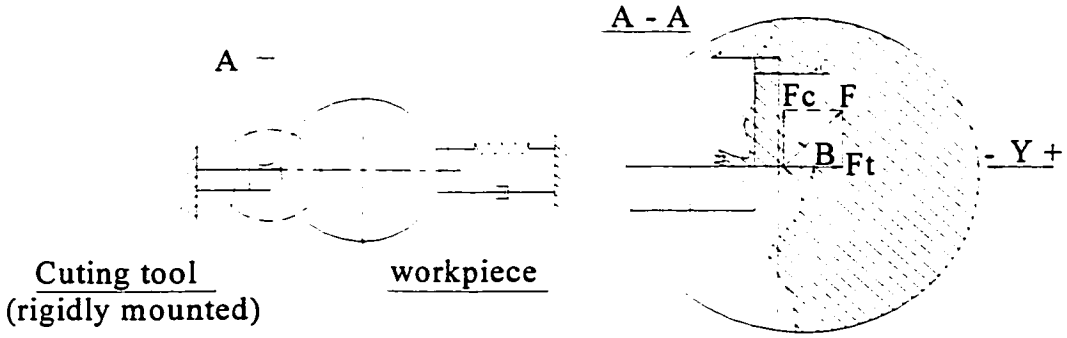

Figure 2.16 The schematic of the cutting tool in a turning

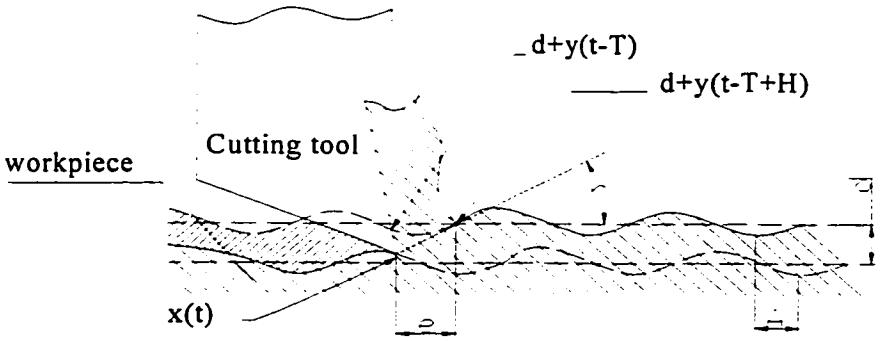

Figure 2.17 Vibratory system of the workpiece

In order to describe the chip thickness variation due to the different effect, Merrit [3] provided an equation for uncut chip thickness, defining the primary and regenerative chatter by the parameter of the overlap factor μ,

$$u(t) = y(t) - \mu \cdot y(t-T) \tag{2.19}$$

where $u(t)$ is the instantaneous chip thickness variation at time t and y(t) is the relative displacement between cutting tool and workpiece normal to machining surface, and μ is the overlap factor and $0 \le \mu \le 1$.

As mentioning early, considering the geometrical relations of shear angle, it was proposed by Ota and Kono [9] that the chip thickness variation will be

$$u(t) = y(t+H) - \mu \cdot y(t-T+H) \tag{2.20}$$

where the definition of H in Eq. 2.17.

In order to derive the feedback loop representing chatter, the cutting processes will be illustrated with a single-point tool performing orthogonal cutting on a lathe shown in Fig. 2.16. The cutting tool is mounted rigidly and the feed rate is adjusted to obtain an average or steady state depth of cut $u_0(t)$. In this steady state condition, the structure maintains a certain deflection caused by the steady state cutting force. The equations will be written about this point of equilibrium.

In Fig. 2.16, the instantaneous depth of cut $u(t)$ is decreased as the workpiece moves away from the cutting tool, i.e., y(t) increases. Further if the workpiece moves away form the cutting tool, a lump is left on the workpiece. This lump increases the uncut chip thickness in one revolution of the workpiece or time delay T.

Hence the instantaneous uncut chip thickness can be written

$$u(t) = u_0(t) - y(t) + \mu \cdot y(t-T) \tag{2.21}$$

where $u(t)$ is the instantaneous uncut chip thickness, $u_0(t)$ is the nominal uncut chip thickness, $y(t)$ the workpiece or cutting tool displacement, T is delay time, (the value of T is the inverse of the lathe speed v in cps), and μ is the overlap factor in this system.

Laplace transforming Eq. 2.21, yield

$$u(s) = u_0(s) - y(s) + \mu \cdot e^{-Ts} \cdot y(s) \tag{2.22}$$

The overlap factor μ accounts for the overlapping of successive cuts; i.e., it defines the portion of the previous cut that is overlapped by the present cut. In a turning operation, such as threading, the previously machined surface does not affect the present uncut chip thickness, then $\mu = 0$. However for most machining operations, such as orthogonal cutting, $\mu = 1$.

The overlap factor μ also may be used to account for the geometrical effects of rounding at the tool cutting edge and of tool clearance angle. Both of these effects tend to smear the machined surface and thereby reduce the amplitude of periodic variation in the machined surface. It is difficult to make a precise definition for the overlap factor μ; however, it is certainly bounded between zero and unity $0 \le \mu \le 1$. An overlap factor of unity is the most critical value from the viewpoint of chatter.

2.5 The Closed Loop of Metal Cutting System

Based on some theoretical and experimental analyses, the mathematical models representing the blocks in Fig. 2.2 are derived into the Eqs. 2.5, 2.11, 2.14, 2.15, 2.16 and 2.21 for two-dimensional and three-dimensional force models respectively. These equations will be placed into Fig. 2.2. Thus, Two block diagrams of metal cutting process for both two-dimensional and three-dimensional force models are plotted as shown in Figs. 2.18 and 2.19.

In Figs. 2.18 and 2.19, the blocks of G1(s) and G2(s) will be replaced by using Eqs. 2.2 and 2.4; three hysteretic relationships between the cutting forces, namly, $F_c(t)$, $F_t(t)$, $F_f(t)$ and uncut chip thickness will be defined by using Eqs. 2.14, 2.15 and 2.16 respectively; the block of the regenerative feedback (time delay) $g(s)$ is denoted as

$$g(s) = \mu \cdot e^{-Ts} \tag{2.23}$$

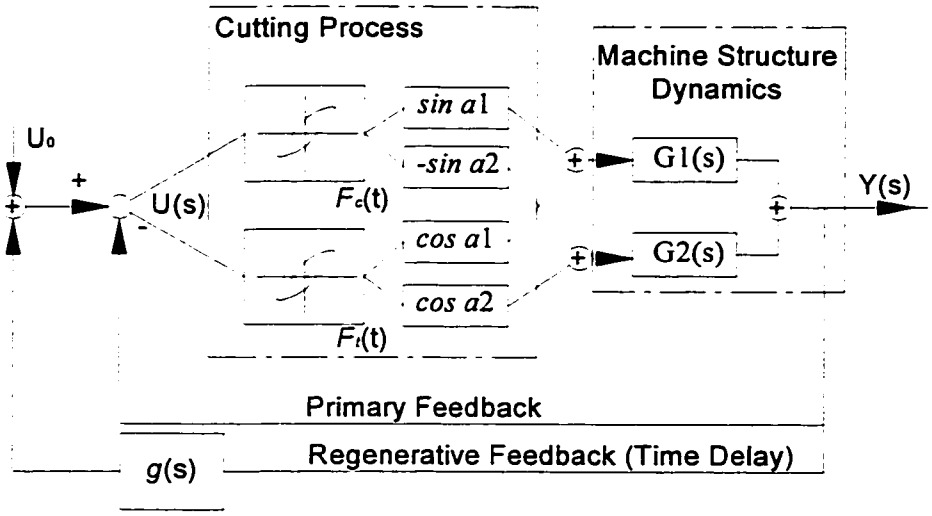

Figure 2. 18 Block diagram of chatter loop with two-dimensional forces

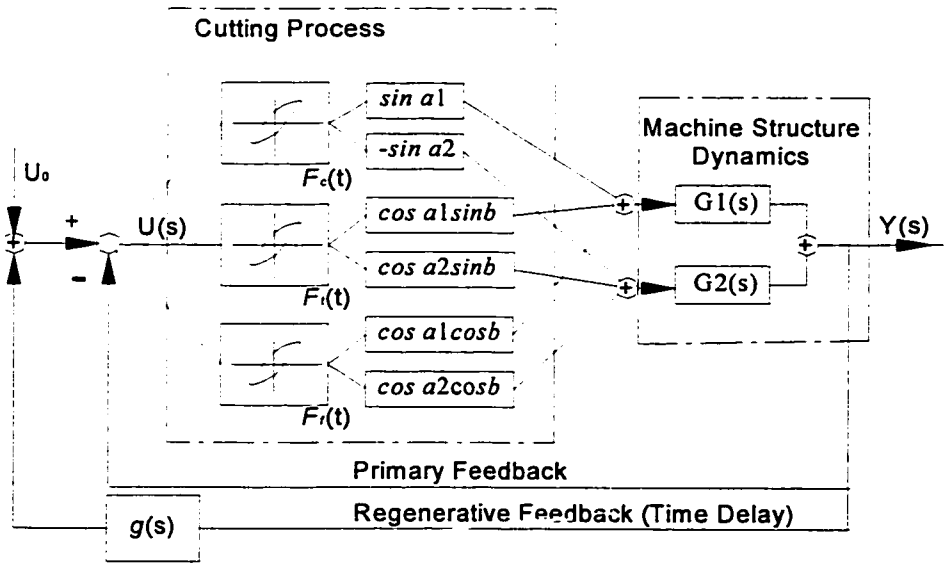

Figure 2. 19 Block diagram of chatter loop with three-dimensional forces

The closed loop dynamic metal cutting systems, including cutting process, machine structure and feedback, have already been built as shown in Figs. 2.18 and 2.19. In the following chapter, the several mathematical models corresponding to different blocks in Figs. 2.18 and 2.19 will be used for the designs of the control laws.

2.6 Simulation Results

In order to determine the actual effects of active hysteretic characteristics in the situations of primary chatter and regenerative chatter vibrations in metal cutting processes, the simulations are introduced as follows.

A metal cutting system will be described as

$$\begin{cases} m\ddot{y}_1(t) + c_1\dot{y}_1(t) + k_1 y_1(t) = F_1(t) \\ m\ddot{y}_2(t) + c_1\dot{y}_2(t) + k_1 y_2(t) = F_2(t) \end{cases} \tag{2.24}$$

where the values of the equivalent mass, damping ratios and spring coefficients for the metal cutting system in each equation are listed in the appendix of Table A.

2.6.1 Simulations of the Dynamic System Responses without Forces

With respect to Eq. 2.24 and the initial conditions of $y_0(t) = 0.01\ (mm)$ and $F_1(t) = F_2(t) = 0$, the response of the system in Eq. 2.24 under this condition is illustrated in Fig. 2.20

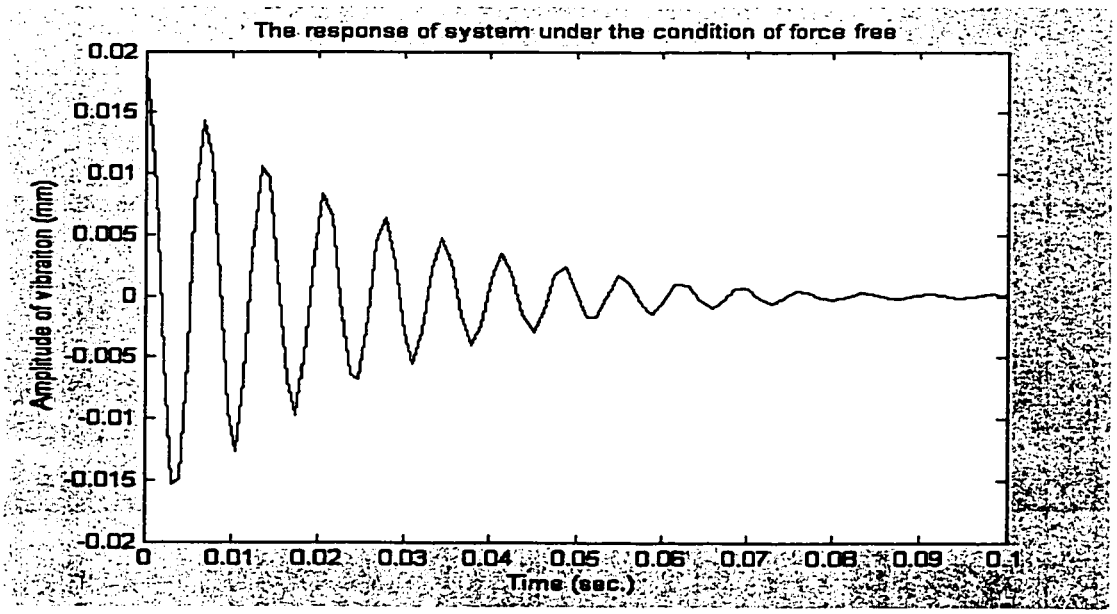

Figure 2.20 The dynamic response of metal cutting system without 2-dimensional or 3-dimensional forces

By Fig. 2.20, It is clear that the cutting system responses is decreasing exponentially onto equilibrium state of the system with two degree-of-freedom due to damping ratios c_1, c_2, while external forces are zero.

2.6.2 Simulations of the Dynamic System Responses with Hysteresis Effect

The active hysteretic characteristics between the cutting forces and uncut chip thickness in the metal cutting process should exist commonly. In order to demonstrate the effect of the hysteretic characteristics, the primary and regenerative chatter will be simulated. The coefficients of hysteresis models and other parameters involved in the simulations are listed in Table A and B.

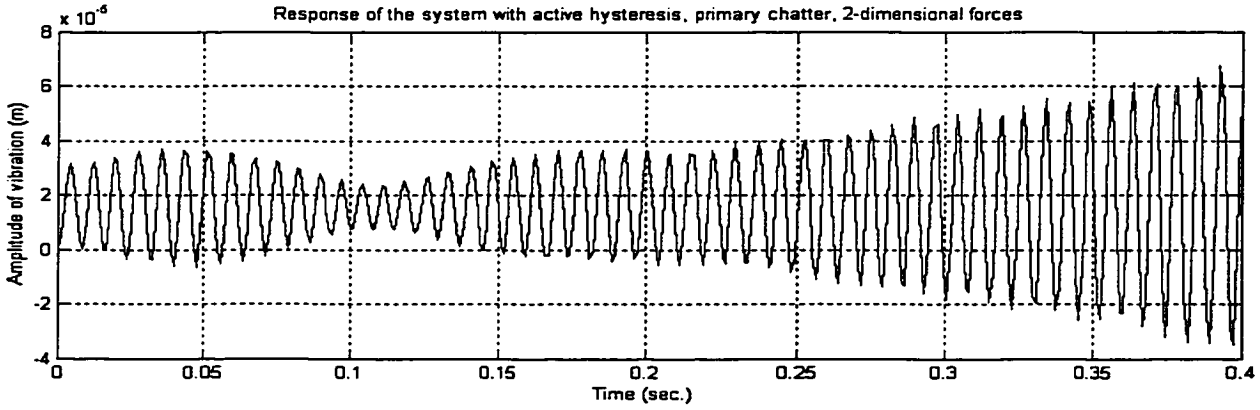

Figure 2.21 Response of the system with active hysteresis, primary chatter, 2-dimensional forces

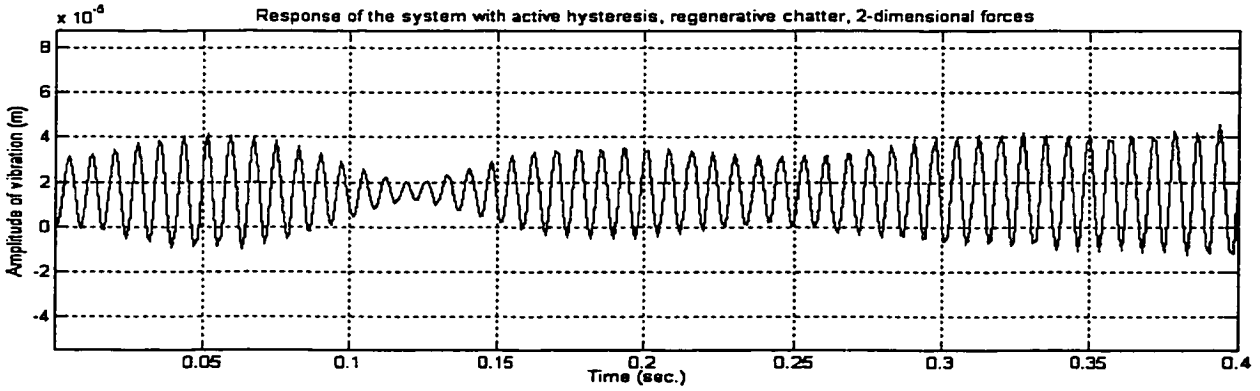

Figure 2.22 Response of the system with active hysteresis, regenerative chatter, 2-dimensional forces

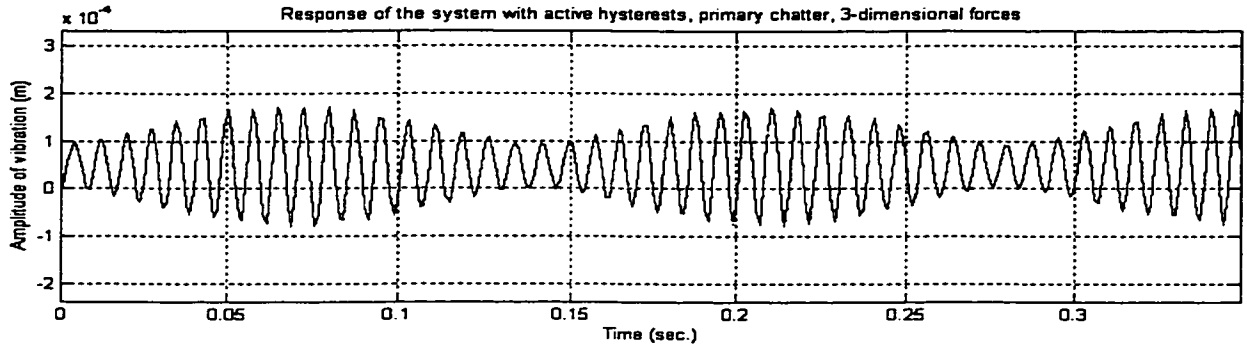

Figure 2.23 Response of the system with active hysteresis, primary chatter, 3-dimensional forces

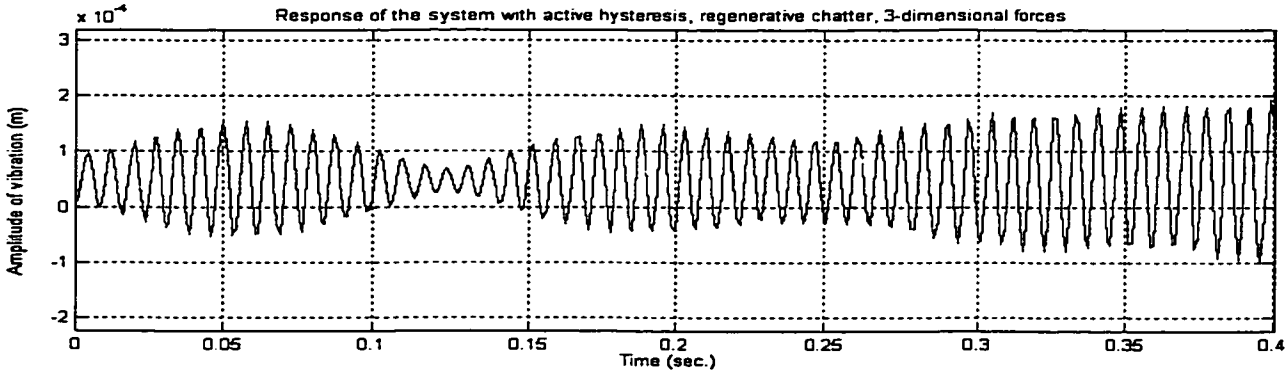

Figure 2.24 Response of the system with active hysteresis, regenerative chatter, 3-dimensional forces

In Fig. 2.21, the dynamic response of the system that is described as two degree-of-freedom and two-dimensional force model is plotted, meanwhile, the chatter is considered as primary type, i.e., $\mu = 0$ in Eq. 2.21.

In Fig. 2.22, the dynamic response of the system that is described as two degree-of-freedom and two-dimensional force model is plotted, meanwhile, the chatter is considered as regenerative type, i.e., $\mu = 0.75$ in Eq. 2.21.

In Fig. 2.23, the dynamic response of the system that is described as two degree-of-freedom and three-dimensional force model is plotted, meanwhile, the chatter is considered as primary type, i.e., $\mu = 0$ in Eq. 2.21.

In Fig. 2.24, the dynamic response of the system that is described as two degree-of-freedom and three-dimensional force models is plotted, meanwhile, the chatter is considered as regenerative type, i.e., $\mu = 0.75$ in Eq. 2.21.

In Fig. 2.21 through 2.24, under both conditions of two and three-dimensional forces, either primary or regenerative chatter, it can seen that the vibrations of the metal cutting systems will be growing as time is going on. Theoretically, chatter can grow as metal cutting process stay in the oscillation state, it is indicated also that chatter can not grow infinitely during cutting process due to the regenerative or even multi-regenerative effects [35].

2.7 Summary

With respect to the metal cutting process in turning, the machine structure, the dynamic cutting process with the hysteretic characteristic are presented in mathematic approaches. Furthermore, based on theoretical analyses and experimental results, the closed-loop diagram of dynamic system is plotted. An active hysteresis in metal cutting process is proved to be the main cause of chatter occurrence as it provides the energy for chatter excitation and maintenance. The simplified mathematical equations of the hysteresis models are given. The simulations of the systems indicate the behaviors of the self-exited vibrations in the metal cutting systems under the conditions of regenerative and primary effects, while the cutting forces acting onto the workpiece are either two-dimensional or three-dimensional models.

Chapter 3

Applications of Piezoactuators in the Suppression of Chatter

Introduction – the main characteristics and applications of piezoelectricity will be analyzed; the preceding applications of piezoactuators in the suppression of chatter in metal cutting process will be surveyed; the mathematical models of the relationships between the applied voltages and the deflections of piezactuators will be presented; two dynamic systems of the metal cutting with both dependent and independent piezoactuators from the tool holders will be constructed.

3.1 Surveys on Control Schemes on Chatter Suppression in Turning

In order to suppress the chatter occurrence during the metal cutting process, proper control schemes are proposed. Rasmussen [36] reviewed the progress in machine tool control during the last three decades; three types of controls are discussed as following:

a. Servo-control loops that control the individual axes of the machines

b. Interpolators that coordinate the motion of several axes

c. Adaptive control that adjusts the cutting variables in real time to maximize system performance.

Rasmussen [37] improved the workpiece surface by employing a digital repetitive servo-control with the design of a piezoelectric actuated cutting tool.

Tarng [35] developed an adaptive fuzzy control system for the turning processes with highly nonlinear and time-varying cutting characteristics.

Recht [38] obtained satisfactory chatter vibration control by implemented a fixed gain PI control and an adaptive pole assignment control technique with the feed force feedback.

Chen [39] and Yang [40] considered the system to be linear with nonlinear time-varying perturbation and employed PI controller to treat this stabilization problem.

Mahmoud and Al-Muthairi [41] presented an adaptive turning force controller that has optimal robustness under the constraint of the feed rate.

Recently, with the advent of piezoelectric devices, increasing attention is attracted to the applications of piezoactuators in the metal cutting systems. Piezoactuators have a prominent characteristic that is fast expansions with short response time. The properties of piezoactuators have made them the high-precision positioning elements in the metal cutting processes.

3.2 Main Characteristics and Applications of Piezoelectricity

In 1880, Jacques and Pierre Curie [42] discovered that pressure applied to a quartz crystal creates an electrical charge in the crystal. They called this phenomenon the piezo effect. Later they also verified that an electrical field applied to the crystal would lead to a deflection of the material. This effect is referred to as the inverse piezo effect. After the discovery, it took several decades to utilize the piezoelectric phenomenon. The first commercial applications were ultrasonic submarine

detectors developed during World War I. In the 1940s scientists discovered that barium titanate ceramics could be made piezoelectricity in an electric field.

Piezoelectricity materials can be used to convert electrical energy into mechanical energy and vice versa. As the actuators, the piezoactuators first became available around 20 years ago and have changed the world of precision positioning.

Piezoactuators (PZTs) offer several benefits and advantages over other motion techniques:

- Repeatable nanometer and sub-nanometer sized steps at high frequency can be achieved with PZTs because they derive their motion through solid state crystal effects. There are no moving parts (no "stick-slip" effect).
- PZTs can be designed to move heavy loads (several tons) or can be made to move lighter loads at frequencies of several 10 kHz.
- PZTs act as capacitive loads and require very little power in static operation, simplifying power supply needs.
- PZTs require no maintenance because they are solid state and their motion is based on molecular effects within the ferroelectric's crystals.

With high-reliability of PZTs' materials, a strain on the order of 1/1000 can be achieved. This means that a 100 mm long PZT actuators can expand by 100 micrometers when the maximum allowable field is applied.

Main applications of piezoactuators in mechanical engineering show as follows [43]:

Microelectronics

- Nano-metrology
- Wafer and mask positioning
- Critical dimensions measurement
- Microlithography
- Inspection systems
- Vibration cancellation

Precision Mechanics and Mechanical Engineering

- Vibration cancellation
- Structural deformation
- Out-of-roundness grinding, drilling, turning
- Tool adjustment
- Wear correction
- Needle valve actuation
- Micro pumps
- Linear drives
- Piezo hammers
- Knife edge control in extrusion tools

3.3 Dynamic Behavior and Mathematical Modeling of Piezoactuators

Piezoactuators can reach the nominal displacement in approximately 1/3 of the period of the resonant frequency. Rise times on the order of microseconds and accelerations of more than 10,000 g's are possible. This feature permits rapid switching applications. Injector nozzle valves, hydraulic valves, electrical relays, adaptive optics and optical switches are a few examples of fast-switching applications of piezactuators.

Resonant frequencies of industrial piezoactuators range from a few tens of kHz for actuators with total travel of a few microns to a few kHz for actuators with travel more than 100 microns. An additional load will decrease the resonant frequency as a function of the square root of the mass (quadrupling the mass will halve the resonant frequency).

Piezoactuators are not designed to be driven at resonant frequency (with full stroke and load), as the resulting high dynamic forces might endanger the structural integrity of the ceramic material.

3.3.1 Hysteretic Characteristics of Piezoactuators

In Cuttino and Fripps' experiments [2], it was proved that the relationships between the stimulated piezoelectricities' deflections and the applied voltages were the nonlinear hysteretic characteristics. Even for piezoelectric products of some commercial companies, the measured data about piezoelectric dynamic behavior also have shown that the hysteretic characteristics exist.

In most applications, piezoactuators are used to produce displacements. If used in the restraint, they can generate forces. The generations of the restraint forces are always coupled with reductions in displacements. The maximum forces (blocked force) that piezoactuators can generate depend on the stiffness and maximum displacement of piezoactuators as Eq. 3.1.

$$F_{\max} \approx K_p \Delta L_o \tag{3.1}$$

where ΔL_o is maximum value of nominal displacement without external force or restraint [m]; K_p is denoted as PZT actuator stiffness [N/m].

Maximum forces that can be generated in infinitely rigid restraints, namely, infinite spring constants. Under the condition of the maximum blocked force, the displacements of piezoactuators are zero.

In Fig. 3.1, it plots that dynamic behavior curve of the piezoactuator, which type is TS18-H5-104 in Piezo System, INC [42], low voltage piezoelectric stack. In Fig. 3.1(a), it shows the relationship between the voltage applied to piezoactuator and the deflection due to the voltage. In fig. 3.1(b), the two lines, which represents the different performance of each type of the piezoactuators, present the relationships between the deflections and forces (pushing and pulling) acting on the piezoactuators due to the inertias of the PZT masses (plus any additional masses),

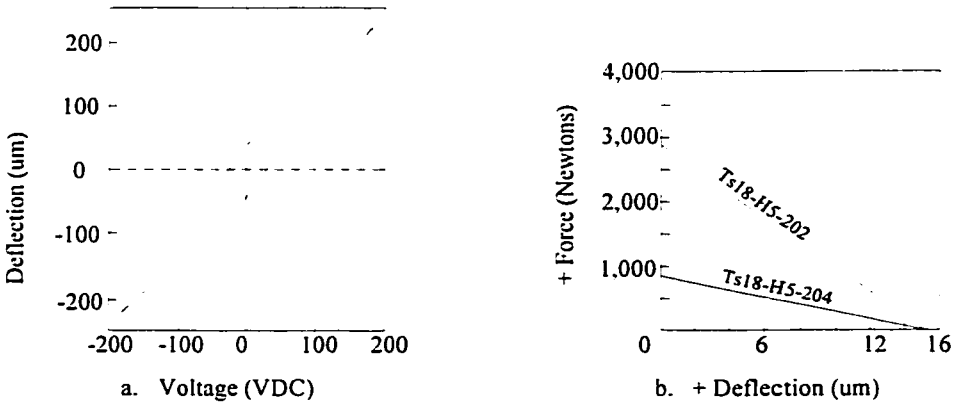

Figure 3.1 Hysteretic characteristics between the voltage and deflection of piezo

3.3.2 Mathematical Modeling of Piezoactuators

Hysteresis is known to be non-differentiable and severely limits the performance of the system by causing undesirable chatter. Moreover, the hysteresis behavior demonstrated in the actuator signals makes it impossible to achieve a high accuracy positioning. Most of the hysteresis mathematical models proposed, like a backlash, are very complicated and may not be amenable to controller design for the nonlinear systems.

For the controller design, instead of traditional backlash hysteresis nonlinear models, a continuous-time dynamic model of hysteresis to describe a class of backlash-like is defined in [34]:

$$\frac{dL(t)}{dt} = \alpha\left|\frac{dv(t)}{dt}\right| \cdot (pv(t) - L(t)) + B\frac{dv(t)}{dt} \tag{3.2}$$

where $v(t)$ denotes as the voltage applied to piezoactuators, $L(t)$ is the deflection of piezoactuators, α, p and B are constants, satisfying $c>B$.

To describe the hysteresis in the system, Difference equation about Eq. 3.2 is

$$L[i+1] = \frac{L[i] + (\alpha|v[i+1] - v[i]|p + B)v[i+1] - Bv[i]}{1 + \alpha|v[i+1] - v[i]|} \qquad (i = 1, 2, 3, \cdots\cdots) \tag{3.2a}$$

As the proof in [34], Eq. 3.2 can be solved explicitly for $v(t)$ piecewise monotone

$$L(t) = pv(t) + g(v(t)) \tag{3.3}$$

with $g(v(t)) = [L(0) - pv(0)]e^{-\alpha(v(t)-v(0))\operatorname{sgn}\dot{v}} + e^{-\alpha v \operatorname{sgn}\dot{v}}\int_{v(0)}^{v(t)}[B-p]e^{\alpha\varsigma(\operatorname{sgn}\dot{v})}d\varsigma$, and $g(v(t))$ is uniform bounded, i.e., $\|g(v(t))\| \le \rho_a$, ρ_a is constant.

With $\alpha = 0.5$, $p=3.17$ and $B=0.35$ and input $v(t) = 8.5\sin(10t)$, Fig. 3.2 shows the model (Eq. 3.2) indeed generates the backlash-like hysteretic curves. It will be mentioned that the parameter α determines the rate at which $L(t)$ switches between $-\rho_a$ and ρ_a. However, the backlash distance is determined by ρ_a and the parameter must satisfy $c>B$, therefore, the parameter α cannot be chosen freely.

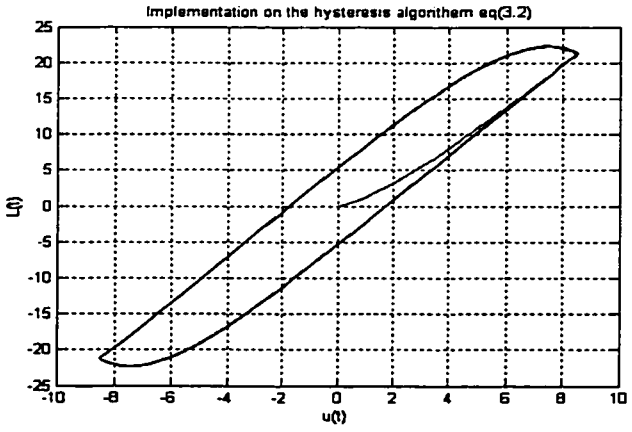

Figure 3.2 Hysteresis response given by using Eq. 3.2

Hence, in the designs of the control laws, the force-expansion relationship $F_p(v)$ of the piezoactuators can be described as,

$$F_p(v) = K_p(pv(t) + g(v(t))) \tag{3.4}$$

where K_p is the stiffness of the piezoactuator, $\|g(v(t))\| \leq \rho_a$ (ρ_a is a constant).

3.4 Applications of Piezoactuators in Turning

One of the schematic of turning metal cutting system is illustrated in Fig. 3.3, in which the cutting tool is mounted on the tool holder with a piezoactuator.

With the advent of improved machines and process, the interests have been growing for a fast tool servomechanism to increase the capability and capacity of existing machines. The purpose of the piezoactuators is to move the tool small displacement into and out of the workpiece, thus generating desired workpiece surface finish.

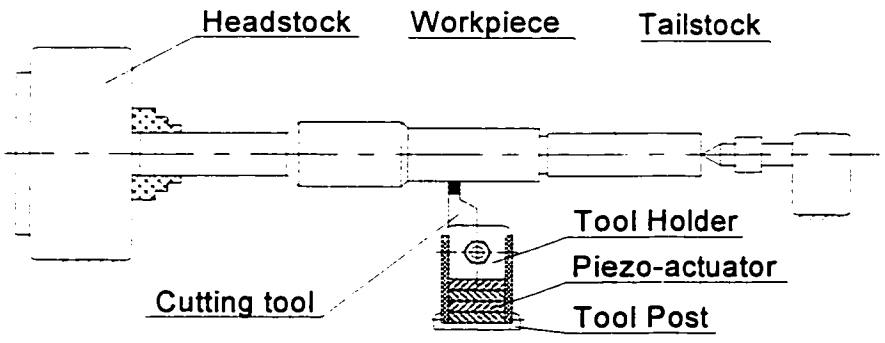

Figure 3.3 The schematic of turning with a piezoactuator

With electrical voltage applied, the piezoactuator can expand and reach its nominal displacement on the order of microseconds and more than 10,000 g's forces are possible, so that the position of the cutting tool can be maneuvered. Therefore, the chatter occurring in metal cutting can be

reduced or suppressed with appropriate control scheme with the help of piezoactuators. In Fig. 3.4, it presents the one of the simplest section view of a piezoactuator structure.

Many piezoactuator models are offered with a mechanical preload so that it is possible to apply larger pulling forces to the positioning element. In order to present the description of a piezoactuator model, the mechanical preload is not indicated in Fig. 3.4.

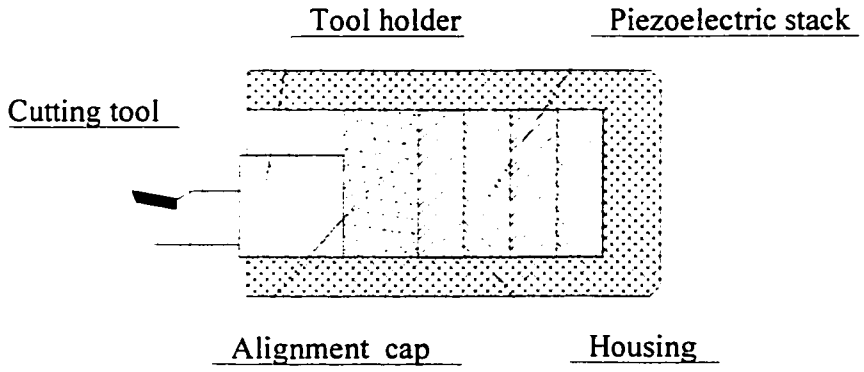

Figure 3.4 the section view of piezoactuator structure

Whether the piezoactuators can generate forces depend on their stiffnesses and expansion capacities. If the piezoactuators are attached between two rigid walls so as not to expand, then the piezoactuators generate the maximum forces, called blocking force. However, it is only true for ideal restraints, whose spring constant *Kp* is infinitely large. In practice, due to fast expanding of the piezoactuators and the inertia of the mass loads connected to the piezoactuators, the pushing or pulling forces can be excited and described.

3.5 Structure of the Dependent Piezoactuator on Tool Holder

To simplify the mechanical structures of the metal cutting systems with the piezoactuators, Liu [44] [45] presented a dynamic model for the turning as follows:

$$m \cdot \ddot{y}(t) + c \cdot \dot{y}(t) + k \cdot y(t) = F(t) - F_p(t) \tag{3.5}$$

where the equivalent mass of the cutting system is m; the damping coefficient of modes of the system is c; the dynamic stiffness is k; the F represents the cutting forces; and F_p is the force generated by the piezoactuator.

The structures of the dependent piezoactuators on the tool holder in the metal cutting system are shown simply in Fig. 3.5.

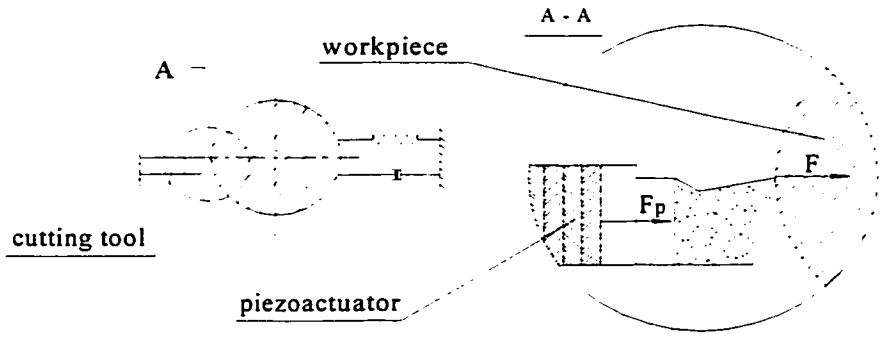

Figure 3.5 Dynamic model of dependent piezactuator on tool holder

3.6 Structure of the Independent Piezoactuator from Tool Holder

Considering the independent piezoactuators from the tool holders while mount the piezoactuators in metal cutting systems, the structure of a piezoactuator can be described in Fig. 3.6. The equations of the dynamic systems are presented as follows:

$$m \cdot \ddot{y}(t) + c \cdot \dot{y}(t) + k \cdot y(t) = F(t) - F_p(t) \tag{3.6}$$

$$F_p(t) = F_V(t) - m_p \ddot{y}_p(t) \tag{3.7}$$

where the equivalent mass of the cutting system is m; the damping coefficient of modes of the cutting system is c; the dynamic stiffness of the cutting system is k; the equivalent mass of the piezoactuator is m_p; the cutting forces between cutting tool and workpiece are F(t); the reaction

force between piezoactuator and cutting tool is F_p(t); the force generated by the piezoactuator due to the expansion while voltage is applied is F_v(t); the relative displacement between cutting tool and workpiece is y(t); the displacement between cutting tool and independent tool holder (in Fig 3.6) is y_p, which the direction is parallel to one of y(t).

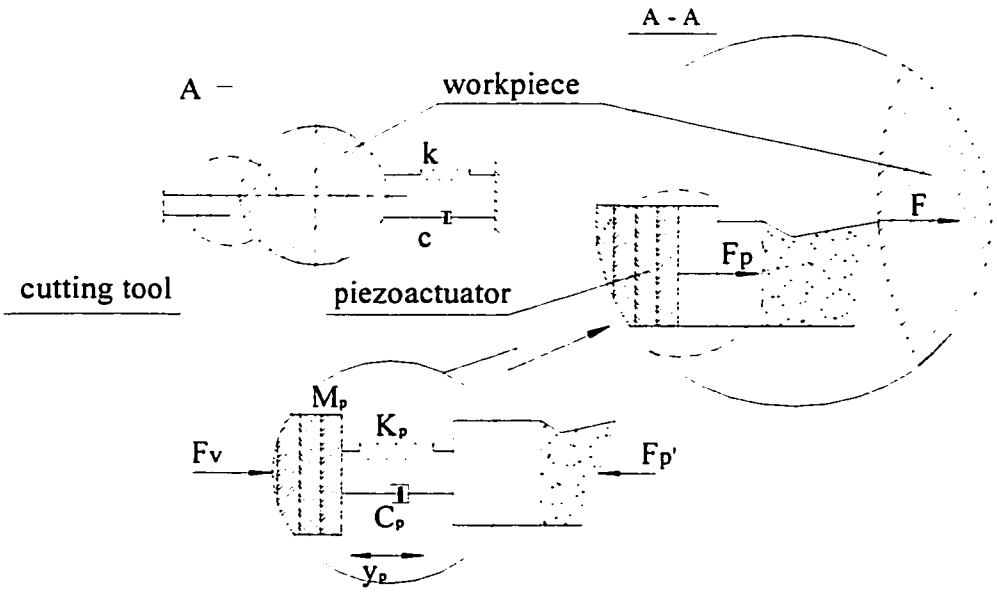

Figure 3.6 Dynamic model of independent piezoactuator from tool holder

3.7 Summary

Based on the analyses of the principles and applications of the piezoactuators in the metal cutting process, the backlash-like model of the hysteretic characteristics is given, two different models of both dependent and independent piezactuators from the tool holders are presented.

Chapter 4

Chatter Suppression for the Controlled System with 2-D Model and Dependent Piezoactuator

Introduction – in order to suppress chatter in the metal cutting processes, a piezoactuator is introduced for the regulation of the displacement in the metal cutting process with two degree-of-freedom. The closed-loop dynamic of the metal cutting system with two-dimensional force model is presented. The piezoactutor in the systems exhibits the hysteretic characteristics. The adaptive control law is designed. The simulations of the dynamic performances of the system with the piezoactuator are shown.

4.1 Dynamic Model of Turning Process

The schematic model of the metal cutting system with two degree-of-freedom is illustrated in Fig. 4.1. The dynamic cutting process is demonstrated in the magnified contact parts of the workpiece and cutting tool. In this thesis, the work focuses on the type A of chatter that is normal to the machining surface of the workpiece. Considering the piezoactuator tool holder assemble as a lumped mass system, the structural turning system may be represented as illustrated in the follows.

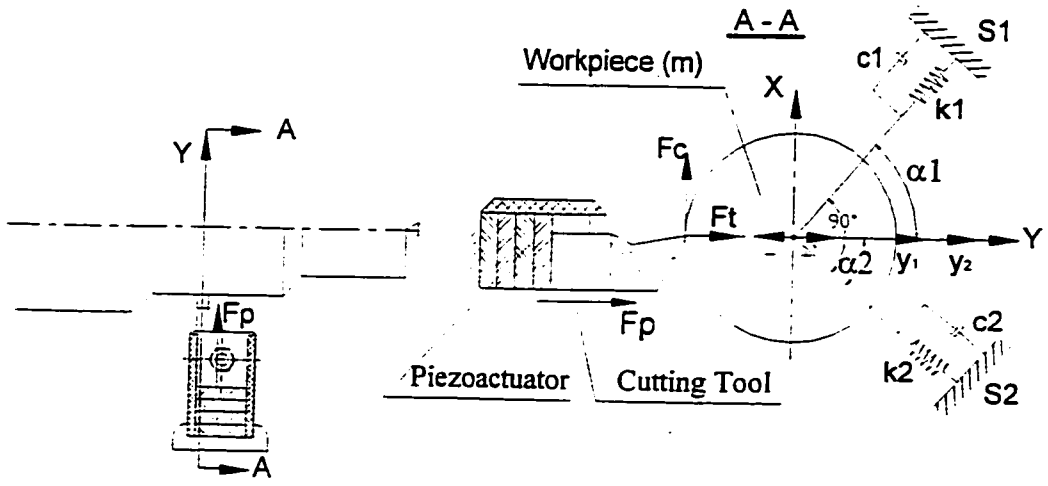

Figure 4.1 Schematic model of turning system with dependent piezoactuators and 2-D force models

In Fig. 4.1, the dynamic process of the metal cutting system can be described with a linear second order function as following:

$$\begin{pmatrix} \frac{m}{\cos\alpha_1} & 0 \\ 0 & \frac{m}{\cos\alpha_2} \end{pmatrix}\begin{pmatrix} \frac{d^2y_1}{dt^2} \\ \frac{d^2y_2}{dt^2} \end{pmatrix}+\begin{pmatrix} \frac{c_1}{\cos\alpha_1} & 0 \\ 0 & \frac{c_2}{\cos\alpha_2} \end{pmatrix}\begin{pmatrix} \frac{dy_1}{dt} \\ \frac{dy_2}{dt} \end{pmatrix}+\begin{pmatrix} \frac{k_1}{\cos\alpha_1} & 0 \\ 0 & \frac{k_2}{\cos\alpha_2} \end{pmatrix}\begin{pmatrix} y_1 \\ y_2 \end{pmatrix}$$
$$=\begin{pmatrix} \cos\alpha_1 & \sin\alpha_1 \\ \cos\alpha_2 & \sin\alpha_2 \end{pmatrix}\begin{pmatrix} F_t \\ F_c \end{pmatrix}+\begin{pmatrix} \cos\alpha_1 \\ \cos\alpha_2 \end{pmatrix}F_p \qquad (4.1)$$

where y_1, y_2 represent the relative displacements between the cutting tool and workpiece normal to the machined surface in each degree-freedom direction; m, c_i, k_i are the equivalent mass, equivalent damping coefficient and equivalent spring stiffness of vibration structure, respectively, in each direction: F_t, F_c are the thrust and main cutting forces exciting the structure; F_p results from the piezoactuator: α_1, α_2 are geometrical angles of models of the vibrations of the structure relative to the line normal to the machined surface.

According to the analyses in Eq. 3.4 in the chapter 3, the reaction force F_p between the cutting tool and workpiece is defined as

$$F_p(v) = K_p(p \cdot v(t) + g(v(t))) \tag{4.2}$$

where K_p is the stiffness of the piezoactuator, v(t) denotes as the applied voltage, other parameters are defined in the chapter 3.

The closed-loop dynamic system of the metal cutting in turning with the piezoactuator and the adaptive controller designed in the next section is illustrated as follows,

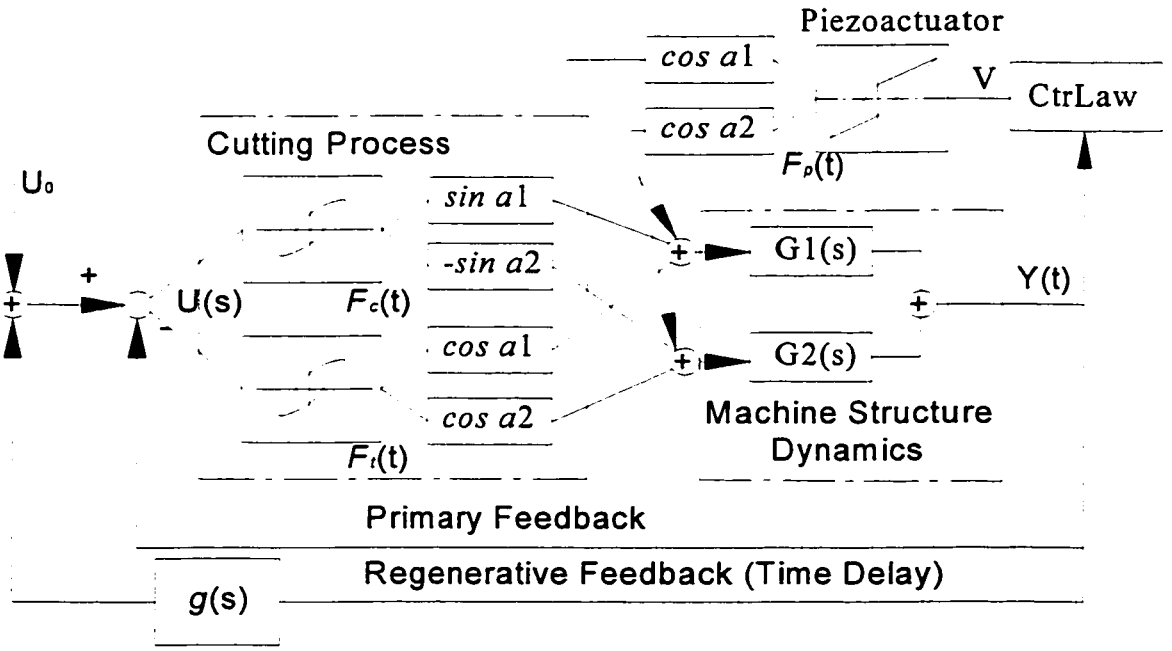

Figure 4.2 Block diagram of turning system with piezoactuator and controller

4.2 Adaptive Controller design

Based on the mathematical model of the closed-loop dynamic system described in Eq. 4.1, the control law will be designed in order to suppress the chatter effect in metal cutting process. Based on Eq. 4.1, we can transform and calculate it further as follows,

$$\frac{m}{\cos\alpha_1}\frac{d^2y_1(t)}{dt^2}+\frac{c_1}{\cos\alpha_1}\frac{d\,y_1(t)}{dt}+\frac{k_1}{\cos\alpha_1}y_1(t)=\cos\alpha_1F_t(t)+\sin\alpha_1F_c(t)+\cos\alpha_1F_p(t)$$

$$y_1(s)=\frac{\cos\alpha_1F_t(s)+\sin\alpha_1F_c(s)+\cos\alpha_1F_p(s)}{\frac{m}{\cos\alpha_1}s^2+\frac{c_1}{\cos\alpha_1}s+\frac{k_1}{\cos\alpha_1}} \tag{4.3}$$

$$\frac{m}{\cos\alpha_2}\frac{d^2y_2(t)}{dt^2}+\frac{c_2}{\cos\alpha_2}\frac{d\,y_2(t)}{dt}+\frac{k_2}{\cos\alpha_2}y_2(t)=\cos\alpha_2F_t(t)+\sin\alpha_2F_c(t)+\cos\alpha_2F_p(t)$$

$$y_2(s)=\frac{\cos\alpha_2F_t(s)+\sin\alpha_2F_c(s)+\cos\alpha_2F_p(s)}{\frac{m}{\cos\alpha_2}s^2+\frac{c_2}{\cos\alpha_2}s+\frac{k_2}{\cos\alpha_2}} \tag{4.4}$$

The combination of Eqs. 4.3 and. 4.4 yields

$$\begin{aligned}y(s)&=y_1(s)+y_2(s)\\&=\frac{\cos\alpha_1F_t(s)+\sin\alpha_1F_c(s)+\cos\alpha_1F_p(s)}{\frac{m}{\cos\alpha_1}s^2+\frac{c_1}{\cos\alpha_1}s+\frac{k_1}{\cos\alpha_1}}+\frac{\cos\alpha_2F_t(s)+\sin\alpha_2F_c(s)+\cos\alpha_2F_p(s)}{\frac{m}{\cos\alpha_2}s^2+\frac{c_2}{\cos\alpha_2}s+\frac{k_2}{\cos\alpha_2}}\\&=\frac{\cos\alpha_1F_t(s)+\sin\alpha_1F_c(s)+\cos\alpha_1F_p(s)}{m_{11}s^2+c_{11}s+k_{11}}+\frac{\cos\alpha_2F_t(s)+\sin\alpha_2F_c(s)+\cos\alpha_2F_p(s)}{m_{22}s^2+c_{22}s+k_{22}}\end{aligned} \tag{4.5}$$

where

$$m_{11}=\frac{m}{\cos\alpha_1},\quad c_{11}=\frac{c_1}{\cos\alpha_1},\quad k_{11}=\frac{k_1}{\cos\alpha_1},\quad m_{22}=\frac{m}{\cos\alpha_2},\quad c_{22}=\frac{c_2}{\cos\alpha_2},\quad k_{22}=\frac{k_2}{\cos\alpha_2}$$

Eq. 4.5 can be further written as

$$\begin{aligned}&y(s)(m_{11}s^2+c_{11}s+k_{11})(m_{22}s^2+c_{22}s+k_{22})\\&=(\cos\alpha_1F_t(s)+\sin\alpha_1F_c(s)+\cos\alpha_1F_p(s))(m_{22}s^2+c_{22}s+k_{22})\\&+(\cos\alpha_2F_t(s)+\sin\alpha_2F_c(s)+\cos\alpha_2F_p(s))(m_{11}s^2+c_{11}s+k_{11})\end{aligned} \tag{4.6}$$

For simplicity, Eq. 4.6 can be rewritten as

$$\begin{aligned}&y(s)(a_4s^4+a_3s^3+a_2s^2+a_1s+a_0)\\&=(F_t(s)+F_p(s))(b_{tp2}s^2+b_{tp1}s+b_{tp0})+F_c(s)(b_{c2}s^2+b_{c1}s+b_{c0})\end{aligned} \tag{4.7}$$

where

$$a_4=m_{11}m_{22},\quad a_3=c_{11}m_{22}+c_{22}m_{11},\quad a_2=k_{11}m_{22}+k_{22}m_{11}+c_{11}c_{22},\quad a_1=k_{11}c_{22}+k_{22}c_{11},\quad a_0=k_{11}k_{22}$$

$$b_{tp2} = \cos\alpha_1 m_{22} + \cos\alpha_2 m_{11}, \quad b_{tp1} = \cos\alpha_1 c_{22} + \cos\alpha_2 c_{11}, \quad b_{tp0} = \cos\alpha_1 k_{22} + \cos\alpha_2 k_{11}$$

$$b_{c2} = \sin\alpha_1 m_{22} + \sin\alpha_2 m_{11}, \quad b_{c1} = \sin\alpha_1 c_{22} + \sin\alpha_2 c_{11}, \quad b_{c0} = \sin\alpha_1 k_{22} + \sin\alpha_2 k_{11}$$

Hence by the inverse Laplace transformation, one can yield.

$$\begin{aligned} &a_4 y^{(4)}(t) + a_3 y^{(3)}(t) + a_2 y^{(2)}(t) + a_1 y^{(1)}(t) + a_0 y(t) \\ &= b_{tp2} F_t^{(2)}(t) + b_{tp1} F_t^{(1)}(t) + b_{tp0} F_t(t) + b_{c2} F_c^{(2)}(t) + b_{c1} F_c^{(1)}(t) + b_{c0} F_c(t) \\ &+ b_{tp2} F_p^{(2)}(t) + b_{tp1} F_p^{(1)}(t) + b_{tp0} F_p(t) \end{aligned} \tag{4.8}$$

based on the analyses in Chapter 2, the uncut chip thickness u(t):

$$u(t) = u_0(t) - y(t) + \mu \cdot y(t-\tau) \tag{4.9}$$

where $\mu$is the overlapping coefficient, τ is time delay of the system, y(t) is the displacement.

Due to the effect of hysteresis between the forces and uncut chip thickness,

$$F_t(t) = p_t u(t) + g_t(u(t)) = p_t(u_0(t) - y(t) + \mu y(t-\tau)) + g_t(u_0(t) - y(t) + \mu y(t-\tau)) \tag{4.10}$$

$$F_c(t) = p_c u(t) + g_c(u(t)) = p_c(u_0(t) - y(t) + \mu y(t-\tau)) + g_c(u_0(t) - y(t) + \mu y(t-\tau)) \tag{4.11}$$

To simplify Eqs. 4.10 and 4.11, the corresponding backlashes can replace the above equations,

$$\begin{aligned} F_t(t) &= A_t u(t) \pm B_t^{'} = A_t(u_0(t) - y(t) + \mu y_\tau(t)) \pm B_t^{'} = -A_t y(t) + A_t \mu y_\tau(t) \pm B_t \\ F_c(t) &= A_c u(t) \pm B_c^{'} = A_c(u_0(t) - y(t) + \mu y_\tau(t)) \pm B_c^{'} = -A_c y(t) + A_c \mu y_\tau(t) \pm B_c \end{aligned} \tag{4.12}$$

where $y_\tau(t) = y(t-\tau)$; $B_t = A_t u_0(t) \pm B_t^{'}$; $B_c = A_c u_0(t) \pm B_c^{'}$; other parameters are defined in Eqs. 2.14 and 2.15.

Substitute Eq. 4.12 into Eq. 4.8, the dynamic equation will be as following:

$$\begin{aligned} &a_4 y^{(4)}(t) + a_3 y^{(3)}(t) + a_2 y^{(2)}(t) + a_1 y^{(1)}(t) + a_0 y(t) \\ &= b_{tp2}(-A_t y^{(2)}(t) + \mu A_t y_\tau^{(2)}(t)) + b_{tp1}(-A_t y^{(1)}(t) + \mu A_t y_\tau^{(1)}(t)) + b_{tp0}(-A_t y(t) + \mu A_t y_\tau(t) \pm B_t) \\ &+ b_{c2}(-A_c y^{(2)}(t) + \mu A_c y_\tau^{(2)}(t)) + b_{c1}(-A_c y^{(1)}(t) + \mu A_c y_\tau^{(1)}(t)) + b_{c0}(-A_c y(t) + \mu A_c y_\tau(t) \pm B_c) \\ &+ b_{tp2} F_p^{(2)}(t) + b_{tp1} F_p^{(1)}(t) + b_{tp0} F_p(t) \end{aligned} \tag{4.13}$$

Eq. 4.13 can be simplified into the form below,

$$\overline{a_4}y^{(4)}(t)+\overline{a_3}y^{(3)}(t)+\overline{a_2}y^{(2)}(t)+\overline{a_1}y^{(1)}(t)+\overline{a_0}y(t)$$
$$=r_2y_r^{(2)}(t)+r_1y_r^{(1)}(t)+r_0y_r(t)+b_{tp0}F_p(t)+e(t,F_p^{(1)},F_p^{(2)}) \quad (4.14)$$

where

$$\overline{a_4}=a_4,\quad \overline{a_3}=a_3,\quad \overline{a_2}=a_2+b_{pt2}A_t+b_{c2}A_c,\quad \overline{a_1}=a_1+b_{pt1}A_t+b_{c1}A_c,$$

$$\overline{a_0}=a_0+b_{pt0}A_t+b_{c0}A_c$$

$$r_2=\mu\ (b_{tp2}A_t+b_{c2}A_c)$$

$$r_1=\mu\ (b_{tp1}A_t+b_{c1}A_c)$$

$$r_0=\mu\ (b_{tp0}A_t+b_{c0}A_c)$$

$$e(t,F_p^{(1)},F_p^{(2)})=r_{\pm b}+b_{tp2}F_p^{(2)}(t)+b_{tp1}F_p^{(1)}(t)$$

$$r_{\pm b}=\pm b_{tp0}B_t\pm b_{c0}B_c$$

Remark A: the term $e(t,F_p^{(1)},F_p^{(2)})$ is the lumped uncertain element in Eq. 4.1. Its upper boundness is assumed to be known, i.e. $\| e(t,F_p^{(1)},F_p^{(2)}) \| \le \rho(t)$.

4.2.1 Designed Control Law

Define the switching surface as:

$$\sigma(t)=S\cdot x(t)=s_1x_1(t)+s_2x_2(t)+s_3x_3(t)+s_4x_4(t)=0 \quad (4.15)$$

where $S\in R^{1\times4}$, $x(t)\in R^{4\times1}$, and s_1, s_2, s_3, s_4 are positive coefficients, $x_1(t)$, $x_2(t)$, $x_3(t)$, $x_4(t)$ are the state variables in Eq. 4.1.

A tuning error σ_t is defined as follows,

$$\sigma_t(t)=\sigma(t)-\varepsilon\cdot sat\ (\frac{\sigma(t)}{\varepsilon})$$

where ε is an arbitrary positive constant vector, sat(·) is the saturation function and $\sigma(t)$ is the sliding surface.

Differentiating $\sigma(t)$ with respect to time t, and substituting Eq. 4.2, one obtain:

$$\dot{\sigma}(t) = \frac{\partial \sigma(t)}{\partial x}\dot{x}(t) = s_1 y^{(1)} + s_2 y^{(2)} + s_3 y^{(3)} + s_4 y^{(4)}$$

$$= (s_1 - s_4 \frac{\bar{a}_1}{\bar{a}_4}) y^{(1)} + (s_2 - s_4 \frac{\bar{a}_2}{\bar{a}_4}) y^{(2)} + (s_3 - s_4 \frac{\bar{a}_3}{\bar{a}_4}) y^{(3)} - s_4 \frac{\bar{a}_0}{\bar{a}_4} y(t)$$

$$+ \frac{s_4}{\bar{a}_4}(r_2 y_r^{(2)} + r_1 y_r^{(1)} + r_0 y_r + e(t)) + s_4 \frac{b_{tpo}\, p}{\bar{a}_4} v(t) + s_4 \frac{b_{tpo}}{\bar{a}_4} g(v(t)) \qquad (4.16)$$

where $b_{tpo} = K_p b_{tp0}$, K_p is the stiffness of the piezoactuator in Eq. 4.2.

Define $N = \dfrac{\bar{a}_4}{s_4 b_{tpo} p}$, ($N$>0), $\theta_1 = N(s_1 - s_4 \dfrac{\bar{a}_1}{\bar{a}_4})$, $\theta_2 = N(s_2 - s_4 \dfrac{\bar{a}_2}{\bar{a}_4})$, $\theta_3 = N(s_3 - s_4 \dfrac{\bar{a}_3}{\bar{a}_4})$,

$\theta_4 = N(-s_4)\dfrac{\bar{a}_0}{\bar{a}_4}$, $\theta_5 = N\dfrac{s_4}{\bar{a}_4} r_2$, $\theta_6 = N\dfrac{s_4}{\bar{a}_4} r_1$, $\theta_7 = N\dfrac{s_4}{\bar{a}_4} r_0$.

For the design of the control laws, the following assumptions concerning the systems and hysteresis are required.

Assumption 1:

There exist positive scalars q_1, q_2, q_3, such that $\| y^{(2)}(t+\tau) \| \le q_1 \| y^{(2)}(t) \|$, $\| y^{(1)}(t+\tau) \| \le q_2 \| y^{(1)}(t) \|$ and $\|y(t+\tau)\| \le q_3 \|y(t)\|$.

Assumption 2:

There exist known constants $b_{tpo\min}$ and $b_{tpo\max}$, such that the control gain b_{tpo} in Eq. 4.16 satisfies $b_{tpo} \in [b_{tpo\min}, b_{tpo\max}]$.

Assumption 3:

There exist known constants $p_{\min}$ and $p_{\max}$ such that the control gain p in Eq. 4.16 satisfies $p \in [p_{\min}, p_{\max}]$.

Assumption 4:

Define $\theta \in \Omega_\theta = \{\theta : \theta_{i\min} \le \theta_i \le \theta_{i\max}, \forall i \in \{1, r\}\}$, where $\theta_{i\min}$, $\theta_{i\max}$ are known real numbers.

Assumption 5:

In Eq. 4.2, $\|g(v(t))\| \le \rho_a$, ρ_a is a constant.

With respect to the plant and hysteresis models subject to the above assumptions, the following control law and adaptation mechanism are presented:

$$v(t) = -[k_r\sigma(t) + \hat{\theta}_1(t)y^{(1)}(t) + \hat{\theta}_2(t)y^{(2)}(t) + \hat{\theta}_3(t)y^{(3)}(t) + \hat{\theta}_4(t)y(t) + \hat{\theta}_5(t)\|y^{(2)}(t)\| + \hat{\theta}_6(t)\|y^{(1)}(t)\| + \hat{\theta}_7(t)\|y(t)\| + k^* sat(\frac{\sigma(t)}{\varepsilon})] \tag{4.17}$$

where $\dot{\hat{\theta}}_i = proj\ (\hat{\theta}_i, -\gamma_i\omega_i)$ $(i = 1, 2, 3, 4, 5, 6, 7)$; k_r, k^* are constant positive gains.

$proj(\cdot,\cdot)$ is a projection function as follows

$$proj(\hat{\theta}_i, -\gamma_i\omega_i) = \begin{cases} 0 & if(\hat{\theta}_i > \theta_{\max} \text{ and } \gamma_i\omega_i < 0) \text{ or } (\hat{\theta}_i < \theta_{\min} \text{ and } \gamma_i\omega_i > 0) \\ -\gamma_i\omega_i & if(\theta_{\min} < \hat{\theta}_i < \theta_{\max}) \text{ or } (\hat{\theta}_i > \theta_{\max} \text{ and } \gamma_i\omega_i \ge 0) \\ & \text{or } \hat{\theta}_i < \theta_{\min} \text{ and } \gamma_i\omega_i \le 0) \end{cases} \tag{4.18}$$

where ω_i are defined as

$\omega_1(t) = \sigma_t(t)\,y^{(1)}(t)$, $\omega_2(t) = \sigma_t(t)y^{(2)}(t)$, $\omega_3(t) = \sigma_t(t)y^{(3)}(t)$, $\omega_4(t) = \sigma_t(t)y(t)$,

$\omega_5(t) = \sigma_t(t)\| y^{(2)}(t) \|$, $\omega_6(t) = \sigma_t(t)\| y^{(1)}(t) \|$, $\omega_7(t) = \sigma_t(t)\| y(t) \|$;

and scalars $\gamma_i (i = 1, 2, 3, 4, 5, 6, 7)$ are coefficients chosen by the designers practically.

4.2.2 Stability Analysis of the System

To establish global bound, we define a Lyapunov function candidate for the system in Eq. 4.1:

$$V(t) = \frac{1}{2}\left[N\sigma_t^2(t) + \sum_{i=1}^{4}[\frac{1}{\gamma_i}(\hat{\theta}_i(t) - \theta_i)^2] + \sum_{i=5}^{i=7}[\frac{1}{\gamma_i}(\hat{\theta}_i(t) - q_{i-4}\theta_i)^2] \right] \tag{4.19}$$

Case 1: when $|\sigma(t)| \le \varepsilon$, the derivative $\dot{V}(t)$ exists for all $\sigma(t)$, which is $\dot{V}(t) = 0$.

Case 2: when $|\sigma(t)| > \varepsilon$, using Eq. 4.16 and the fact $\dot{\sigma} = \dot{\sigma}_t$, one obtain

$$\dot{V}(t) \le N\sigma_t \dot{\sigma} + \sum_{i=1}^{4}[\frac{1}{\gamma_i}(\hat{\theta}_i(t)-\theta_i)\dot{\hat{\theta}}_i] + \sum_{i=5}^{i=7}[\frac{1}{\gamma_i}(\hat{\theta}_i(t)-q_{i-4}\theta_i)\dot{\hat{\theta}}_i]$$

$$= \sum_{i=1}^{4}[\frac{1}{\gamma_i}(\hat{\theta}_i(t)-\theta_i)\dot{\hat{\theta}}_i] + \sum_{i=5}^{i=7}[\frac{1}{\gamma_i}(\hat{\theta}_i(t)-q_{i-4}\theta_i)\dot{\hat{\theta}}_i] + \sigma_t(v(t)+\frac{1}{p}g(v))$$

$$+\sigma_t(\theta_1 y^{(1)} + \theta_2 y^{(2)} + \theta_3 y^{(3)} + \theta_4 y + \theta_5 y_\tau^{(2)} + \theta_6 y_\tau^{(1)} + \theta_7 y_\tau + \frac{e(t)}{b_{ipo}p}) \tag{4.20}$$

As a projection function, $(\hat{\theta}_i - m_i\theta_i)proj(\hat{\theta}_i, r_i\varpi_i) \le (\hat{\theta}_i - m_i\theta_i)r_i\varpi_i$, m_i are positive scalars. Then

$$\dot{V}(t) \le \sigma_t(\theta_1 y^{(1)} + \theta_2 y^{(2)} + \theta_3 y^{(3)} + \theta_4 y + \theta_5 y_\tau^{(2)} + \theta_6 y_\tau^{(1)} + \theta_7 y_\tau + \frac{e(t)}{b_{ipo}p})$$

$$+\sigma_t\ (v(t)+\frac{1}{p}g(v(t))) + \sigma_t((\hat{\theta}_1-\theta_1)y^{(1)} + (\hat{\theta}_2-\theta_2)y^{(2)} + (\hat{\theta}_3-\theta_3)y^{(3)}$$

$$+(\hat{\theta}_4-\theta_4)y + (\hat{\theta}_5-q_i\theta_5)\| y^{(2)} \| + (\hat{\theta}_6-q_2\theta_6)\| y^{(1)} \| + (\hat{\theta}_7-q_3\theta_7)\| y \|) \tag{4.21}$$

According to the *assumption 1*, we can get

$$\dot{V}(t) \le \sigma_t(\theta_1 y^{(1)} + \theta_2 y^{(2)} + \theta_3 y^{(3)} + \theta_4 y + q_2\theta_5 \| y^{(2)} \| + q_1\theta_6 \| y^{(1)} \| + q_1\theta_7 \| y \| + \frac{e(t)}{b_{ipo}p})$$

$$+\sigma_t\ (v(t)+\frac{1}{p}g(v(t))) + \sigma_t((\hat{\theta}_1-\theta_1)y^{(1)} + (\hat{\theta}_2-\theta_2)y^{(2)} + (\hat{\theta}_3-\theta_3)y^{(3)}$$

$$+(\hat{\theta}_4-\theta_4)y + (\hat{\theta}_5-q_1\theta_5)\| y^{(2)} \| + (\hat{\theta}_6-q_2\theta_6)\| y^{(1)} \| + (\hat{\theta}_7-q_3\theta_7)\| y \|)$$

$$\le \sigma_t(\frac{e(t)}{b_{ipo}p} + \frac{g(v)}{p}) + \sigma_t v(t) + \sigma_t(\hat{\theta}_1 y^{(1)} + \hat{\theta}_2 y^{(2)} + \hat{\theta}_3 y^{(3)} + \hat{\theta}_4 y + \hat{\theta}_5 \| y^{(2)} \| + \hat{\theta}_6 \| y^{(1)} \| + \hat{\theta}_7 \| y \|)$$

$$\le \sigma_t(\frac{e(t)}{b_{ipo}p} + \frac{g(v)}{p}) + \sigma_t(\hat{\theta}_1 y^{(1)} + \hat{\theta}_2 y^{(2)} + \hat{\theta}_3 y^{(3)} + \hat{\theta}_4 y + \hat{\theta}_5 \| y^{(2)} \| + \hat{\theta}_6 \| y^{(1)} \| + \hat{\theta}_7 \| y \|)$$

$$-\sigma_t(k_\tau\sigma + \hat{\theta}_1 y^{(1)} + \hat{\theta}_2 y^{(2)} + \hat{\theta}_3 y^{(3)} + \hat{\theta}_4 y + \hat{\theta}_5\|y^{(2)}\| + \hat{\theta}_6\|y^{(1)}\|) + \hat{\theta}_7\|y\| + k^* sat(\frac{\sigma(t)}{\varepsilon}))$$

$$= -k_\tau\sigma_t(t)\sigma(t) - \sigma_t k^* sat(\frac{\sigma(t)}{\varepsilon}) + \sigma_t(\frac{1}{p}g(v) + \frac{e(t)}{b_{ipo}p})$$

$$\le -k_\tau\sigma_t^2(t) - \sigma_t k^* sat(\frac{\sigma(t)}{\varepsilon}) + \sigma_t(\frac{1}{p}g(v) + \frac{e(t)}{b_{ipo}p})$$

$$\le -k_\tau\sigma_t^2(t) - |\sigma_t|k^* + |\sigma_t|(\frac{1}{p}|g(v)| + \frac{|e(t)|}{b_{ipo}p}) \tag{4.22}$$

In the *assumption 5* and the *Remark A*, $|g(v)| \le \rho_a$ and $|e(t)| \le \rho(t)$ are defined.

While defines $k^* = k^*_{\max} \ge \frac{1}{p}(\rho_a + \frac{\rho(t)+v(t)}{b_{ipo}})$, it yields

$$\dot{V}(t) \le -k_r \sigma_t^2(t) - |\sigma_t| \hat{k}_{\max}^{\bullet} + |\sigma_t| (\frac{1}{p} |g(v)| + \frac{|e(t)|}{b_{tpo} p}) \le -k_r \sigma_t^2 \qquad \forall |\sigma(t)| > \varepsilon \tag{4.23}$$

Based on the above analyses and proof, the following theorem regarding the stability of the closed-loop system described by Eqs. (4.2), (4.14) and (4.17) can be established.

Theorem: For the plant in Eq. (4.1) subject to *Assumptions 1-5* and *Remark A*, the robust adaptive controller specified by Eq. (4.17) ensures that all the closed-loop signals are bounded and the state variable $y(t)$ converges to zero for $\forall t \ge t_0$.

4.3 Simulation Results

The adaptive controller developed in Eq. 4.17 is introduced into the system in Eq. 4.1. The parameters involved in all equations in the simulations are listed in Table A. Fig. 4.3 shows the dynamic response of the metal cutting system (in Eq. 4.1) combined with the control law (in Eq. 4.17); Fig. 4.4 illustrates the dynamic response of the main cutting force $F_c(t)$ during the cutting process; Fig. 4.5 presents the dynamic response of the thrust force $F_t(t)$ in the same process.

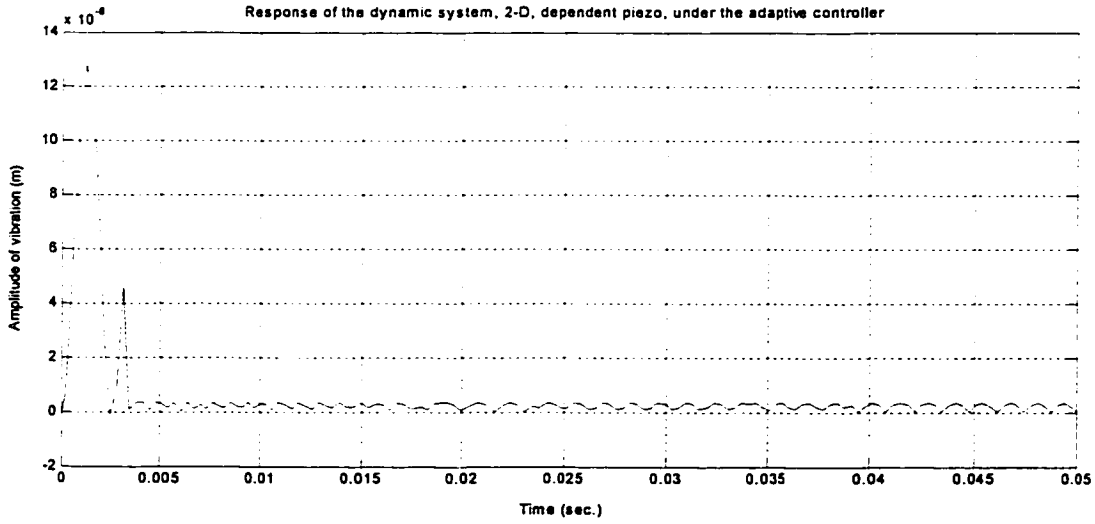

Figure 4.3 Response y(t) of dynamic system with the control law

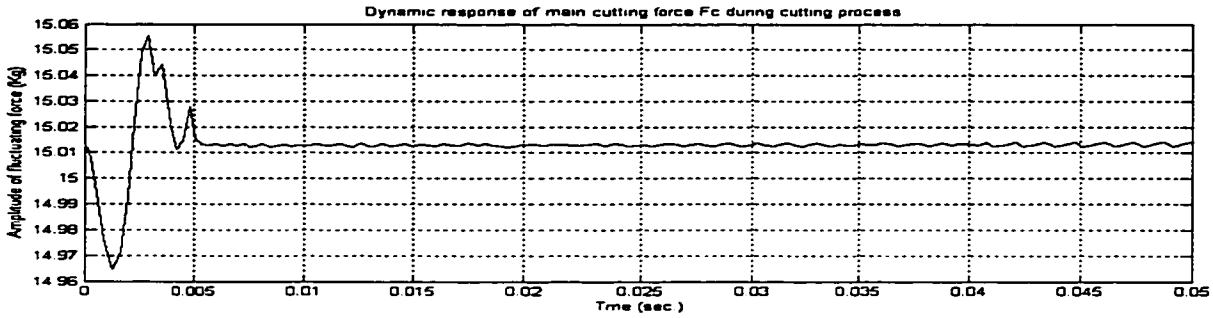

Figure 4.4 Response of main cutting force $F_c(t)$ during cutting process

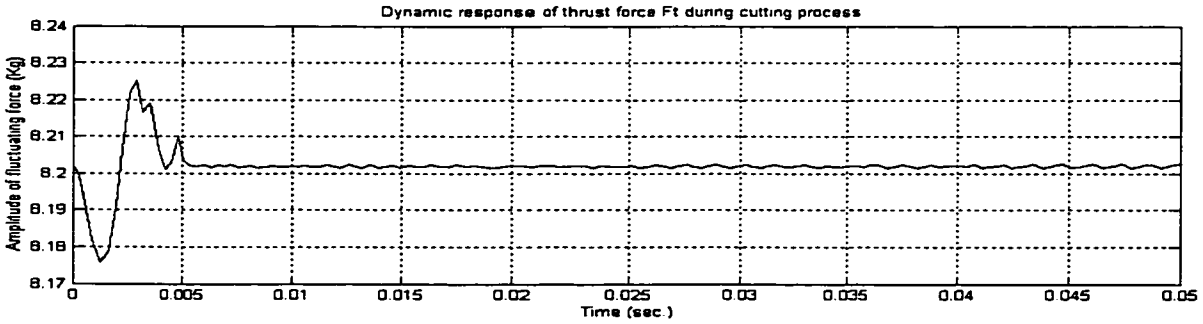

Figure 4.5 Response of thrust force $F_t(t)$ during cutting process

From Fig. 4.3 through Fig. 4.5, the simulations of the system with the adaptive controller show clearly that: 1) the proposed adaptive controller results in the suppression to chatter; 2) the cutting forces during the cutting process are stable eventually.

4.4 Summary

In order to suppress the chatter in the metal cutting system, a piezoactuator is introduced into the system; the system is modeled as a class of uncertain linear system with hysteresis and time lag; an adaptive control law for the system is presented. The simulation results show that the designed control law significantly eliminates the chatter effect in the metal cutting process.

Chapter 5

Chatter Suppression for the Controlled System with 3-D Model and Dependent Piezoactuators

Introduction – in order to suppress chatter in the metal cutting processes, the piezoactuators are introduced for the regulation of the displacement in the system with two degree-of-freedom. The closed-loop dynamics of the metal cutting processes with three-dimensional models of forces is presented. The piezoactutors exhibit the hysteretic characteristics. Two adaptive control laws are designed. The simulations for the dynamic performance of the system with the piezoactuators are shown.

5.1 Dynamic Model of Turning Process

The schematic model of the metal cutting process with two degree-of-freedom and three-dimensional force models is illustrated in Fig. 5.1. The dynamic cutting process is demonstrated in the magnified contact parts of the workpiece and cutting tool. The work will focus on the typy A of chatter that is normal to the cutting surface of workpiece. Considering the piezoactuator tool holders assemble as a lumped mass system, the structural turning system may be represented in the following Fig. 5.1.

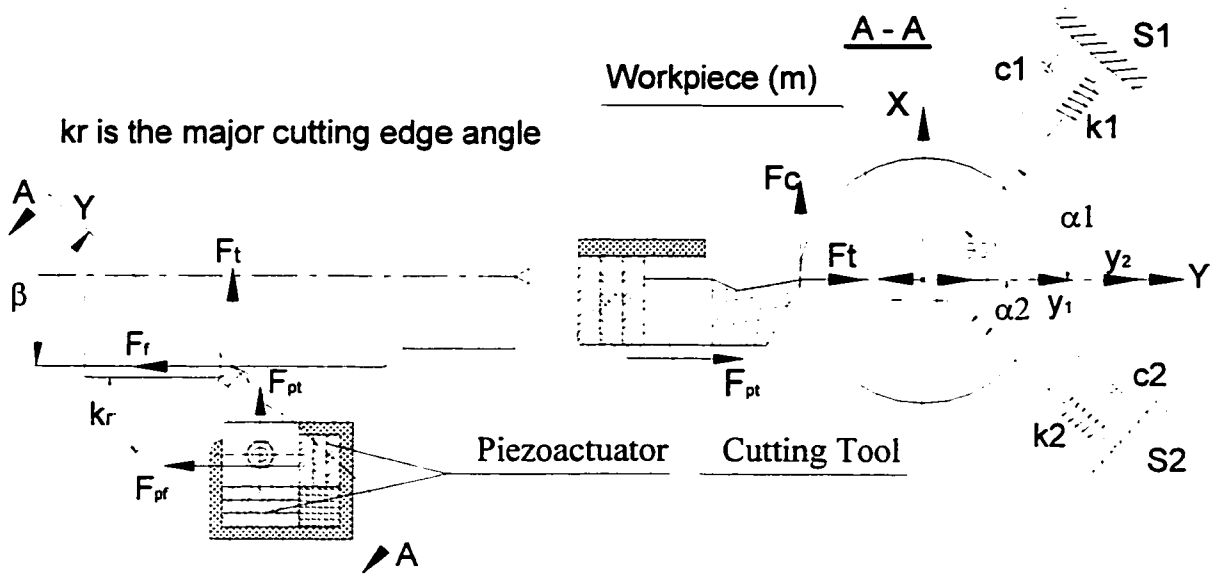

Figure 5.1 Schematic model of turning system with dependent piezoactuators and 3-D force models

In Fig. 5.1, the dynamic process of the metal cutting system can be described with a linear second order function as following:

$$\begin{pmatrix} \frac{m}{\cos\alpha_1} & 0 \\ 0 & \frac{m}{\cos\alpha_2} \end{pmatrix}\begin{pmatrix} \frac{d^2y_1}{dt^2} \\ \frac{d^2y_2}{dt^2} \end{pmatrix}+\begin{pmatrix} \frac{c_1}{\cos\alpha_1} & 0 \\ 0 & \frac{c_2}{\cos\alpha_2} \end{pmatrix}\begin{pmatrix} \frac{dy_1}{dt} \\ \frac{dy_2}{dt} \end{pmatrix}+\begin{pmatrix} \frac{k_1}{\cos\alpha_1} & 0 \\ 0 & \frac{k_2}{\cos\alpha_1} \end{pmatrix}\begin{pmatrix} y_1 \\ y_2 \end{pmatrix}$$

$$=\begin{pmatrix} \cos\alpha_1\sin\beta & \sin\alpha_1 & \cos\alpha_1\cos\beta \\ \cos\alpha_2\sin\beta & -\sin\alpha_2 & \cos\alpha_2\cos\beta \end{pmatrix}\begin{pmatrix} F_t \\ F_c \\ F_f \end{pmatrix}+\begin{pmatrix} \cos\alpha_1\sin\beta & \cos\alpha_1\cos\beta \\ \cos\alpha_2\sin\beta & \cos\alpha_2\cos\beta \end{pmatrix}\begin{pmatrix} F_{pt} \\ F_{pf} \end{pmatrix} \tag{5.1}$$

where y_1, y_2 represent the relative displacement between tools and workpiece normal to machined surface in each degree-freedom direction; m, c_i, k_i are the equivalent mass, equivalent damping coefficient and equivalent spring stiffness of vibration structure, respectively, in each direction; F_t, F_c, F_f are defined as the thrust, main cutting and feeding forces exciting the structure; F_{pt}, F_{pf} are denoted as the forces resulted from the piezoactuators in both directions of thrust and

feed forces; α_1, α_2 are geometrical angles of models of vibration of structure relative to a line normal to the machined surface; β is the angle between the horizontal line and the area normal to the machined surface.

The closed-loop dynamic system of the metal cutting in turning with the piezoactuators and two adaptive controllers designed in next section is illustrated as follows:

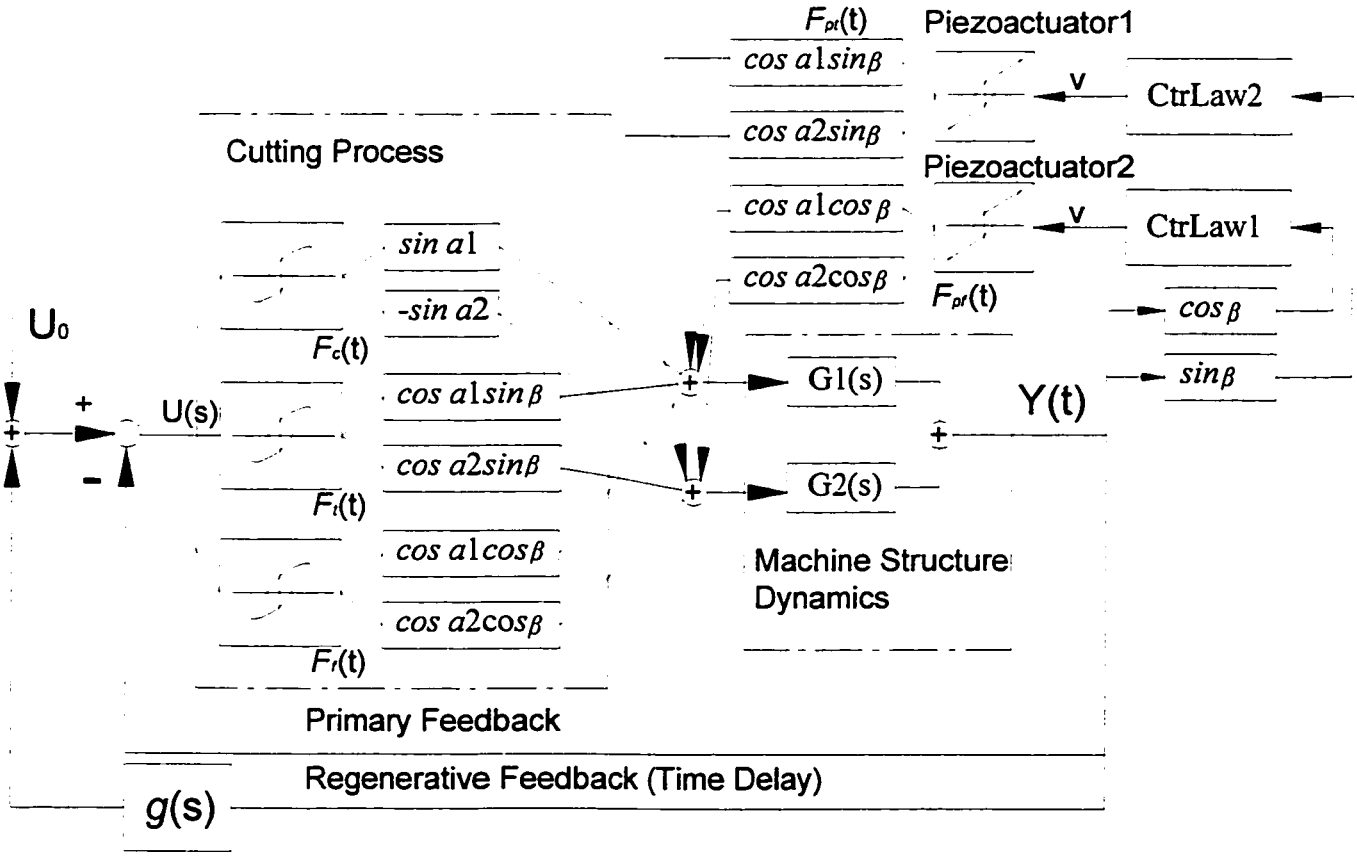

Figure 5.2 Block diagram of turning system with the piezoactuators and controllers

According to the analyses in Eq. 3.4 in the Chapter 3, the reaction forces between the cutting tool and workpiece are defined as:

$$F_{pt}(v) = K_{pt}(p_t \cdot v_t(t) + g_t(v_t(t))) \tag{5.2}$$

$$F_{pf}(v) = K_{pf}(p_f \cdot v_f(t) + g_f(v_f(t))) \tag{5.3}$$

where K_{pt} *and* K_{pf} are the stiffness of the each piezoactuator, $v_t(t)$ and $v_f(t)$ denote as the applied voltages and other parameters are defined in the Chapter 3.

5.2 Adaptive Controller design

Based on the mathematical model of the closed-loop dynamic system described in Eq. 5.1, the control laws will be designed in order to suppress the chatter in the metal cutting process.

Based on Eq. 5.1, we can transform and calculate it further as follows:

$$\frac{m}{\cos\alpha_1}\frac{d^2y_1(t)}{dt^2}+\frac{c_1}{\cos\alpha_1}\frac{d\ y_1(t)}{dt}+\frac{k_1}{\cos\alpha_1}y_1(t) \tag{5.4}$$
$$=\cos\alpha_1\sin\beta F_t(t)+\sin\alpha_1F_c(t)+\cos\alpha_1\cos\beta F_f(t)+\cos\alpha_1\sin\beta F_{pt}(t)+\cos\alpha_1\cos\beta F_{pf}(t)$$
$$y_1(s)=\frac{\cos\alpha_1\sin\beta F_t(s)+\sin\alpha_1F_c(s)+\cos\alpha_1\cos\beta F_f(s)+\cos\alpha_1\sin\beta F_{pt}(s)+\cos\alpha_1\cos\beta F_{pf}(s)}{\frac{m}{\cos\alpha_1}s^2+\frac{c_1}{\cos\alpha_1}s+\frac{k_1}{\cos\alpha_1}}$$

$$\frac{m}{\cos\alpha_2}\frac{d^2y_2(t)}{dt^2}+\frac{c_2}{\cos\alpha_2}\frac{d\ y_2(t)}{dt}+\frac{k_2}{\cos\alpha_2}y_2(t) \tag{5.5}$$
$$=\cos\alpha_2\sin\beta F_t(t)-\sin\alpha_2F_c(t)+\cos\alpha_2\cos\beta F_f(t)+\cos\alpha_2\sin\beta F_{pt}(t)+\cos\alpha_2\cos\beta F_{pf}(t)$$
$$y_2(s)=\frac{\cos\alpha_2\sin\beta F_t(t)-\sin\alpha_2F_c(t)+\cos\alpha_2\cos\beta F_f(t)+\cos\alpha_2\sin\beta F_{pt}(t)+\cos\alpha_2\cos\beta F_{pf}(t)}{\frac{m}{\cos\alpha_2}s^2+\frac{c_2}{\cos\alpha_2}s+\frac{k_2}{\cos\alpha_2}}$$

The combination of Eqs. 5.4 and 5.5 yields

$$y(s)=y_1(s)+y_2(s) \tag{5.6}$$

where

$$y_1(s)=\frac{\cos\alpha_1\sin\beta F_t(s)+\sin\alpha_1F_c(s)+\cos\alpha_1\cos\beta F_f(s)+\cos\alpha_1\sin\beta F_{pt}(s)+\cos\alpha_1\cos\beta F_{pf}(s)}{\frac{m}{\cos\alpha_1}s^2+\frac{c_1}{\cos\alpha_1}s+\frac{k_1}{\cos\alpha_1}}$$

$$y_2(s)=\frac{\cos\alpha_2\sin\beta F_t(t)-\sin\alpha_2F_c(t)+\cos\alpha_2\cos\beta F_f(t)+\cos\alpha_2\sin\beta F_{pt}(t)+\cos\alpha_2\cos\beta F_{pf}(t)}{\frac{m}{\cos\alpha_2}s^2+\frac{c_2}{\cos\alpha_2}s+\frac{k_2}{\cos\alpha_2}}.$$

From Eq. 5.6, we can obtain:

$$
\begin{aligned}
&y(s)(m_{11}s^2+c_{11}s+k_{11})(m_{22}s^2+c_{22}s+k_{22})\\
&=(\cos\alpha_1\sin\beta F_t(s)+\sin\alpha_1 F_c(s)+\cos\alpha_1\cos\beta F_f(s)+\cos\alpha_1\sin\beta F_{pt}(s)+\cos\alpha_1\cos\beta F_{pf}(s))\\
&\times(m_{22}s^2+c_{22}s+k_{22})\\
&+(\cos\alpha_2\sin\beta F_t(t)-\sin\alpha_2 F_c(t)+\cos\alpha_2\cos\beta F_f(t)+\cos\alpha_2\sin\beta F_{pt}(t)+\cos\alpha_2\cos\beta F_{pf}(t))\\
&\times(m_{11}s^2+c_{11}s+k_{11})
\end{aligned}
\tag{5.7}
$$

where

$$
m_{11}=\frac{m}{\cos\alpha_1},\quad c_{11}=\frac{c_1}{\cos\alpha_1},\quad k_{11}=\frac{k_1}{\cos\alpha_1},\quad m_{22}=\frac{m}{\cos\alpha_2},\quad c_{22}=\frac{c_2}{\cos\alpha_2},\quad k_{22}=\frac{k_2}{\cos\alpha_2}
$$

For simplicity, rewrite Eq. 5.7 as

$$
\begin{aligned}
&y(s)(a_4s^4+a_3s^3+a_2s^2+a_1s+a_0)=(F_t(s)+F_{pt}(s))(b_{tp2}s^2+b_{tp1}s+b_{tp0})\\
&+F_c(s)(b_{c2}s^2+b_{c1}s+b_{c0})+(F_f(s)+F_{pf}(s))(b_{fp2}s^2+b_{fp1}s+b_{fp0})
\end{aligned}
\tag{5.8}
$$

where

$$
a_4=m_{11}m_{22},\quad a_3=c_{11}m_{22}+c_{22}m_{11},\quad a_2=k_{11}m_{22}+k_{22}m_{11}+c_{11}c_{22},\quad a_1=k_{11}c_{22}+k_{22}c_{11},\quad a_0=k_{11}k_{22}
$$

$$
b_{tp2}=\cos\alpha_1\sin\beta\cdot m_{22}+\cos\alpha_2\sin\beta\cdot m_{11},\quad b_{tp1}=\cos\alpha_1\sin\beta\cdot c_{22}+\cos\alpha_2\sin\beta\cdot c_{11}
$$

$$
b_{tp0}=\cos\alpha_1\sin\beta\cdot k_{22}+\cos\alpha_2\sin\beta\cdot k_{11}
$$

$$
b_{c2}=\sin\alpha_1 m_{22}+\sin\alpha_2 m_{11},\quad b_{c1}=\sin\alpha_1 c_{22}+\sin\alpha_2 c_{11},\quad b_{c0}=\sin\alpha_1 k_{22}+\sin\alpha_2 k_{11}
$$

$$
b_{fp2}=\cos\alpha_1\cos\beta\cdot m_{22}+\cos\alpha_2\cos\beta\cdot m_{11},\quad b_{fp1}=\cos\alpha_1\cos\beta\cdot c_{22}+\cos\alpha_2\cos\beta\cdot c_{11}
$$

$$
b_{fp0}=\cos\alpha_1\cos\beta\cdot k_{22}+\cos\alpha_2\cos\beta\cdot k_{11}.
$$

By the inverse Laplace transformation of Eq. 5.8, one can obtain:

$$
\begin{aligned}
&a_4y^{(4)}(t)+a_3y^{(3)}(t)+a_2y^{(2)}(t)+a_1y^{(1)}(t)+a_0y(t)\\
&=b_{tp2}F_t^{(2)}(t)+b_{tp1}F_t^{(1)}(t)+b_{tp0}F_t(t)+b_{c2}F_c^{(2)}(t)+b_{c1}F_c^{(1)}(t)+b_{c0}F_c(t)\\
&+b_{fp2}F_f^{(2)}(t)+b_{fp1}F_f^{(1)}(t)+b_{fp0}F_f(t)+b_{tp2}F_{pt}^{(2)}(t)+b_{tp1}F_{pt}^{(1)}(t)+b_{tp0}F_{pt}(t)\\
&+b_{fp2}F_{pf}^{(2)}(t)+b_{fp1}F_{pf}^{(1)}(t)+b_{fp0}F_{pf}(t)
\end{aligned}
\tag{5.9}
$$

In terms of the analyses in Chapter 2, the uncut chip thickness u(t) is

$$
u(t)=u_0(t)-y(t)+\mu\cdot y(t-\tau) \tag{5.10}
$$

where μ is the overlapping coefficient, τ is time delay of the system, and y(t) is the displacement. Due to the effect of hysteresis between the forces and uncut chip thickness, the forces can be expressed as:

$$F_t(t) = p_t u(t) + g_t(u(t)) = p_t(u_0(t) - y(t) + \mu y(t-\tau)) + g_t(u_0(t) - y(t) + \mu y(t-\tau)) \quad (5.11)$$

$$F_c(t) = p_c u(t) + g_c(u(t)) = p_c(u_0(t) - y(t) + \mu y(t-\tau)) + g_c(u_0(t) - y(t) + \mu y(t-\tau)) \quad (5.12)$$

$$F_f(t) = p_f u(t) + g_f(u(t)) = p_f(u_0(t) - y(t) + \mu y(t-\tau)) + g_f(-y(t) + \mu y(t-\tau)) \quad (5.13)$$

To simplify the above equations, the corresponding backlashes can replace them,

$$\begin{aligned} F_t(t) &= A_t u(t) \pm B_t^{'} = A_t(u_0(t) - y(t) + \mu \cdot y_\tau(t)) \pm B_t^{'} = -A_t y(t) + A_t \mu \cdot y_\tau(t) \pm B_t \\ F_c(t) &= A_c u(t) \pm B_c^{'} = A_c(u_0(t) - y(t) + \mu \cdot y_\tau(t)) \pm B_c^{'} = -A_c y(t) + A_c \mu \cdot y_\tau(t) \pm B_c \\ F_f(t) &= A_f u(t) \pm B_f^{'} = A_f(u_0(t) - y(t) + \mu\ y_\tau(t)) \pm B_f^{'} = -A_f y(t) + A_f \mu \cdot y_\tau(t) \pm B_f \end{aligned} \quad (5.14)$$

where $y_\tau(t) = y(t-\tau)$; $B_t = A_t u_0(t) \pm B_t^{'}$; $B_c = A_c u_0(t) \pm B_c^{'}$; $B_f = A_f u_0(t) \pm B_f^{'}$; other parameters are defined in Eq. 2.14 and 2.15.

Substitute Eq. 5.14 into Eq. 5.9, the dynamic equation of the system will be as following:

$$\begin{aligned} &a_4 y^{(4)}(t) + a_3 y^{(3)}(t) + a_2 y^{(2)}(t) + a_1 y^{(1)}(t) + a_0 y(t) \\ &= b_{tp2}(-A_t y^{(2)}(t) + \mu A_t y_\tau^{(2)}(t)) + b_{tp1}(-A_t y^{(1)}(t) + \mu A_t y_\tau^{(1)}(t)) + b_{tp0}(-A_t y(t) + \mu A_t y_\tau(t) \pm B_t) \\ &+ b_{c2}(-A_c y^{(2)}(t) + \mu A_c y_\tau^{(2)}(t)) + b_{c1}(-A_c y^{(1)}(t) + \mu A_c y_\tau^{(1)}(t)) + b_{c0}(-A_c y(t) + \mu A_c y_\tau(t) \pm B_c) \\ &+ b_{fp2}(-A_f y^{(2)}(t) + \mu A_f y_\tau^{(2)}(t)) + b_{fp1}(-A_f y^{(1)}(t) + \mu A_f y_\tau^{(1)}(t)) + b_{fp0}(-A_f y(t) + \mu A_f y_\tau(t) \pm B_f) \\ &+ b_{tp2} F_{pt}^{(2)}(t) + b_{tp1} F_{pt}^{(1)}(t) + b_{tp0} F_{pt}(t) + b_{fp2} F_{pf}^{(2)}(t) + b_{fp1} F_{pf}^{(1)}(t) + b_{fp0} F_{pf}(t) \end{aligned} \quad (5.15)$$

So, the Eq. 5.15 can be simplified into the following form,

$$\begin{aligned} &\overline{a_4} y^{(4)}(t) + \overline{a_3} y^{(3)}(t) + \overline{a_2} y^{(2)}(t) + \overline{a_1} y^{(1)}(t) + \overline{a_0} y(t) \\ &= r_2 y_\tau^{(2)}(t) + r_1 y_\tau^{(1)}(t) + r_0 y_\tau(t) + b_{tp0} F_{pt}(t) + b_{fp0} F_{pf}(t) + e(t, F_{pt}^{(2)}, F_{pt}^{(1)}, F_{pf}^{(2)}, F_{pf}^{(1)}) \end{aligned} \quad (5.16)$$

where $\overline{a_4} = a_4$, $\overline{a_3} = a_3$, $\overline{a_2} = a_2 + b_{pt2} A_t + b_{fp2} A_f + b_{c2} A_c$, $\overline{a_1} = a_1 + b_{pt1} A_t + b_{fp1} A_f + b_{c1} A_c$, $\overline{a_0} = a_0 + b_{pt0} A_t + b_{fp0} A_f + b_{c0} A_c$, $r_2 = \mu\,(b_{tp2} A_t + b_{fp2} A_f + b_{c2} A_c)$, $r_1 = \mu\,(b_{tp1} A_t + b_{fp1} A_f + b_{c1} A_c)$, $r_0 = \mu\,(b_{tp0} A_t + b_{fp0} A_f + b_{c0} A_c)$, $r_{\pm b} = \pm(b_{tp0} B_t + b_{fp0} B_f + b_{c0} B_c)$, $e\,(t, F_{pt}^{(2)}, F_{pt}^{(1)}, F_{pf}^{(2)}, F_{pf}^{(1)}) = r_{\pm b} + b_{tp2} F_{pt}^{(2)}(t) + b_{tp1} F_{pt}^{(1)}(t) + b_{fp2} F_{pf}^{(2)}(t) + b_{fp1} F_{pf}^{(1)}(t)$.

Remark A: The term $e(t, F_{pt}^{(2)}, F_{pt}^{(1)}, F_{pf}^{(2)}, F_{pf}^{(1)})$ is the lumped uncertain element in Eq. 5.1; Its upper bound is assumed to be known, i.e., $\| e(t, F_{pt}^{(2)}, F_{pt}^{(1)}, F_{pf}^{(2)}, F_{pf}^{(1)}) \| \le \rho(t)$.

5.2.1 Design Control Law

Proceeding in the usual fashion, define the switching surface $\sigma(t) \in R^{2\times 1}$

$$\sigma(t) = \begin{pmatrix} \sigma_1(t) \\ \sigma_2(t) \end{pmatrix} = S \cdot X(t) = \begin{pmatrix} s_{11}x_1(t) + s_{12}x_2(t) + s_{13}x_3(t) + s_{14}x_4(t) \\ s_{21}x_1(t) + s_{22}x_2(t) + s_{23}x_3(t) + s_{24}x_4(t) \end{pmatrix} = 0 \tag{5.20}$$

where $S \in R^{2\times 4}$, $X(t) \in R^{4\times 1}$, s_{11}, s_{12}, s_{13}, s_{14}, s_{21}, s_{22}, s_{23}, s_{24} are positive coefficients respectively, $x_1(t)$, $x_2(t)$, $x_3(t)$, $x_4(t)$ are the state variables in Eq. 5.1.

Similar to Chapter 4, a tuning error σ_t is defined:

$$\sigma_{it}(t) = \sigma_i(t) - \varepsilon \cdot sat\left(\frac{\sigma_i(t)}{\varepsilon}\right), \quad (i = 1,\ 2) \tag{5.21}$$

where ε is an arbitrary positive constant, $sat(\cdot)$ is the saturation function and $\sigma(t)$ is the sliding surface defined by Eq. 5.20.

Differentiating $\sigma(t)$ with respect to time t, and substituting Eq. 5.2 and 5.3, one has

$$\dot{\sigma}(t) = \frac{\partial \sigma(t)}{\partial x}\dot{x}(t) = \begin{pmatrix} s_{11} & s_{12} & s_{13} & s_{14} \\ s_{21} & s_{22} & s_{23} & s_{24} \end{pmatrix} \begin{pmatrix} \dot{x}_1(t) \\ \dot{x}_2(t) \\ \dot{x}_3(x) \\ \dot{x}_4(x) \end{pmatrix} \tag{5.22}$$

The above state variables are chosen as:

$x_1(t) = y(t)$, $x_2(t) = \dot{x}_1(t)$, $x_3(t) = \dot{x}_2(t)$, $x_4(t) = \dot{x}_3(t)$. Therefore

$$\dot{\sigma}(t) = \frac{\partial \sigma(t)}{\partial x}\dot{x}(t) = \begin{pmatrix} s_{11} & s_{12} & s_{13} & s_{14} \\ s_{21} & s_{22} & s_{23} & s_{24} \end{pmatrix} \begin{pmatrix} \dot{y}(t) \\ \ddot{y}(t) \\ \dddot{y}(x) \\ \Omega(x) \end{pmatrix} \tag{5.23}$$

where $Y_r(t) = r_2 y_r^{(2)}(t) + r_1 y_r^{(1)} + r_0 y_r(t)$, $e(t) = e(t, F_{pt}^{(2)}, F_{pt}^{(1)}, F_{pf}^{(2)}, F_{pf}^{(1)})$,

$$\Omega(x) = -\frac{\overline{a_0}}{a_4} y(t) - \frac{\overline{a_1}}{a_4} y^{(1)}(t) - \frac{\overline{a_2}}{a_4} y^{(2)}(t) - \frac{\overline{a_3}}{a_4} y^{(3)}(t) + \frac{1}{a_4}(Y_r(t) + e(t)) + \frac{b_{fp0}}{a_4} F_{pf}(t) + \frac{b_{tp0}}{a_4} F_{pt}(t).$$

Each element of the sliding surface $\sigma(t)$ is

$$\begin{aligned}
\dot{\sigma}_1(t) = {} & (s_{11} - s_{14}\frac{\overline{a_1}}{a_4}) y^{(1)}(t) + (s_{12} - s_{14}\frac{\overline{a_2}}{a_4}) y^{(2)}(t) + (s_{13} - s_{14}\frac{\overline{a_3}}{a_4}) y^{(3)}(t) \\
& - s_{14}\frac{\overline{a_0}}{a_4} y(t) + \frac{s_{14}}{a_4}(Y_r(t) + e(t)) + s_{14}\frac{b_{tpo}\, p_t}{a_4} v_t(t) + s_{14}\frac{b_{tpo}}{a_4} g_t(v_t(t)) \\
& + s_{14}\frac{b_{fpo}\, p_f}{a_4} v_f(t) + s_{14}\frac{b_{fpo}}{a_4} g_f(v_f(t))
\end{aligned} \tag{5.24}$$

$$\begin{aligned}
\dot{\sigma}_2(t) = {} & (s_{21} - s_{24}\frac{\overline{a_1}}{a_4}) y^{(1)}(t) + (s_{22} - s_{24}\frac{\overline{a_2}}{a_4}) y^{(2)}(t) + (s_{23} - s_{24}\frac{\overline{a_3}}{a_4}) y^{(3)}(t) \\
& - s_{24}\frac{\overline{a_0}}{a_4} y(t) + \frac{s_{24}}{a_4}(Y_r(t) + e(t)) + s_{24}\frac{b_{tpo}\, p_t}{a_4} v_t(t) + s_{24}\frac{b_{tpo}}{a_4} g_t(v_t(t)) \\
& + s_{24}\frac{b_{fpo}\, p_f}{a_4} v_f(t) + s_{24}\frac{b_{fpo}}{a_4} g_f(v_f(t))
\end{aligned} \tag{5.25}$$

where $b_{pto} = K_{pt} b_{pt0}$, $b_{pfo}(v) = K_{pf} b_{pf0}$, K_{pt} and K_{pf} are the stiffness of the each piezoactuator.

The above equation can be transformed to the matrix form as follows

$$\begin{aligned}
\begin{pmatrix} \dot{\sigma}_1(t) \\ \dot{\sigma}_2(t) \end{pmatrix} = {} & \begin{pmatrix} A_{11} \\ A_{21} \end{pmatrix} y^{(1)}(t) + \begin{pmatrix} A_{12} \\ A_{22} \end{pmatrix} y^{(2)}(t) + \begin{pmatrix} A_{13} \\ A_{23} \end{pmatrix} y^{(3)}(t) + \begin{pmatrix} A_{14} \\ A_{24} \end{pmatrix} y(t) + \begin{pmatrix} A_{15} \\ A_{25} \end{pmatrix} y_r^{(2)}(t) + \begin{pmatrix} A_{16} \\ A_{26} \end{pmatrix} y_r^{(1)}(t) \\
& + \begin{pmatrix} A_{17} \\ A_{27} \end{pmatrix} y_r(t) + \begin{pmatrix} A_{18} \\ A_{28} \end{pmatrix} e(t) + \begin{pmatrix} N_{11} & N_{12} \\ N_{21} & N_{22} \end{pmatrix} \begin{pmatrix} v_t(t) \\ v_f(t) \end{pmatrix} + \begin{pmatrix} M_{11} & M_{12} \\ M_{21} & M_{22} \end{pmatrix} \begin{pmatrix} g_t(v_t) \\ g_f(v_f) \end{pmatrix}
\end{aligned} \tag{5.26}$$

where $A_{11} = s_{11} - s_{14}\frac{\overline{a_1}}{a_4}$, $A_{21} = s_{21} - s_{24}\frac{\overline{a_1}}{a_4}$, $A_{12} = s_{12} - s_{14}\frac{\overline{a_2}}{a_4}$, $A_{22} = s_{22} - s_{24}\frac{\overline{a_2}}{a_4}$,

$A_{13} = s_{13} - s_{14}\frac{\overline{a_3}}{a_4}$, $A_{23} = s_{23} - s_{24}\frac{\overline{a_3}}{a_4}$, $A_{14} = -s_{14}\frac{\overline{a_0}}{a_4}$, $A_{24} = -s_{24}\frac{\overline{a_0}}{a_4}$, $A_{15} = \frac{s_{14} r_2}{a_4}$,

$A_{25} = \frac{s_{24} r_2}{a_4}$, $A_{16} = \frac{s_{14} r_1}{a_4}$, $A_{26} = \frac{s_{24} r_1}{a_4}$, $A_{17} = \frac{s_{14} r_0}{a_4}$, $A_{27} = \frac{s_{24} r_0}{a_4}$, $A_{18} = \frac{s_{14}}{a_4}$, $A_{28} = \frac{s_{24}}{a_4}$,

$N_{11} = \frac{s_{14} b_{tpo} p_t}{a_4}$, $N_{12} = \frac{s_{14} b_{fpo} p_f}{a_4}$, $N_{21} = \frac{s_{24} b_{tpo} p_t}{a_4}$, $N_{22} = \frac{s_{24} b_{fpo} p_f}{a_4}$,

$M_{11} = \frac{s_{14} b_{tpo}}{a_4}$, $M_{12} = \frac{s_{14} b_{fpo}}{a_4}$, $M_{21} = \frac{s_{24} b_{tpo}}{a_4}$, $M_{22} = \frac{s_{24} b_{fpo}}{a_4}$.

Define $\overline{A_1} = \begin{pmatrix} A_{11} \\ A_{21} \end{pmatrix}$, $\overline{A_2} = \begin{pmatrix} A_{12} \\ A_{22} \end{pmatrix}$, $\overline{A_3} = \begin{pmatrix} A_{13} \\ A_{23} \end{pmatrix}$, $\overline{A_4} = \begin{pmatrix} A_{14} \\ A_{24} \end{pmatrix}$, $\overline{A_5} = \begin{pmatrix} A_{15} \\ A_{25} \end{pmatrix}$, $\overline{A_6} = \begin{pmatrix} A_{16} \\ A_{26} \end{pmatrix}$ $\overline{A_7} = \begin{pmatrix} A_{17} \\ A_{27} \end{pmatrix}$

$\overline{A_8} = \begin{pmatrix} A_{18} \\ A_{28} \end{pmatrix}$, $\overline{N} = \begin{pmatrix} N_{11} & N_{12} \\ N_{21} & N_{22} \end{pmatrix}$, $\overline{M} = \begin{pmatrix} M_{11} & M_{12} \\ M_{21} & M_{22} \end{pmatrix}$, $v(t) = \begin{pmatrix} v_t(t) \\ v_f(t) \end{pmatrix}$, $g(v) = \begin{pmatrix} g_t(v_t) \\ g_f(v_f) \end{pmatrix}$.

In terms of the above definitions, the Eq. 5.26 can be rewritten as:

$$\dot{\sigma}(t) = \overline{A_1} y^{(1)}(t) + \overline{A_2} y^{(2)}(t) + \overline{A_3} y^{(3)}(t) + \overline{A_4} y(t) + \overline{A_5} y_\tau^{(2)}(t) + \overline{A_6} y_\tau^{(1)}(t) + \overline{A_7} y_\tau(t) + \overline{A_8} e(t) + \overline{N} v(t) + \overline{M} g(v). \tag{5.27}$$

Define $\theta_1 = \overline{N}^{-1}\overline{A_1}$, $\theta_2 = \overline{N}^{-1}\overline{A_2}$, $\theta_3 = \overline{N}^{-1}\overline{A_3}$, $\theta_4 = \overline{N}^{-1}\overline{A_4}$, $\theta_5 = \overline{N}^{-1}\overline{A_5}$, $\theta_6 = \overline{N}^{-1}\overline{A_6}$, $\theta_7 = \overline{N}^{-1}\overline{A_7}$.

$\theta_i \in R^{2\times 1}$ ($i = 1,\ 2,\ 3,\ 4,\ 5,\ 6,\ 7$).

For the designs of the control laws, the following assumptions concerning the systems and hysteresis are required,

Assumption 1:

There exist positive scalars q_1, q_2, q_3, such that $\| y^{(2)}(t+\tau) \| \le q_1 \| y^{(2)}(t) \|$, $\| y^{(1)}(t+\tau) \| \le q_2 \| y^{(1)}(t) \|$ and $\| y(t+\tau) \| \le q_3 \| y(t) \|$.

Assumption 2:

There exist known constants $b_{tp0\min}$ and $b_{tp0\max}$ such that the control gain b_{tp0} in Eq. 5.16 satisfies $b_{tp0} \in \lfloor b_{tp0\min}, b_{tp0\max} \rfloor$.

There also exist known constants $b_{fp0\min}$ and $b_{fp0\max}$ such that the control gain b_{fp0} in Eq. 5.16 satisfies $b_{fp0} \in \lfloor b_{fp0\min}, b_{fp0\max} \rfloor$.

Assumption 3:

There exist known constants $p_{t\min}$ and $p_{t\max}$ such that the control gain p_t in Eq. 5.16 satisfies $p_t \in [p_{t\min}, p_{t\max}]$.

There also exist known constants $p_{f\min}$ and $p_{f\max}$ such that the control gain p_f in Eq. 5.16 satisfies $p_f \in [p_{f\min}, p_{f\max}]$.

Assumption 4:

Define $\theta \in \Omega_\theta = \{\theta : \theta_{i\min} \le \theta_i \le \theta_{i\max}. \forall i \in \{1, r\}\}$, where $\theta_{i\min}$ and $\theta_{i\max}$ are known real numbers.

Assumption 5:

In Eqs. 5.2 and 5.3, $\| g(v) \| \le \rho_a$, ρ_a is constant.

With respect to the plant and hysteresis models subject to the assumptions, the following control law and adaptation mechanism are presented:

$$v(t) = -[k_r \sigma(t) + \hat{\theta}_1(t) y^{(1)}(t) + \hat{\theta}_2(t) y^{(2)}(t) + \hat{\theta}_3(t) y^{(3)}(t) + \hat{\theta}_4(t) y + \hat{\theta}_5(t) \| y^{(2)}(t) \| + \hat{\theta}_6(t) \| y^{(1)}(t) \| + \hat{\theta}_7(t) \| y(t) \| + k^* sat(\frac{\sigma(t)}{\varepsilon})] \quad (5.28)$$

where $v(t) \in R^{2X1}$; k_r, k^* are constant positive gains; $\dot{\hat{\theta}}_i = proj(\hat{\theta}_i, -\gamma_i \omega_i)$ $(i = 1, 2, 3, 4, 5, 6, 7)$, $proj(\cdot,\cdot)$ is a projection function defined as

$$proj(\hat{\theta}_i, -\gamma_i \omega_i) = \begin{cases} 0 & if\ (\hat{\theta}_i > \theta_{\max}\ and\ \gamma_i \omega_i < 0)\ or\ (\hat{\theta}_i < \theta_{\min}\ and\ \gamma_i \omega_i > 0) \\ -\gamma_i \omega_i & if\ (\theta_{\min} < \hat{\theta}_i < \theta_{\max})\ or\ (\hat{\theta}_i > \theta_{\max}\ and\ \gamma_i \omega_i \ge 0) \\ & or\ \hat{\theta}_i < \theta_{\min}\ and\ \gamma_i \omega_i \le 0) \end{cases} \quad (5.29)$$

Define $\omega_1(t) = \sigma_t(t) y^{(1)}(t)$, $\omega_2(t) = \sigma_t(t) y^{(2)}(t)$, $\omega_3(t) = \sigma_t(t) y^{(3)}(t)$, $\omega_4(t) = \sigma_t(t) y(t)$,

$\omega_5(t) = \sigma_t(t) \| y^{(2)}(t) \|$, $\omega_6(t) = \sigma_t(t) \| y^{(1)}(t) \|$, $\omega_7(t) = \sigma_t(t) \| y(t) \|$;

and scalars $\gamma_i (i = 1, 2, 3, 4, 5, 6, 7)$ are coefficients selected by the designers.

5.2.2 Stability Analysis of the System

To establish global bound, a Lyapunov function candidate for the system in Eq. 5.1 is defined as:

$$V(t)=\frac{1}{2}\{\sigma_t^T N\sigma_t(t)+\sum_{i=1}^{4}[\frac{1}{\gamma_i}(\hat{\theta}_i(t)-\theta_i)^T(\hat{\theta}_i(t)-\theta_i)]+\sum_{i=5}^{7}[\frac{1}{\gamma_i}(\hat{\theta}_i(t)-q_{i-4}\theta_i)^T(\hat{\theta}_i(t)-q_{i-4}\theta_i)]\} \quad (5.30)$$

Case 1: when $\| \sigma(t) \| \le \varepsilon$, the derivative $\dot{V}(t)$ exists for all $\sigma(t)$, which is $\dot{V}(t)=0$.

Case 2: When $\| \sigma(t) \| > \varepsilon$, using Eq. 5.27 and the fact $\dot{\sigma}=\dot{\sigma}_t$, one can obtain:

$$\begin{aligned}\dot{V}(t) &= \sigma_t^T \overline{N}^{-1}\dot{\sigma}+\sum_{i=1}^{4}[\frac{1}{\gamma_i}(\hat{\theta}_i(t)-\theta_i)^T\dot{\hat{\theta}}_i]+\sum_{i=5}^{7}[\frac{1}{\gamma_i}(\hat{\theta}_i(t)-q_{i-4}\theta_i)^T\dot{\hat{\theta}}_i] \\ &= \sum_{i=1}^{4}[\frac{1}{\gamma_i}(\hat{\theta}_i(t)-\theta_i)^T\dot{\hat{\theta}}_i]+\sum_{i=5}^{7}[\frac{1}{\gamma_i}(\hat{\theta}_i(t)-q_{i-4}\theta_i)^T\dot{\hat{\theta}}_i]+\sigma_t^T\overline{N}^{-1}(\overline{A}_1 y^{(1)}(t)+\overline{A}_2 y^{(2)}(t)+\overline{A}_3 y^{(3)}(t)+\overline{A}_4 y(t) \\ &+\overline{A}_5 y_r^{(2)}(t)+\overline{A}_6 y_r^{(1)}(t)+\overline{A}_7 y_r(t)+\overline{A}_8 e(t)+\overline{N}v(t)+\overline{M}g(v)) \end{aligned} \quad (5.31)$$

As a projection function, $(\hat{\theta}_i-m_i\theta_i)proj(\hat{\theta}_i,r_i\varpi_i)\le(\hat{\theta}_i-m_i\theta_i)r_i\varpi_i$, m_i is positive scalars. Then

$$\begin{aligned}\dot{V}(t) &\le \sigma_t^T(\theta_1 y^{(1)}+\theta_2 y^{(2)}+\theta_3 y^{(3)}+\theta_4 y+\theta_5 y_r^{(2)}+\theta_6 y_r^{(1)}+\theta_7 y_r+\overline{N}^{-1}\overline{A}_8 e(t)) \\ &+\sigma_t^T(v(t)+\overline{N}^{-1}\overline{M}g(v))+\sigma_t^T((\hat{\theta}_1-\theta_1)y^{(1)}+(\hat{\theta}_2-\theta_2)y^{(2)}+(\hat{\theta}_3-\theta_3)y^{(3)} \\ &+(\hat{\theta}_4-\theta_4)y+(\hat{\theta}_5-q_1\theta_5)\| y^{(2)}\|+(\hat{\theta}_6-q_2\theta_6)\| y^{(1)}\|+(\hat{\theta}_7-q_3\theta_7)\| y\|) \\ &\le \sigma_t^T(\theta_1 y^{(1)}+\theta_2 y^{(2)}+\theta_3 y^{(3)}+\theta_4 y+\theta_5 q_3\| y^{(2)}\|+\theta_6 q_2\| y^{(1)}\|+\theta_7 q_1\| y\|+\overline{N}^{-1}\overline{A}_8 e(t)) \\ &+\sigma_t^T(v(t)+\overline{N}^{-1}\overline{M}g(v))+\sigma_t^T((\hat{\theta}_1-\theta_1)y^{(1)}+(\hat{\theta}_2-\theta_2)y^{(2)}+(\hat{\theta}_3-\theta_3)y^{(3)} \\ &+(\hat{\theta}_4-\theta_4)y+(\hat{\theta}_5-q_1\theta_5)\| y^{(2)}\|+(\hat{\theta}_6-q_2\theta_6)\| y^{(1)}\|+(\hat{\theta}_7-q_3\theta_7)\| y\|) \\ &\le \sigma_t^T(\overline{N}^{-1}\overline{A}_8 e(t)+\overline{N}^{-1}\overline{M}g(v))-\sigma_t^T(k_r\sigma(t)+\hat{\theta}_1 y^{(1)}(t)+\hat{\theta}_2 y^{(2)}(t) \\ &+\hat{\theta}_3 y^{(3)}(t)+\hat{\theta}_4 y+\hat{\theta}_5\| y^{(2)}(t)\|+\hat{\theta}_6\| y^{(1)}(t)\|+\hat{\theta}_7\| y(t)\|+k^* sat(\frac{\sigma}{\varepsilon})) \\ &+\sigma_t^T(\hat{\theta}_1 y^{(1)}+\hat{\theta}_2 y^{(2)}+\hat{\theta}_3 y^{(3)}+\hat{\theta}_4 y+\hat{\theta}_5\| y^{(2)}\|+\hat{\theta}_6\| y^{(1)}\|+\hat{\theta}_7\| y\|) \\ &\le -\sigma_t^T k_r\sigma(t)-\sigma_t^T k^* sat(\frac{\sigma}{\varepsilon})+\sigma_t^T(\overline{N}^{-1}\overline{A}_8 e(t)+\overline{N}^{-1}\overline{M}g(v)) \\ &\le -\sigma_t^T k_r\sigma_t(t)-\sigma_t^T k^* sat(\frac{\sigma}{\varepsilon})+\sigma_t^T(\overline{N}^{-1}\overline{A}_8 e(t)+\overline{N}^{-1}\overline{M}g(v)) \end{aligned} \quad (5.32)$$

As the definition in Eq 5.21, $\sigma(t)\in R^{2X1}$ and $sat(\frac{\sigma(t)}{\varepsilon})=\left[sat(\frac{\sigma_1(t)}{\varepsilon}) \quad sat(\frac{\sigma_2(t)}{\varepsilon})\right]^T$,

$$\text{So } \sigma_t^T k^* sat(\frac{\sigma}{\varepsilon}) = (|\sigma_1| + |\sigma_2|) \cdot k^* = \| \sigma_t \| \cdot k^* \tag{5.33}$$

Eq. 5.32 can be rewritten as:

$$\dot{V}(t) \le -\sigma_t^T k_\tau \sigma_t(t) - \| \sigma_t^T \| k^* + \| \sigma_t^T \| \cdot \| \overline{N}^{-1} \| (\| \overline{A}_s \| \cdot \| e(t) \| + \| \overline{M} \| \cdot \| g(v) \|) \tag{5.34}$$

In the *Assumption 5* and the *Remark A*, $\|g(v)\| \le \rho_a$ and $\|e(t)\| \le \rho(t)$ are assumed.

While defines $k^* = k^*_{\max} \ge \| \overline{N}^{-1} \| (\| \overline{A}_s \| \cdot \rho(t) + \| \overline{M} \| \cdot \rho_a)$. We can yield

$$\begin{aligned} \dot{V}(t) &\le -k_\tau \| \sigma_t(t) \|^2 - \| \sigma_t^T \| \cdot k^*_{\max} + \| \sigma_t^T \| \cdot \| \overline{N}^{-1} \| (\| \overline{A}_s \| \cdot \| e(t) \| + \| \overline{M} \| \cdot \| g(v) \|) \\ &\le -k_\tau \| \sigma_t(t) \|^2 \qquad \forall \| \sigma(t) \| > \varepsilon \end{aligned} \tag{5.35}$$

Based on the above analyses and proof, the following theorem regarding the stability of the closed-loop system described by Eqs. (5.2), (5.3), (5.16) and (5.28) can be established.

Theorem: For the plant in Eq. (5.1) subject to *Assumptions 1-5* and *Remark A*, the robust adaptive controller specified by Eq. (5.28) ensures that all the closed-loop signals are bounded and the state variable $y(t)$ converges to zero for $\forall t \ge t_0$.

5.3 Simulation Results

In order to eliminate the chatter in metal cutting processes, the adaptive controller developed in Eq. 5.28 is introduced into the system in Eq. 5.1. The parameters involved in all equations in the simulations are listed in Table B. Fig. 5.3 shows the dynamic response of the metal cutting system in Eq. 5.1 combined with the control law in Eq. 5.28; Fig. 5.4 illustrates the dynamic response of the main cutting force $F_c(t)$ during the cutting process; Fig. 5.5 represents the dynamic response of the thrust force $F_t(t)$ during the cutting process; Fig. 5.6 plots the dynamic response of the feed force $F_f(t)$ during the cutting process.

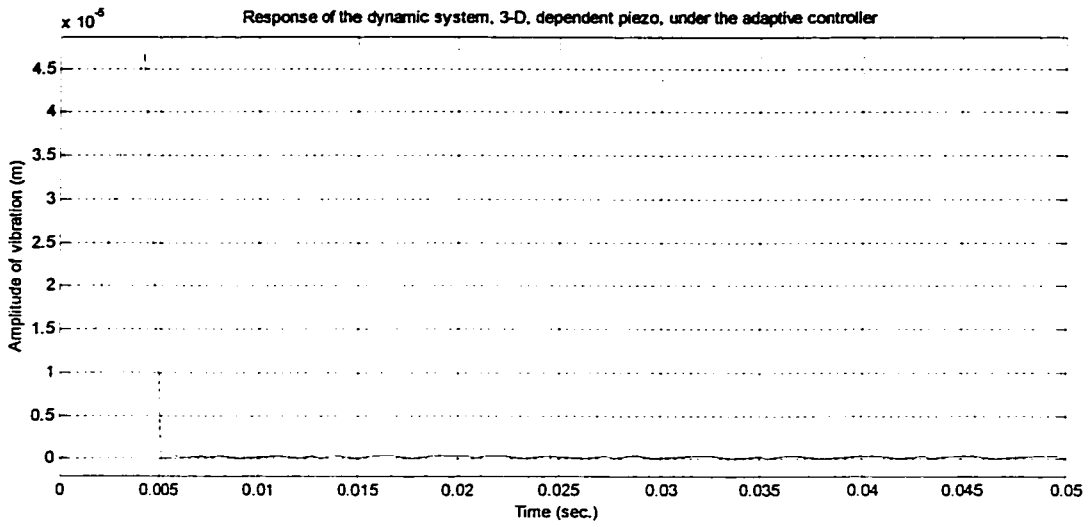

Figure 5.3 Response of dynamic system with the control law

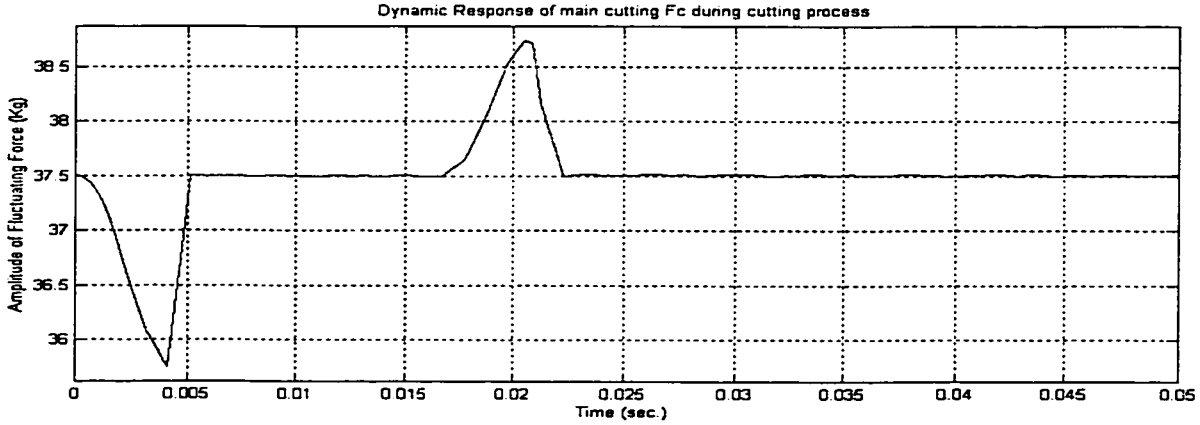

Figure 5.4 Response of main cutting force $F_c(t)$ during cutting process

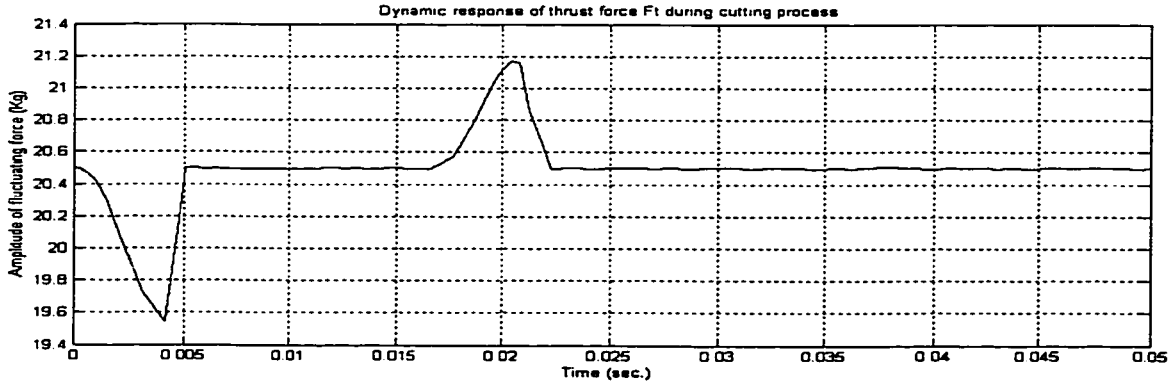

Figure 5.5 Response of thrust force $F_t(t)$ during cutting process

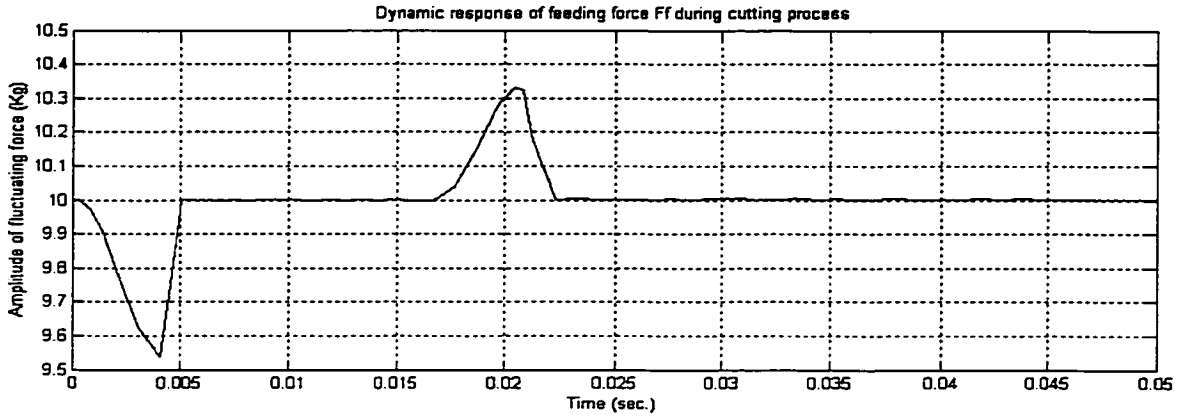

Figure 5.6 Response of feed force $F_f(t)$ during cutting process

From Fig. 5.3 through Fig. 5.6, the simulations of the turning system with the adaptive control laws in Eq. 5.28 show clearly that the proposed adaptive controllers can significantly suppress the chatter during the metal cutting processes.

5.4 Summary

In this chapter, in order to suppress the chatter in the metal cutting processes, two piezoactuators are introduced the system; the metal cutting process is modeled as a class of uncertain linear system with the hysteretic characteristic and time lag; two adaptive control laws for the suppression of chatter in the system are designed; the simulation results show that the designed control laws significantly eliminates the chatter effect in the metal cutting process.

Chapter 6

Chatter Suppression for the Controlled System with 2-D Model and Independent Piezoactuator

Introduction – in the metal cutting system with two degree-of-freedom, a piezoactuator is introduced for the regulation of the displacement between the cutting tool and workpiece. The closed-loop dynamic of the metal cutting system involving two-dimensional force model is presented. The piezoactutor, the structure of which is independent from the tool holder, exhibits the hysteretic characteristics. For overcoming the chatter, the adaptive control law is presented. The simulations for the dynamic performances of this system with a piezoactuator are shown.

6.1 Dynamic Model of Turning Process

The schematic model of the metal cutting system with two degree-of-freedom and two-dimensional force models is illustrated in Fig. 6.1. The dynamic cutting process is demonstrated in the magnified contact parts of workpiece and cutting tool. The work focuses on the type A of chatter that is normal to the cutting surface of work-piece. Considering the structure of the piezoactuator as an independent free mechanical body with the cutting tool, the structural turning system may be represented as in Fig. 6.1.

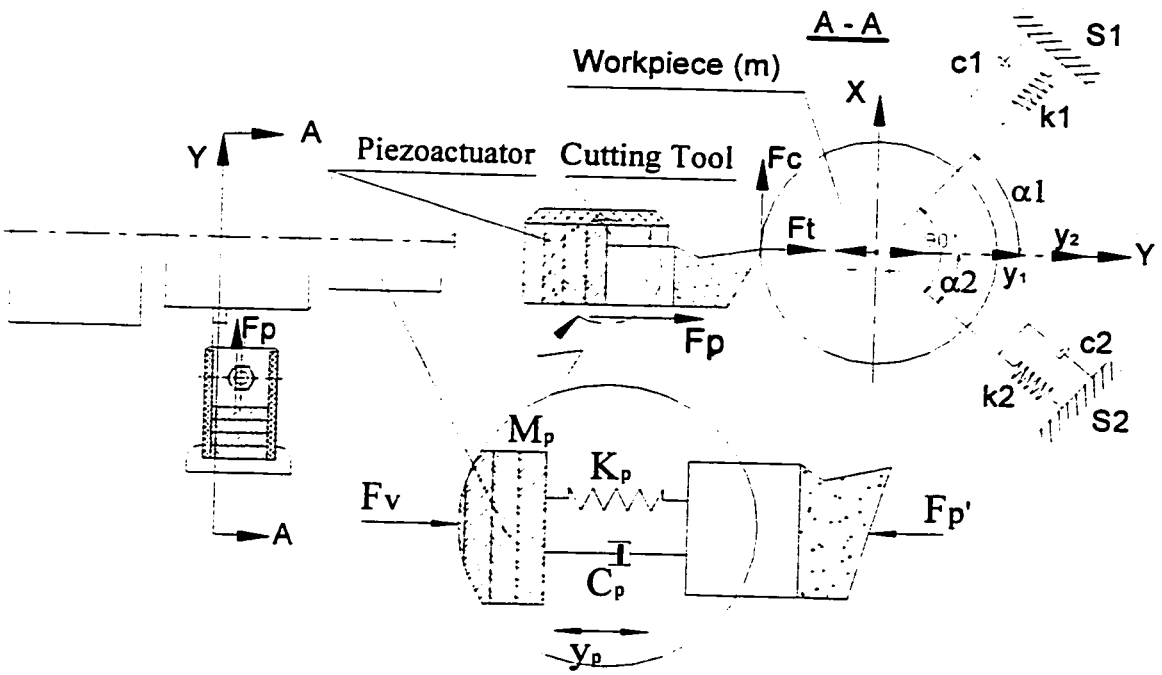

Figure 6.1 Schematic model of turning system with independent piezoactuators and 2-D force models

In Fig. 6.1, the dynamic process of above metal cutting system can be described with a linear second order function as following:

$$\begin{pmatrix} \frac{m}{\cos\alpha_1} & 0 \\ 0 & \frac{m}{\cos\alpha_2} \end{pmatrix} \begin{pmatrix} \frac{d^2y_1}{dt^2} \\ \frac{d^2y_2}{dt^2} \end{pmatrix} + \begin{pmatrix} \frac{c_1}{\cos\alpha_1} & 0 \\ 0 & \frac{c_2}{\cos\alpha_2} \end{pmatrix} \begin{pmatrix} \frac{dy_1}{dt} \\ \frac{dy_2}{dt} \end{pmatrix} + \begin{pmatrix} \frac{k_1}{\cos\alpha_1} & 0 \\ 0 & \frac{k_2}{\cos\alpha_2} \end{pmatrix} \begin{pmatrix} y_1 \\ y_2 \end{pmatrix}$$

$$= \begin{pmatrix} \cos\alpha_1 & \sin\alpha_1 \\ \cos\alpha_2 & \sin\alpha_2 \end{pmatrix} \begin{pmatrix} F_t \\ F_c \end{pmatrix} + \begin{pmatrix} \cos\alpha_1 \\ \cos\alpha_2 \end{pmatrix} F_p \qquad (6.1)$$

$$F_v = m_p \frac{d^2y_p}{dt^2} + F_p \qquad (6.2)$$

where y_1, y_2 represent the relative displacements between the tool and workpiece normal to machined surface in each degree-freedom direction; m, c_i, k_i are the equivalent mass, equivalent damping coefficient and equivalent spring stiffness of vibration structure respectively in each

direction S1 or S2; F_t, F_c are the thrust and main cutting forces exciting the structure; F_v represents the force generated by the piezoactuator; F_p is reaction force between the piezoactuator and workpiece; α_1, α_2 are geometrical angles of models of vibrations of structure relative to a line normal to machined surface; the definition of the $y_p(t)$ is given in the section 3.6 in Chapter 3; m_p is an equivalent mass of the piezoactuator.

The closed-loop dynamic system of the metal cutting system in turning with a piezoactuator and a adaptive control law designed in next section is illustrated as following:

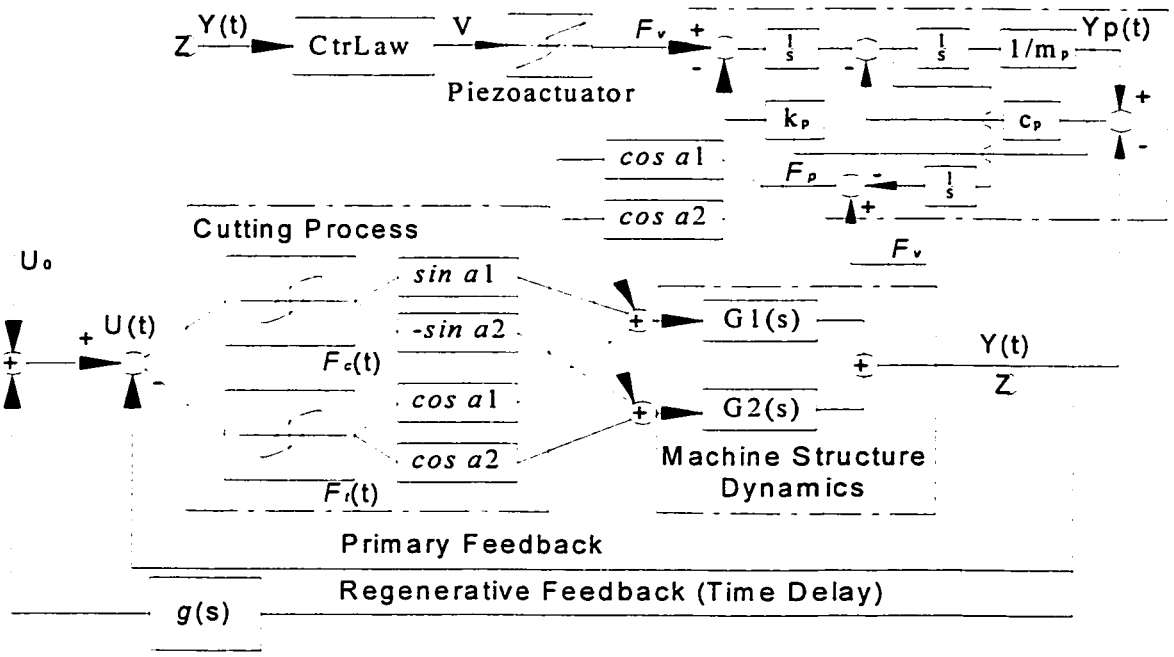

Figure 6.2 Block diagram of turning system with the piezoactuator and controller

According to the analyses in Eq. 3.4 in Chapter 3, the force F_v generated by the piezoactuator is defined as:

$$F_v(v) = K_p(p \cdot v(t) + g(v(t))) \tag{6.3}$$

where K_p is the stiffness of the piezoactuator, v(t) denotes as the applied voltage, other parameters are defined in Chapter 3.

6.2 Adaptive Controller design

Based on the mathematical model of the closed-loop dynamic system described in Eq. 6.1, the control law will be designed in order to suppress the chatter effect in the metal cutting process.

Based on Eq. 6.1, we can transform and calculate it further as follows:

$$\frac{m}{\cos\alpha_1}\frac{d^2y_1(t)}{dt^2}+\frac{c_1}{\cos\alpha_1}\frac{d\ y_1(t)}{dt}+\frac{k_1}{\cos\alpha_1}y_1(t)=\cos\alpha_1F_t(t)+\sin\alpha_1F_c(t)+\cos\alpha_1(F_v(t)-m_p\frac{d^2y_p(t)}{dt^2})$$

$$y_1(s)=\frac{\cos\alpha_1F_t(s)+\sin\alpha_1F_c(s)+\cos\alpha_1F_v(s)-\cos\alpha_1m_py_p(s)s^2}{\frac{m}{\cos\alpha_1}s^2+\frac{c_1}{\cos\alpha_1}s+\frac{k_1}{\cos\alpha_1}} \tag{6.4}$$

$$\frac{m}{\cos\alpha_2}\frac{d^2y_2(t)}{dt^2}+\frac{c_2}{\cos\alpha_2}\frac{d\ y_2(t)}{dt}+\frac{k_2}{\cos\alpha_2}y_2(t)=\cos\alpha_2F_t(t)+\sin\alpha_2F_c(t)+\cos\alpha_2(F_v(t)-m_p\frac{d^2y_p(t)}{dt^2})$$

$$y_2(s)=\frac{\cos\alpha_2F_t(s)+\sin\alpha_2F_c(s)+\cos\alpha_2F_v(s)-\cos\alpha_1m_py_p(s)s^2}{\frac{m}{\cos\alpha_2}s^2+\frac{c_2}{\cos\alpha_2}s+\frac{k_2}{\cos\alpha_2}} \tag{6.5}$$

The combination of Eqs. 6.4 and 6.5 yields

$$y(s)=y_1(s)+y_2(s)=\frac{\cos\alpha_1F_t(s)+\sin\alpha_1F_c(s)+\cos\alpha_1F_v(s)-\cos\alpha_1m_py_p(s)s^2}{\frac{m}{\cos\alpha_1}s^2+\frac{c_1}{\cos\alpha_1}s+\frac{k_1}{\cos\alpha_1}}$$
$$+\frac{\cos\alpha_2F_t(s)+\sin\alpha_2F_c(s)+\cos\alpha_2F_v(s)-\cos\alpha_2m_py_p(s)s^2}{\frac{m}{\cos\alpha_2}s^2+\frac{c_1}{\cos\alpha_2}s+\frac{k_1}{\cos\alpha_2}} \tag{6.6}$$

$$y(s)(m_{11}s^2+c_{11}s+k_{11})(m_{22}s^2+c_{22}s+k_{22})$$
$$=(\cos\alpha_1F_t(s)+\sin\alpha_1F_c(s)+\cos\alpha_1F_v(s)-\cos\alpha_1m_py_p(s)s^2)(m_{22}s^2+c_{22}s+k_{22})$$
$$+(\cos\alpha_2F_t(s)+\sin\alpha_2F_c(s)+\cos\alpha_2F_v(s)-\cos\alpha_2m_py_p(s)s^2)(m_{11}s^2+c_{11}s+k_{11}) \tag{6.7}$$

where

$$m_{11}=\frac{m}{\cos\alpha_1},\quad c_{11}=\frac{c_1}{\cos\alpha_1},\quad k_{11}=\frac{k_1}{\cos\alpha_1},\quad m_{22}=\frac{m}{\cos\alpha_2},\quad c_{22}=\frac{c_2}{\cos\alpha_2},\quad k_{22}=\frac{k_2}{\cos\alpha_2}.$$

For simplicity, rewrite Eq. 6.7 as:

$$y(s)(a_4s^4+a_3s^3+a_2s^2+a_1s+a_0)=$$
$$(F_t(s)+F_v(s))(b_{tp2}s^2+b_{tp1}s+b_{tp0})+F_c(s)(b_{c2}s^2+b_{c1}s+b_{c0})-y_p(s)s^2(m_{p4}s^2+m_{p3}s+m_{p2}) \quad (6.8)$$

where

$$a_4=m_{11}m_{22},\quad a_3=c_{11}m_{22}+c_{22}m_{11},\quad a_2=k_{11}m_{22}+k_{22}m_{11}+c_{11}c_{22},\quad a_1=k_{11}c_{22}+k_{22}c_{11},\quad a_0=k_{11}k_{22}$$

$$b_{tp2}=\cos\alpha_1m_{22}+\cos\alpha_2m_{11},\quad b_{tp1}=\cos\alpha_1c_{22}+\cos\alpha_2c_{11},\quad b_{tp0}=\cos\alpha_1k_{22}+\cos\alpha_2k_{11}$$

$$b_{c2}=\sin\alpha_1m_{22}+\sin\alpha_2m_{11},\quad b_{c1}=\sin\alpha_1c_{22}+\sin\alpha_2c_{11},\quad b_{c0}=\sin\alpha_1k_{22}+\sin\alpha_2k_{11}$$

$$m_{p4}=(\cos\alpha_1m_{22}+\cos\alpha_2m_{11})m_p,\quad m_{p3}=(\cos\alpha_1c_{22}+\cos\alpha_2c_{11})m_p,\quad m_{p2}=(\cos\alpha_1k_{22}+\cos\alpha_2k_{11})m_p$$

By the inverse Laplace transformation, one can obtain.

$$a_4y^{(4)}(t)+a_3y^{(3)}(t)+a_2y^{(2)}(t)+a_1y^{(1)}(t)+a_0y(t)$$
$$=b_{tp2}F_t^{(2)}(t)+b_{tp1}F_t^{(1)}(t)+b_{tp0}F_t(t)+b_{c2}F_c^{(2)}(t)+b_{c1}F_c^{(1)}(t)+b_{c0}F_c(t)$$
$$+b_{tp2}F_v^{(2)}(t)+b_{tp1}F_v^{(1)}(t)+b_{tp0}F_v(t)-(m_{p4}y_p^{(4)}(t)+m_{p3}y_p^{(3)}(t)+m_{p2}y_p^{(2)}(t)) \quad (6.9)$$

Based on the analyses in Chapter 2, the uncut chip thickness u(t):

$$u(t)=u_0(t)-y(t)+\mu\cdot y(t-\tau) \quad (6.10)$$

where μ is the overlapping coefficient, τ is time delay of the system, y(t) is the displacement

Due to the effect of hysteresis between the forces and uncut chip thickness, the forces are

$$F_t(t)=p_tu(t)+g_t(u(t))=p_t(u_0(t)-y(t)+\mu\cdot y(t-\tau))+g_t(u_0(t)-y(t)+\mu\cdot y(t-\tau)) \quad (6.11)$$
$$F_c(t)=p_cu(t)+g_c(u(t))=p_c(u_0(t)-y(t)+\mu\cdot y(t-\tau))+g_c(u_0(t)-y(t)+\mu\cdot y(t-\tau)) \quad (6.12)$$

To simplify the above Equations, the corresponding backlashes can be simplified as:

$$F_t(t)=A_tu(t)\pm B_t^{'}=A_t(u_0(t)-y(t)+\mu\cdot y_\tau(t))\pm B_t^{'}=-A_ty(t)+A_t\mu\cdot y_\tau(t)\pm B_t \quad (6.13)$$
$$F_c(t)=A_cu(t)\pm B_c^{'}=A_c(u_0(t)-y(t)+\mu\cdot y_\tau(t))\pm B_c^{'}=-A_cy(t)+A_c\mu\cdot y_\tau(t)\pm B_c \quad (6.14)$$

where $y_\tau(t)=y(t-\tau)$; $B_t=A_tu_0(t)\pm B_t^{'}$, $B_c=A_cu_0(t)\pm B_c^{'}$; other parameters are defined in Eqs. 2.14 and 2.15.

Substitute Eqs. 6.13 and 6.14 into Eq. 6.9, the dynamic system is

$$
\begin{aligned}
&a_4 y^{(4)}(t) + a_3 y^{(3)}(t) + a_2 y^{(2)}(t) + a_1 y^{(1)}(t) + a_0 y(t) \\
&= b_{tp2}(-A_t y^{(2)}(t) + \mu A_t y_\tau^{(2)}(t)) + b_{tp1}(-A_t y^{(1)}(t) + \mu A_t y_\tau^{(1)}(t)) + b_{tp0}(-A_t y(t) + \mu A_t y_\tau(t) \pm B_t) \\
&+ b_{c2}(-A_c y^{(2)}(t) + \mu A_c y_\tau^{(2)}(t)) + b_{c1}(-A_c y^{(1)}(t) + \mu A_c y_\tau^{(1)}(t)) + b_{c0}(-A_c y(t) + \mu A_c y_\tau(t) \pm B_c) \\
&+ b_{tp2} F_v^{(2)}(t) + b_{tp1} F_v^{(1)}(t) + b_{tp0} F_v(t) - (m_{p4} y_p^{(4)}(t) + m_{p3} y_p^{(3)}(t) + m_{p2} y_p^{(2)}(t))
\end{aligned}
$$

The above equation can be simplified as

$$
\begin{aligned}
&\overline{a_4} y^{(4)}(t) + \overline{a_3} y^{(3)}(t) + \overline{a_2} y^{(2)}(t) + \overline{a_1} y^{(1)}(t) + \overline{a_0} y(t) \\
&= r_2 y_\tau^{(2)}(t) + r_1 y_\tau^{(1)}(t) + r_0 y_\tau(t) + b_{tp0} F_v(t) + z(t, y_p^{(4)}, y_p^{(3)}, y_p^{(2)}) + e(t, F_v^{(1)}, F_v^{(2)})
\end{aligned} \tag{6.15}
$$

where $\overline{a_4} = a_4$, $\overline{a_3} = a_3$, $\overline{a_2} = a_2 + b_{pt2} A_t + b_{c2} A_c$, $\overline{a_1} = a_1 + b_{pt1} A_t + b_{c1} A_c$, $\overline{a_0} = a_0 + b_{pt0} A_t + b_{co} A_c$,
$r_2 = \mu\ (b_{tp2} A_t + b_{c2} A_c)$, $r_1 = \mu\ (b_{tp1} A_t + b_{c1} A_c)$, $r_0 = \mu\ (b_{tp0} A_t + b_{c0} A_c)$, $r_{\pm b} = \pm(b_{tp0} B_t + b_{c0} B_c)$,
$e\ (t, F_v^{(2)}, F_v^{(1)}) = b_{tp2} F_v^{(2)}(t) + b_{tp1} F_v^{(1)}(t)$, $z(t, y_p^{(4)}, y_p^{(3)}, y_p^{(2)}) = -(m_{p4} y_p^{(4)}(t) + m_{p3} y_p^{(3)}(t) + m_{p2} y_p^{(2)}(t)) + r_{\pm b}$.

Remark A: The term $e\ (t, F_v^{(2)}, F_v^{(1)})$ is the lumped uncertain element in Eq. 6.1, its upper bound is assumed to be known, i.e., $\| \ e\ (t, F_v^{(2)}, F_v^{(1)}) \ \| \le \rho(t)$.

6.2.1 Dynamic Estimate of $z(t, y_p^{(4)}, y_p^{(3)}, y_p^{(2)})$

The value of disturbance $z(t, y_p^{(4)}, y_p^{(3)}, y_p^{(2)})$ in Eq. 6.15 will be estimated dynamically. The detailed calculation can be referred to Appendix A. Based on Appendix A,

$$z_e(t) = w_2(t) b(\partial). \tag{6.16}$$

where $z_e(t)$ is denoted as the estimate of $z(t, y_p^{(4)}, y_p^{(3)}, y_p^{(2)})$; the definitions of $w_2(t)$, $b(\partial)$, ∂ refer to Appendix A.

6.2.2 Design Control Law

The state variables $x(t) \in R^4$ of the system in Eq. 6.1 are defined as following:

$x_1(t) = y(t)$, $x_2(t) = \dot{x}_1(t)$, $x_3(t) = \dot{x}_2(t)$, $x_4(t) = \dot{x}_3(t)$.

Define the switching surface as:

$$\sigma(t) = S \cdot x(t) = s_1 x_1(t) + s_2 x_2(t) + s_3 x_3(t) + s_4 x_4(t) = 0 \tag{6.17}$$

where $S \in R^{1\times 4}$, $x(t) \in R^{4\times 1}$, s_1, s_2, s_3, s_4 are positive coefficients respectively, $x_1(t)$, $x_2(t)$, $x_3(t)$, $x_4(t)$ are the state variables of the system in Eq. 6.1.

A tuning error σ_r is defined as follows: $\sigma_r(t) = \sigma(t) - \varepsilon \cdot sat\left(\frac{\sigma(t)}{\varepsilon}\right)$, where ε is an arbitrary positive constant vector, $sat(\cdot)$ is the saturation function, $\sigma(t)$ is the sliding surface.

Differentiating $\sigma(t)$ with respect to time t, and substituting Eq. 6.3, one can obtain

$$\begin{aligned}
\dot{\sigma}(t) &= \frac{\partial \sigma(t)}{\partial x}\dot{x}(t) = s_1 y^{(1)}(t) + s_2 y^{(2)}(t) + s_3 y^{(3)}(t) + s_4 y^{(4)}(t) \\
&= (s_1 - s_4 \frac{\bar{a}_1}{\bar{a}_4}) y^{(1)}(t) + (s_2 - s_4 \frac{\bar{a}_2}{\bar{a}_4}) y^{(2)}(t) + (s_3 - s_4 \frac{\bar{a}_3}{\bar{a}_4}) y^{(3)}(t) \\
&- s_4 \frac{\bar{a}_0}{\bar{a}_4} y(t) + \frac{s_4}{\bar{a}_4}(r_2 y_r^{(2)}(t) + r_1 y_r^{(1)}(t) + r_0 y_r(t) + z_e(t) + e(t)) \\
&+ s_4 \frac{b_{lpo}\, p}{\bar{a}_4} v(t) + s_4 \frac{b_{lpo}}{\bar{a}_4} g(v(t))
\end{aligned} \tag{6.18}$$

where $b_{lpo} = K_p b_{lp0}$, K_p is the stiffness of the piezoactuator in Eq. 6.3.

Define $N = \frac{\bar{a}_4}{s_4 b_{lpo} p}$ (N>0), $\theta_1 = N(s_1 - s_4 \frac{\bar{a}_1}{\bar{a}_4})$, $\theta_2 = N(s_2 - s_4 \frac{\bar{a}_2}{\bar{a}_4})$, $\theta_3 = N(s_3 - s_4 \frac{\bar{a}_3}{\bar{a}_4})$,

$$\theta_4 = N(-s_4)\frac{\bar{a}_0}{\bar{a}_4} \theta_5 = N\frac{s_4}{\bar{a}_4} r_2,\ \theta_6 = N\frac{s_4}{\bar{a}_4} r_1,\ \theta_7 = N\frac{s_4}{\bar{a}_4} r_0.$$

For the designs of the control law, the following assumptions concerning the system and hysteresis are required as follows:

Assumption 1:

There exist positive scalars q_1, q_2, q_3, such that $\| y^{(2)}(t+\tau) \| \le q_1 \| y^{(2)}(t) \|$, $\| y^{(1)}(t+\tau) \| \le q_2 \| y^{(1)}(t) \|$ and $\|y(t+\tau)\| \le q_3 \|y(t)\|$.

Assumption 2:

There exist known constants $b_{lp0\min}$ and $b_{lp0\max}$, such that the control gain b_{lp0} in Eq. 6.15 satisfies $b_{lp0} \in \left[b_{lp0\min}, b_{lp0\max}\right]$.

Assumption 3:

There exist known constants $p_{\min}$ and $p_{\max}$, such that the control gain p in Eq. 6.18 satisfies $p \in \left[p_{\min}, p_{\max}\right]$.

Assumption 4:

Define $\theta \in \Omega_\theta = \{\theta : \theta_{i\min} \le \theta_i \le \theta_{i\max}. \forall i \in \{1, r\}\}$, where $\theta_{i\min}$ and $\theta_{i\max}$ are known real numbers.

Assumption 5:

In Eq. 6.3, $\|g(v(t))\| \le \rho_a$, ρ_a is a constant.

With respect to the plant and hysteresis models subject to the assumptions, the following control law and adaptation mechanism are presented:

$$\begin{aligned} v(t) = -[&k_r \sigma(t) + \hat{\theta}_1(t) y^{(1)}(t) + \hat{\theta}_2(t) y^{(2)}(t) + \hat{\theta}_3(t) y^{(3)}(t) + \hat{\theta}_4(t) y(t) \\ &+ \hat{\theta}_5(t) \|y^{(2)}(t)\| + \hat{\theta}_6(t) \|y^{(1)}(t)\| + \hat{\theta}_7(t) \|y(t)\| + k^* sat(\frac{\sigma(t)}{\varepsilon})] \end{aligned} \tag{6.19}$$

where k_r, k^* are constant positive gains; with $\dot{\hat{\theta}}_i = proj\ (\hat{\theta}_i, -\gamma_i \omega_i)$ $(i = 1, 2, 3, 4, 5, 6, 7)$, $proj(\cdot,\cdot)$ is a projection function as follows

$$proj(\hat{\theta}_i, -\gamma_i \omega_i) = \begin{cases} 0 & if\ (\hat{\theta}_i > \theta_{\max}\ and\ \gamma_i \omega_i < 0)\ or\ (\hat{\theta}_i < \theta_{\min}\ and\ \gamma_i \omega_i > 0) \\ -\gamma_i \omega_i & if\ (\theta_{\min} < \hat{\theta}_i < \theta_{\max})\ or\ (\hat{\theta}_i > \theta_{\max}\ and\ \gamma_i \omega_i \ge 0) \\ & \quad or\ \hat{\theta}_i < \theta_{\min}\ and\ \gamma_i \omega_i \le 0) \end{cases} \tag{6.20}$$

where $\omega_1(t) = \sigma_t(t) y^{(1)}(t)$, $\omega_2(t) = \sigma_t(t) y^{(2)}(t)$, $\omega_3(t) = \sigma_t(t) y^{(3)}(t)$, $\omega_4(t) = \sigma_t(t) y(t)$,

$\omega_5(t) = \sigma_t(t) \| y^{(2)}(t) \|$, $\omega_6(t) = \sigma_t(t) \| y^{(1)}(t) \|$, $\omega_7(t) = \sigma_t(t) \| y(t) \|$,

and scalars $\gamma_i (i = 1,\ 2,\ 3,\ 4,\ 5,\ 6,\ 7)$ are chosen by the designers.

6.2.3 Stability Analysis of the System

A Lyapunov function candidate for the system in Eq. 6.1 is defined as:

$$V(t) = \frac{1}{2}\left[N\sigma_t^2(t) + \sum_{i=1}^{4}[\frac{1}{\gamma_i}(\hat{\theta}_i(t) - \theta_i)^2] + \sum_{i=5}^{i=7}[\frac{1}{\gamma_i}(\hat{\theta}_i(t) - q_{i-4}\theta_i)^2] \right] \tag{6.21}$$

Case 1: when $|\sigma(t)| \le \varepsilon$, the derivative $\dot{V}(t)$ exists for all $\sigma(t)$, which is $\dot{V}(t) = 0$.

Case 2: when $|\sigma(t)| > \varepsilon$, using Eq. 6.18 and the fact $\dot{\sigma} = \dot{\sigma}_t$, one can yield

$$\begin{aligned}
\dot{V}(t) &\le N\sigma_t \dot{\sigma} + \sum_{i=1}^{4}[\frac{1}{\gamma_i}(\hat{\theta}_i(t) - \theta_i)\dot{\hat{\theta}}_i] + \sum_{i=5}^{i=7}[\frac{1}{\gamma_i}(\hat{\theta}_i(t) - q_{i-4}\theta_i)\dot{\hat{\theta}}_i] \\
&= \sum_{i=1}^{4}[\frac{1}{\gamma_i}(\hat{\theta}_i(t) - \theta_i)\dot{\hat{\theta}}_i] + \sum_{i=5}^{i=7}[\frac{1}{\gamma_i}(\hat{\theta}_i(t) - q_{i-4}\theta_i)\dot{\hat{\theta}}_i] + \sigma_t(v(t) + \frac{1}{p}g(v)) \\
&+ \sigma_t(\theta_1 y^{(1)} + \theta_2 y^{(2)} + \theta_3 y^{(3)} + \theta_4 y + \theta_5 y_r^{(2)} + \theta_6 y_r^{(1)} + \theta_7 y_r + \frac{e(t) + z_e(t)}{b_{ipo} p})
\end{aligned} \tag{6.22}$$

As a projection function, it can obtain that $(\hat{\theta}_i - m_i\theta_i)proj(\hat{\theta}_i, r_i\varpi_i) \le (\hat{\theta}_i - m_i\theta_i)r_i\varpi_i$, m_i are positive scalars, then

$$\begin{aligned}
\dot{V}(t) &\le \sigma_t(\theta_1 y^{(1)} + \theta_2 y^{(2)} + \theta_3 y^{(3)} + \theta_4 y + \theta_5 y_r^{(2)} + \theta_6 y_r^{(1)} + \theta_7 y_r + \frac{e(t) + z_e(t)}{b_{ipo} p}) \\
&+ \sigma_t(v(t) + \frac{1}{p}g(v(t))) + \sigma_t((\hat{\theta}_1 - \theta_1)y^{(1)} + (\hat{\theta}_2 - \theta_2)y^{(2)} + (\hat{\theta}_3 - \theta_3)y^{(3)} \\
&+ (\hat{\theta}_4 - \theta_4)y + (\hat{\theta}_5 - q_i\theta_5)\| y^{(2)} \| + (\hat{\theta}_6 - q_2\theta_6)\| y^{(1)} \| + (\hat{\theta}_7 - q_3\theta_7)\| y \|)
\end{aligned} \tag{6.23}$$

According to the *assumption 1*, we can get

$$\begin{aligned}
\dot{V}(t) &\le \sigma_t(\theta_1 y^{(1)} + \theta_2 y^{(2)} + \theta_3 y^{(3)} + \theta_4 y + q_2\theta_5\| y^{(2)} \| + q_1\theta_6\| y^{(1)} \| + q_1\theta_7\| y \| + \frac{e(t) + z_e(t)}{b_{ipo} p}) \\
&+ \sigma_t(v(t) + \frac{1}{p}g(v(t))) + \sigma_t((\hat{\theta}_1 - \theta_1)y^{(1)} + (\hat{\theta}_2 - \theta_2)y^{(2)} + (\hat{\theta}_3 - \theta_3)y^{(3)} + (\hat{\theta}_4 - \theta_4)y \\
&+ (\hat{\theta}_5 - q_1\theta_5)\| y^{(2)} \| + (\hat{\theta}_6 - q_2\theta_6)\| y^{(1)} \| + (\hat{\theta}_7 - q_3\theta_7)\| y \|) \\
&\le \sigma_t(\frac{e(t) + z_e(t)}{b_{ipo} p} + \frac{g(v)}{p}) + \sigma_t v(t) + \sigma_t(\hat{\theta}_1 y^{(1)} + \hat{\theta}_2 y^{(2)} + \hat{\theta}_3 y^{(3)} + \hat{\theta}_4 y + \hat{\theta}_5\| y^{(2)} \| + \hat{\theta}_6\| y^{(1)} \| + \hat{\theta}_7\| y \|)
\end{aligned}$$

$$\leq \sigma_t(\frac{e(t)+z_e(t)}{b_{tpo}p}+\frac{g(v)}{p})+\sigma_t(\hat{\theta}_1 y^{(1)}+\hat{\theta}_2 y^{(2)}+\hat{\theta}_3 y^{(3)}+\hat{\theta}_4 y+\hat{\theta}_5 \| y^{(2)} \|+\hat{\theta}_6 \| y^{(1)} \|+\hat{\theta}_7 \| y \|)$$

$$-\sigma_t(k_r\sigma+\hat{\theta}_1 y^{(1)}+\hat{\theta}_2 y^{(2)}+\hat{\theta}_3 y^{(3)}+\hat{\theta}_4 y+\hat{\theta}_5\|y^{(2)}\|+\hat{\theta}_6\|y^{(1)})\|+\hat{\theta}_7\|y\|+k^* sat(\frac{\sigma(t)}{\varepsilon}))$$

$$=-k_r\sigma_t(t)\sigma(t)-\sigma_t k^* sat(\frac{\sigma(t)}{\varepsilon})+\sigma_t(\frac{1}{p}g(v)+\frac{e(t)+z_e(t)}{b_{tpo}p})$$

$$\leq -k_r\sigma_t^2(t)-\sigma_t k^* sat(\frac{\sigma(t)}{\varepsilon})+\sigma_t(\frac{1}{p}g(v)+\frac{e(t)+z_e(t)}{b_{tpo}p})$$

$$\leq -k_r\sigma_t^2(t)-|\sigma_t|k^*+|\sigma_t|(\frac{1}{p}|g(v)|+\frac{|e(t)|+z_e(t)}{b_{tpo}p}) \qquad (6.24)$$

In the *assumption 5* and the *Remark A*, $|g(v)|\leq \rho_a$ and $|e(t)|\leq \rho(t)$ are defined and $z_e(t)$ is dynamical estimate of $z(t, y_p^{(4)}, y_p^{(3)}, y_p^{(2)})$. While $k^* = k^*_{\max} \geq \frac{1}{p}(\rho_a + \frac{\rho(t)+z_e(t)}{b_{tpo}})$ is defined,

$$\dot{V}(t) \leq -k_r\sigma_t^2(t)-|\sigma_t|k^*_{\max}+|\sigma_t|(\frac{1}{p}|g(v)|+\frac{|e(t)|+z_e(t)}{b_{tp0}p}) \leq -k_r\sigma_t^2 \qquad \forall |\sigma(t)|>\varepsilon \qquad (6.25)$$

Based on the above analyses and proof, the following theorem regarding the stability of the closed-loop system described by Eqs. (6.3), (6.15) and (6.19) can be established.

Theorem: For the plant in Eq. (6.1) subject to *Assumptions 1-5* and *Remark A*, the robust adaptive controller specified by Eq. (6.19) ensures that all the closed-loop signals are bounded and the state variable $y(t)$ converges to zero for $\forall t \geq t_0$.

6.3 Simulation Results

In order to eliminate the chatter in the metal cutting processes, the adaptive controller developed in Eq. 6.19 is introduced into the system in Eq. 6.1. The parameters in the simulations of the dynamic performance of the metal cutting system are listed in Table C. Fig. 6.3 shows the dynamic response of the metal cutting system in Eq. 6.1 combined with the control law in Eq. 6.19; Fig. 6.4

illustrates the steady-state error between the desired value and actual response of the system in Eq. 6.1; Fig. 6.5 plots the dynamic response of the main cutting force $F_c(t)$ during the cutting process; Fig. 6.6 represents the dynamic response of the thrust force $F_t(t)$ during the cutting process; Fig. 6.7 plots the dynamic performance of the piezoactuator during the cutting process.

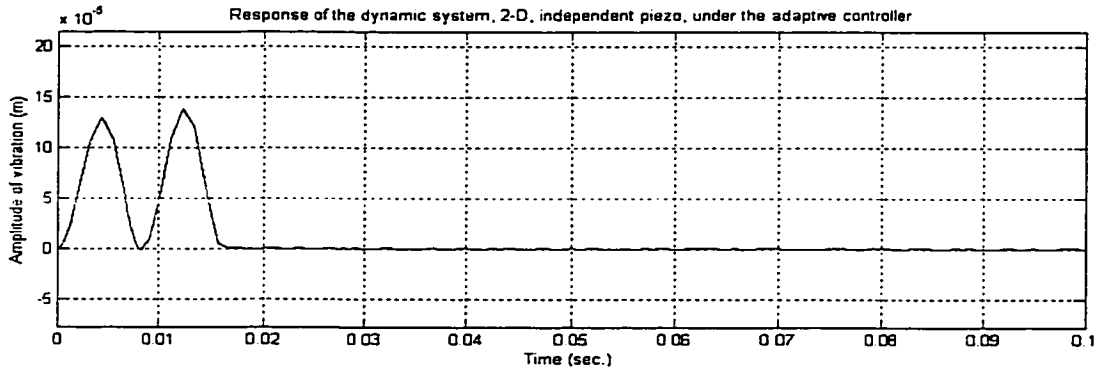

Figure 6.3 Response y(t) of dynamic system with the control law

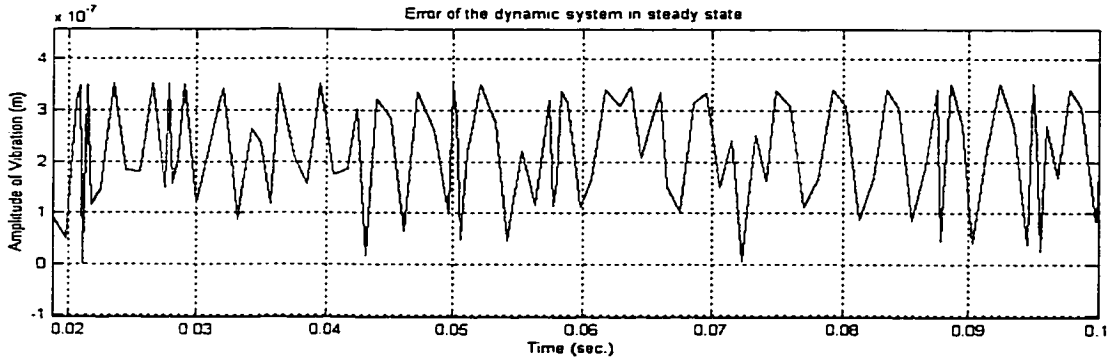

Figure 6.4 Steady-state error of the dynamic system with the control law

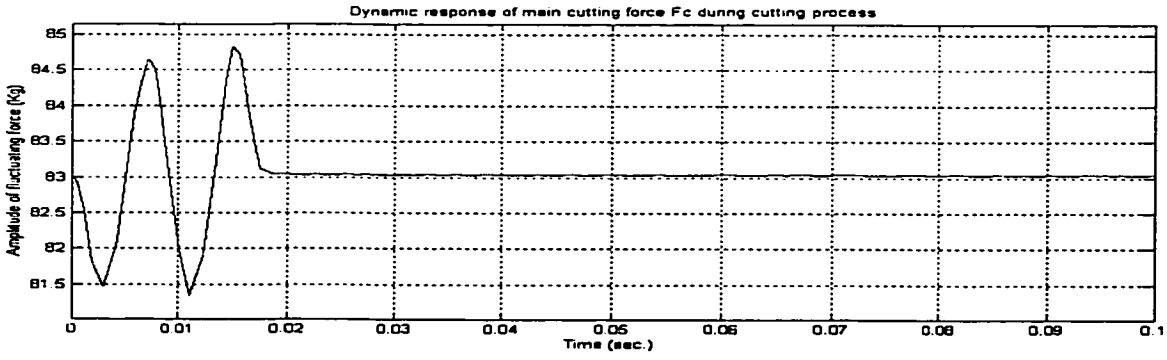

Figure 6.5 Response of main cutting force $F_c(t)$ during cutting process

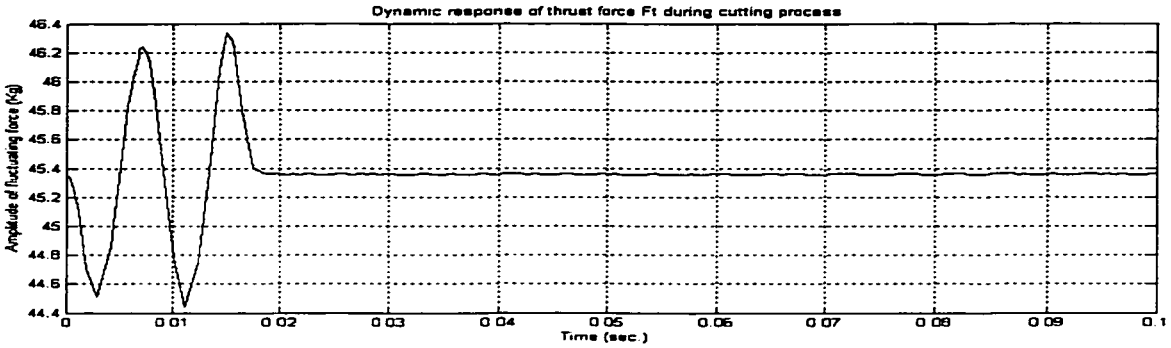

Figure 6.6 Response of thrust force $F_t(t)$ during cutting process

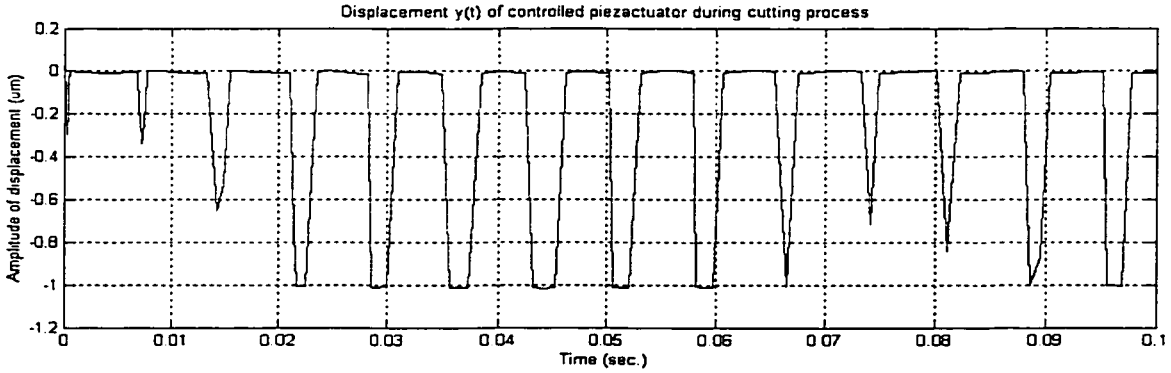

Figure 6.7 Displacement of the controlled piezoactuator during cutting process

From Fig. 6.3 through Fig. 6.7, the simulations of the dynamic performance of the system with the adaptive controller show clearly that the proposed adaptive controller can significantly suppress the chatter during the metal cutting processes.

6.4 Summary

In order to suppress the chatter in the metal cutting with two degree-of-freedom and two-dimensional force models, a piezoactuator independent from the tool holder is introduced into the system; the metal cutting system is modeled as a class of uncertain linear system with hysteresis and time lag; An adaptive control law for the system is presented; The simulation results show that the designed control law significantly eliminates the chatter effect in the metal cutting process.

Chapter 7

Chatter Suppression for the Controlled System with 3-D Model and Independent Piezoactuators

Introduction – in the metal cutting system with two degree-of-freedom and two piezoactuators, the structures of which are independent from the tool holders, are introduced for the regulation of the displacement between the cutting tool and workpiec. The closed-loop dynamic of the metal cutting system involving three-dimensional force models is presented. The piezoactutors exhibit the hysteretic characteristics. To suppress chatter in the system, two adaptive controllers are designed. The simulations for the dynamic performances of this system with two piezoactuatos are shown.

7.1 Dynamic Model of Turning Process

The schematic model of the metal cutting system with two degree-of-freedom and three-dimensional force models is illustrated in Fig. 7.1. The dynamic cutting process is demonstrated in the magnified contact parts of workpiece and the cutting tool. The work focuses on the type A of chatter that is normal to the cutting surface of the workpiece. Considering the structures of the piezoactuators as an independent free mechanical body with the cutting tool, the structural turning system may be represented as in Fig. 7.1.

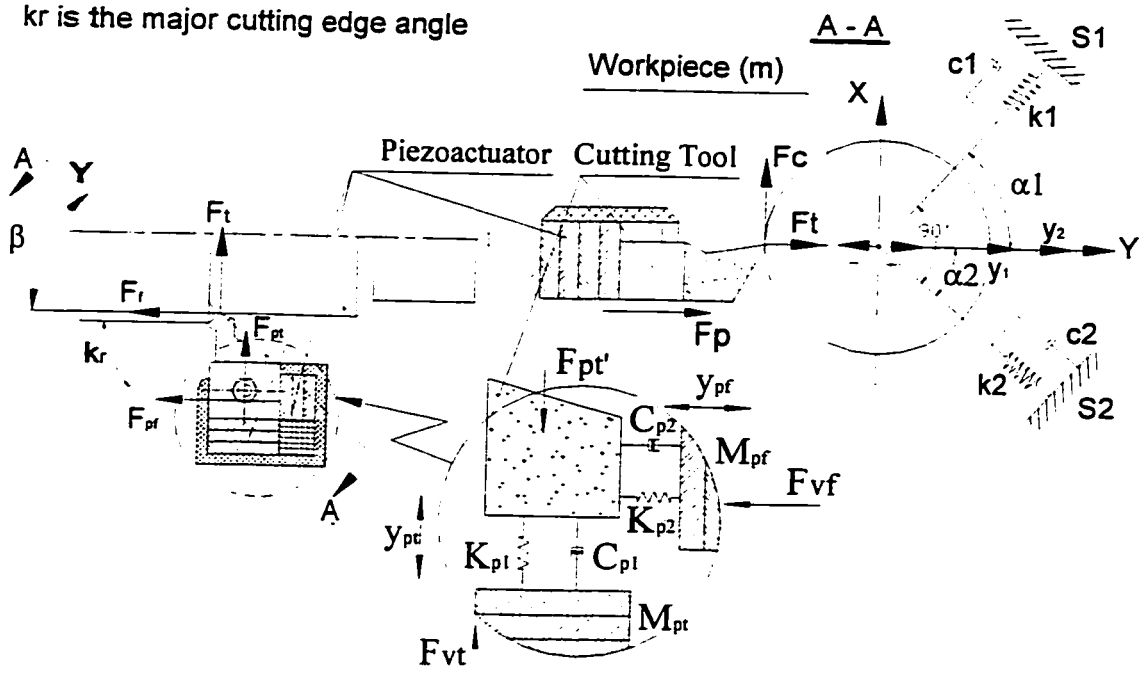

Figure 7.1 Schematic model of turning system with independent piezoactuators and 3-D force models

In Fig. 7.1. the dynamic process of the metal cutting system can be described with a linear second order function as following:

$$\begin{pmatrix} \frac{m}{\cos\alpha_1} & 0 \\ 0 & \frac{m}{\cos\alpha_2} \end{pmatrix}\begin{pmatrix} \frac{d^2y_1}{dt^2} \\ \frac{d^2y_2}{dt^2} \end{pmatrix}+\begin{pmatrix} \frac{c_1}{\cos\alpha_1} & 0 \\ 0 & \frac{c_2}{\cos\alpha_2} \end{pmatrix}\begin{pmatrix} \frac{dy_1}{dt} \\ \frac{dy_2}{dt} \end{pmatrix}+\begin{pmatrix} \frac{k_1}{\cos\alpha_1} & 0 \\ 0 & \frac{k_1}{\cos\alpha_1} \end{pmatrix}\begin{pmatrix} y_1 \\ y_2 \end{pmatrix}$$

$$=\begin{pmatrix} \cos\alpha_1\sin\beta & \sin\alpha_1 & \cos\alpha_1\cos\beta \\ \cos\alpha_2\sin\beta & -\sin\alpha_2 & \cos\alpha_2\cos\beta \end{pmatrix}\begin{pmatrix} F_t \\ F_c \\ F_f \end{pmatrix}+\begin{pmatrix} \cos\alpha_1\sin\beta & \cos\alpha_1\cos\beta \\ \cos\alpha_2\sin\beta & \cos\alpha_2\cos\beta \end{pmatrix}\begin{pmatrix} F_{pt} \\ F_{pf} \end{pmatrix} \tag{7.1}$$

$$F_{pt} = F_{vt} - m_p\frac{d^2y_{pt}}{dt^2} \tag{7.2}$$

$$F_{pf} = F_{vf} - m_p\frac{d^2y_{pf}}{dt^2} \tag{7.3}$$

where y_1, y_2 represent the relative displacements between the cutting tool and workpiece normal to the machined surface in each degree-freedom direction; m, c_i, k_i are the equivalent mass, equivalent damping coefficient and equivalent spring stiffness of the structure in each direction; F_t, F_c, F_f are the thrust, main cutting and feed forces; F_{vt}, F_{vf} represents the forces generated by the two piezoactuators in both directions of thrust and feed forces; F_{pt}, F_{pf} is reaction forces between the piezoactuators and workpiece in both the directions of the thrust and feed forces; α_1, α_2 are geometrical angles of the structure model related to a line normal to the machined surface; the definition of the $y_{pt}(t)$, $y_{pf}(t)$ is given, which represent the displacements in both directions of the thrust and feed forces, in the section 3.6 in Chapter 3; m_p is the equivalent mass of each of the piezoactuators.

With respect to the Eqs. 7.1, 7.2 and 7.3, the schematic of the closed-loop system with the adaptive controllers designed in next section is illustrated in Fig. 7.2.

According to the analyses in Eq. 3.4 in Chapter 3, the forces F_{vt}, F_{vf} resulted from the piezoactuators in two directions are given as follows:

$$F_{vt}(v) = K_{pt}(p_t \cdot v_t(t) + g_t(v_t(t))) \tag{7.4}$$

$$F_{vf}(v) = K_{pf}(p_f \cdot v_f(t) + g_f(v_f(t))) \tag{7.5}$$

where K_{pt} *and* K_{pf} are the stiffnesses of the two piezoactuators; v_t(t), v_f(t) are denoted as the applied voltages; other parameters are defined in Chapter 3.

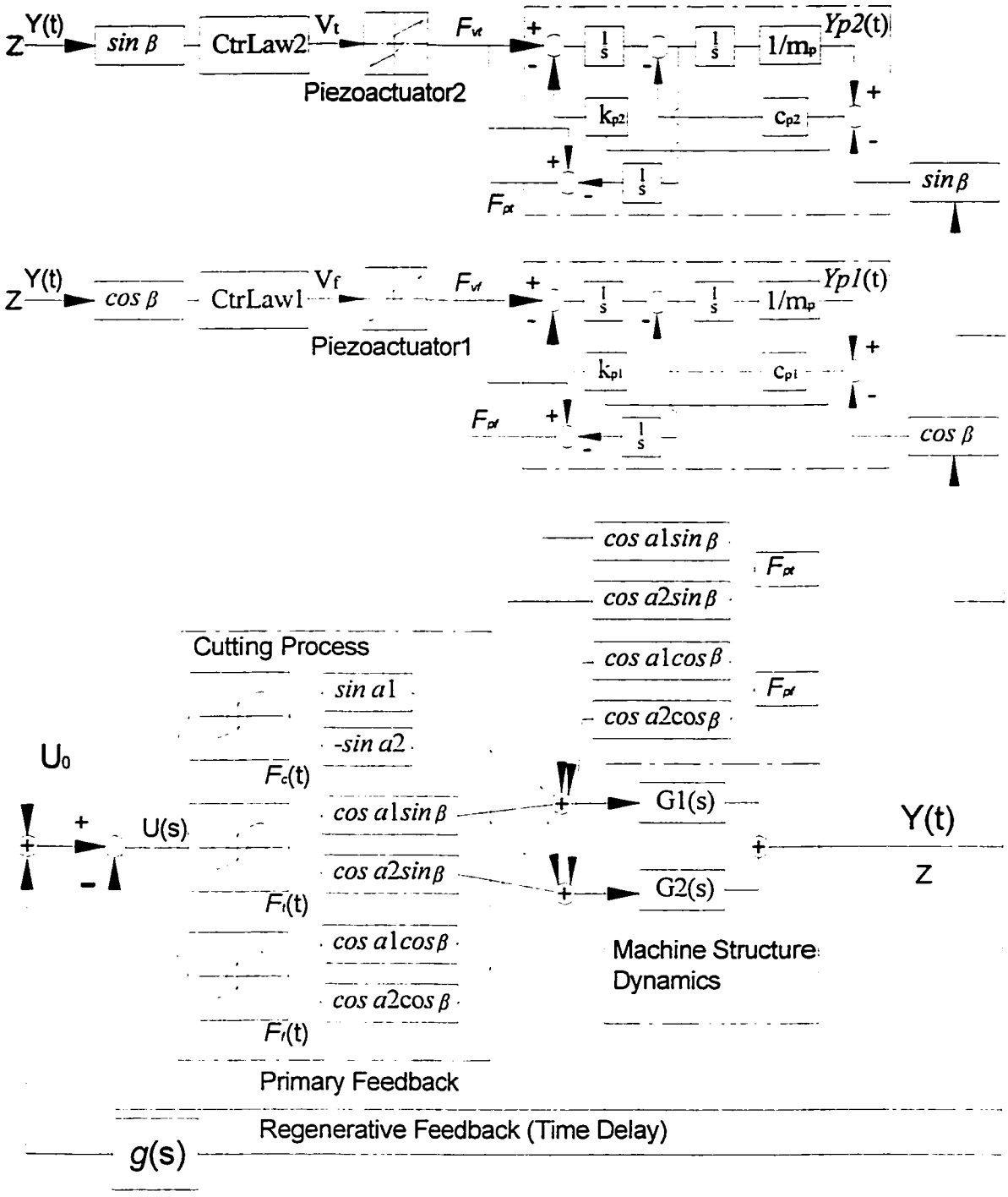

Figure 7.2 Block diagram of turning system with the piezoactuators and controllers

7.2 Adaptive Controller design

Based on the mathematical model of the closed-loop system described in Eq. 7.1, the control laws will be designed in order to suppress the chatter effect in the metal cutting process.

Based on the Eq. 7.1 through Eq. 7.3, we can transform and calculate it further as follows:

$$\frac{m}{\cos\alpha_1}\frac{d^2y_1(t)}{dt^2}+\frac{c_1}{\cos\alpha_1}\frac{d\ y_1(t)}{dt}+\frac{k_1}{\cos\alpha_1}y_1(t)=\cos\alpha_1\sin\beta F_t(t)+\sin\alpha_1F_c(t)+\cos\alpha_1\cos\beta F_f(t)$$
$$+\cos\alpha_1\sin\beta(F_{vt}-m_p\frac{d^2y_{pt}}{dt^2})+\cos\alpha_1\cos\beta(F_{vf}-m_p\frac{d^2y_{pf}}{dt^2}) \tag{7.6}$$

$$\frac{m}{\cos\alpha_2}\frac{d^2y_2(t)}{dt^2}+\frac{c_2}{\cos\alpha_2}\frac{d\ y_2(t)}{dt}+\frac{k_2}{\cos\alpha_2}y_2(t)=\cos\alpha_2\sin\beta F_t(t)-\sin\alpha_2F_c(t)+\cos\alpha_2\cos\beta F_f(t)$$
$$+\cos\alpha_2\sin\beta(F_{vt}-m_p\frac{d^2y_{pt}}{dt^2})+\cos\alpha_2\cos\beta(F_{vf}-m_p\frac{d^2y_{pf}}{dt^2}) \tag{7.7}$$

The combination of Eq. 7.6 and Eq. 7.7 yields

$$y(s)=y_1(s)+y_2(s) \tag{7.8}$$

where $y_1(s)=\dfrac{\cos\alpha_1\sin\beta F_t(s)+\sin\alpha_1F_c(s)+\cos\alpha_1\cos\beta F_f(s)}{\frac{m}{\cos\alpha_1}s^2+\frac{c_1}{\cos\alpha_1}s+\frac{k_1}{\cos\alpha_1}}$

$$+\frac{\cos\alpha_1\sin\beta(F_{vt}(s)-m_ps^2y_{pt}(s))+\cos\alpha_1\cos\beta(F_{vf}(s)-m_ps^2y_{pf}(s))}{\frac{m}{\cos\alpha_1}s^2+\frac{c_1}{\cos\alpha_1}s+\frac{k_1}{\cos\alpha_1}},$$

$$y_2(s)=\frac{\cos\alpha_2\sin\beta F_t(t)-\sin\alpha_2F_c(t)+\cos\alpha_2\cos\beta F_f(t))}{\frac{m}{\cos\alpha_2}s^2+\frac{c_2}{\cos\alpha_2}s+\frac{k_2}{\cos\alpha_2}}$$

$$+\frac{\cos\alpha_2\sin\beta(F_{vt}(s)-m_ps^2y_{pt}(s))+\cos\alpha_2\cos\beta(F_{vf}(s)-m_ps^2y_{pf}(s))}{\frac{m}{\cos\alpha_2}s^2+\frac{c_2}{\cos\alpha_2}s+\frac{k_2}{\cos\alpha_2}}.$$

Eq. 7.8 can be rewritten as

$$
\begin{aligned}
&y(s)(m_{11}s^2 + c_{11}s + k_{11})(m_{22}s^2 + c_{22}s + k_{22}) \\
&= (\cos\alpha_1 \sin\beta F_t(s) + \sin\alpha_1 F_c(s) + \cos\alpha_1 \cos\beta F_f(s) + \cos\alpha_1 \sin\beta (F_{vt}(s) - m_p s^2 y_{pt}(s)) \\
&+ \cos\alpha_1 \cos\beta (F_{vf}(s) - m_p s^2 y_{pf}(s))) \times (m_{22}s^2 + c_{22}s + k_{22}) \\
&+ (\cos\alpha_2 \sin\beta F_t(t) - \sin\alpha_2 F_c(t) + \cos\alpha_2 \cos\beta F_f(t) + \cos\alpha_2 \sin\beta (F_{vt}(s) - m_p s^2 y_{pt}(s)) \\
&+ \cos\alpha_2 \cos\beta (F_{vf}(s) - m_p s^2 y_{pf}(s))) \times (m_{11}s^2 + c_{11}s + k_{11})
\end{aligned} \tag{7.9}
$$

where

$$
m_{11} = \frac{m}{\cos\alpha_1}, \quad c_{11} = \frac{c_1}{\cos\alpha_1}, \quad k_{11} = \frac{k_1}{\cos\alpha_1}, \quad m_{22} = \frac{m}{\cos\alpha_2}, \quad c_{22} = \frac{c_2}{\cos\alpha_2}, \quad k_{22} = \frac{k_2}{\cos\alpha_2}.
$$

For simplicity, Eq. 7.9 can be rewritten

$$
\begin{aligned}
&y(s)(a_4 s^4 + a_3 s^3 + a_2 s^2 + a_1 s + a_0) = (F_t(s) + F_{vt}(s))(b_{tp2}s^2 + b_{tp1}s + b_{tp0}) \\
&+ F_c(s)(b_{c2}s^2 + b_{c1}s + b_{c0}) + (F_f(s) + F_{vf}(s))(b_{fp2}s^2 + b_{fp1}s + b_{fp0}) \\
&- y_{pt}(s)(m_{pt4}s^4 + m_{pt3}s^3 + m_{pt4}s^2) - y_{pf}(s)(m_{pf4}s^4 + m_{pf3}s^3 + m_{pf4}s^2)
\end{aligned} \tag{7.10}
$$

where

$$
a_4 = m_{11}m_{22}, \quad a_3 = c_{11}m_{22} + c_{22}m_{11}, \quad a_2 = k_{11}m_{22} + k_{22}m_{11} + c_{11}c_{22}, \quad a_1 = k_{11}c_{22} + k_{22}c_{11}, \quad a_0 = k_{11}k_{22}
$$

$$
b_{tp2} = \cos\alpha_1 \sin\beta \cdot m_{22} + \cos\alpha_2 \sin\beta \cdot m_{11}, \quad b_{tp1} = \cos\alpha_1 \sin\beta \cdot c_{22} + \cos\alpha_2 \sin\beta \cdot c_{11},
$$

$$
b_{tp0} = \cos\alpha_1 \sin\beta \cdot k_{22} + \cos\alpha_2 \sin\beta \cdot k_{11},
$$

$$
b_{c2} = \sin\alpha_1 m_{22} - \sin\alpha_2 m_{11}, \quad b_{c1} = \sin\alpha_1 c_{22} - \sin\alpha_2 c_{11}, \quad b_{c0} = \sin\alpha_1 k_{22} - \sin\alpha_2 k_{11}
$$

$$
b_{fp2} = \cos\alpha_1 \cos\beta \cdot m_{22} + \cos\alpha_2 \cos\beta \cdot m_{11}, \quad b_{fp1} = \cos\alpha_1 \cos\beta \cdot c_{22} + \cos\alpha_2 \cos\beta \cdot c_{11},
$$

$$
b_{fp0} = \cos\alpha_1 \cos\beta \cdot k_{22} + \cos\alpha_2 \cos\beta \cdot k_{11},
$$

$$
m_{pt4} = (\cos\alpha_1 m_{22} + \cos\alpha_2 m_{11}) \sin\beta \cdot m_p, \quad m_{pt3} = (\cos\alpha_1 c_{22} + \cos\alpha_2 c_{11}) \sin\beta \cdot m_p,
$$

$$
m_{pt2} = (\cos\alpha_1 k_{22} + \cos\alpha_2 k_{11}) \sin\beta \cdot m_p,
$$

$$
m_{pf4} = (\cos\alpha_1 m_{22} + \cos\alpha_2 m_{11}) \cos\beta m_p, \quad m_{pf3} = (\cos\alpha_1 c_{22} + \cos\alpha_2 c_{11}) \cos\beta m_p,
$$

$$
m_{pf2} = (\cos\alpha_1 k_{22} + \cos\alpha_2 k_{11}) \cos\beta m_p.
$$

The inverse Laplace transformation of Eq. 7.10, one can obtain

$$
\begin{aligned}
&a_4 y^{(4)}(t) + a_3 y^{(3)}(t) + a_2 y^{(2)}(t) + a_1 y^{(1)}(t) + a_0 y(t) \\
&= b_{tp2} F_t^{(2)}(t) + b_{tp1} F_t^{(1)}(t) + b_{tp0} F_t(t) + b_{c2} F_c^{(2)}(t) + b_{c1} F_c^{(1)}(t) + b_{c0} F_c(t) \\
&+ b_{fp2} F_f^{(2)}(t) + b_{fp1} F_f^{(1)}(t) + b_{fp0} F_f(t) + b_{tp2} F_{vt}^{(2)}(t) + b_{tp1} F_{vt}^{(1)}(t) + b_{tp0} F_{vt}(t) \\
&+ b_{fp2} F_{vf}^{(2)}(t) + b_{fp1} F_{vf}^{(1)}(t) + b_{fp0} F_{vf}(t) - (m_{pt4} y_{pt}^{(4)}(t) + m_{pt3} y_{pt}^{(3)}(t) + m_{pt2} y_{pt}^{(2)}(t)) \\
&- (m_{pf4} y_{pf}^{(4)}(t) + m_{pf3} y_{pf}^{(3)}(t) + m_{pf2} y_{pf}^{(2)}(t))
\end{aligned} \tag{7.11}
$$

Based on the analyses in Chapter 2, the uncut chip thickness u(t) is expressed as

$$u(t) = u_0(t) - y(t) + \mu \cdot y(t-\tau) \tag{7.12}$$

where μ is the overlapping coefficient, and τ is time delay of the system, y(t) is the displacement.

With respect to the hysteresis relationships between the forces $F_j(t)$ and uncut chip thickness $u(t)$, the forces are

$$F_t(t) = p_t u(t) + g_t(u(t)) = p_t(u_0(t) - y(t) + \mu y(t-\tau)) + g_t(u_0(t) - y(t) + \mu y(t-\tau)) \tag{7.13}$$

$$F_c(t) = p_c u(t) + g_c(u(t)) = p_c(u_0(t) - y(t) + \mu y(t-\tau)) + g_c(u_0(t) - y(t) + \mu y(t-\tau)) \tag{7.14}$$

$$F_f(t) = p_f u(t) + g_f(u(t)) = p_f(u_0(t) - y(t) + \mu y(t-\tau)) + g_f(-y(t) + \mu y(t-\tau)) \tag{7.15}$$

To simplify the above equations, the corresponding backlashes can be simplified as,

$$\begin{aligned} F_t(t) &= A_t u(t) \pm B_t^{'} = A_t(u_0(t) - y(t) + \mu \cdot y_\tau(t)) \pm B_t^{'} = -A_t y(t) + A_t \mu \cdot y_\tau(t) \pm B_t \\ F_c(t) &= A_c u(t) \pm B_c^{'} = A_c(u_0(t) - y(t) + \mu \cdot y_\tau(t)) \pm B_c^{'} = -A_c y(t) + A_c \mu \cdot y_\tau(t) \pm B_c \\ F_f(t) &= A_f u(t) \pm B_f^{'} = A_f(u_0(t) - y(t) + \mu\ y_\tau(t)) \pm B_f^{'} = -A_f y(t) + A_f \mu \cdot y_\tau(t) \pm B_f \end{aligned} \tag{7.16}$$

where $y_\tau(t) = y(t-\tau)$, $B_t = A_t u_0(t) \pm B_t^{'}$; $B_c = A_c u_0(t) \pm B_c^{'}$; $B_f = A_f u_0(t) \pm B_f^{'}$; other parameters are defined in Eq. 2.14 and 2.15.

In term of Eq. 7.16, Eq. 7.11 can be rewritten as follows:

$$\begin{aligned} &a_4 y^{(4)}(t) + a_3 y^{(3)}(t) + a_2 y^{(2)}(t) + a_1 y^{(1)}(t) + a_0 y(t) \\ &= b_{tp2}(-A_t y^{(2)}(t) + \mu A_t y_\tau^{(2)}(t)) + b_{tp1}(-A_t y^{(1)}(t) + \mu A_t y_\tau^{(1)}(t)) + b_{tp0}(-A_t y(t) + \mu A_t y_\tau(t) \pm B_t) \\ &+ b_{c2}(-A_c y^{(2)}(t) + \mu A_c y_\tau^{(2)}(t)) + b_{c1}(-A_c y^{(1)}(t) + \mu A_c y_\tau^{(1)}(t)) + b_{c0}(-A_c y(t) + \mu A_c y_\tau(t) \pm B_c) \\ &+ b_{fp2}(-A_f y^{(2)}(t) + \mu A_f y_\tau^{(2)}(t)) + b_{fp1}(-A_f y^{(1)}(t) + \mu A_f y_\tau^{(1)}(t)) + b_{fp0}(-A_f y(t) + \mu A_f y_\tau(t) \pm B_f) \\ &+ b_{tp2} F_{vt}^{(2)}(t) + b_{tp1} F_{vt}^{(1)}(t) + b_{tp0} F_{vt}(t) + b_{fp2} F_{vf}^{(2)}(t) + b_{fp1} F_{vf}^{(1)}(t) + b_{fp0} F_{vf}(t) \\ &- (m_{pt4} y_{pt}^{(4)}(t) + m_{pt3} y_{pt}^{(3)}(t) + m_{pt2} y_{pt}^{(2)}(t)) - (m_{pf4} y_{pf}^{(4)}(t) + m_{pf3} y_{pf}^{(3)}(t) + m_{pf2} y_{pf}^{(2)}(t)) \end{aligned} \tag{7.17}$$

Further,

$$\begin{aligned} &\overline{a_4} y^{(4)}(t) + \overline{a_3} y^{(3)}(t) + \overline{a_2} y^{(2)}(t) + \overline{a_1} y^{(1)}(t) + \overline{a_0} y(t) \\ &= r_2 y_\tau^{(2)}(t) + r_1 y_\tau^{(1)}(t) + r_0 y_\tau(t) + b_{tp0} F_{vt}(t) + b_{fp0} F_{vf}(t) + z_1(t, y_{pt}^{(4)}, y_{pt}^{(3)}, y_{pt}^{(2)}) + z_2(t, y_{pf}^{(4)}, y_{pf}^{(3)}, y_{pf}^{(2)}) \\ &+ e(t, F_{vt}^{(2)}, F_{vt}^{(1)}, F_{vf}^{(2)}, F_{vf}^{(1)}) \end{aligned} \tag{7.18}$$

where $\overline{a_4} = a_4$, $\overline{a_3} = a_3$, $\overline{a_2} = a_2 + b_{pt2}A_t + b_{fp2}A_f + b_{c2}A_c$, $\overline{a_1} = a_1 + b_{pt1}A_t + b_{fp1}A_f + b_{c1}A_c$,
$\overline{a_0} = a_0 + b_{pt0}A_t + b_{fp0}A_f + b_{c0}A_c$, $r_2 = \mu\ (b_{tp2}A_t + b_{fp2}A_f + b_{c2}A_c)$, $r_1 = \mu\ (b_{tp1}A_t + b_{fp1}A_f + b_{c1}A_c)$,
$r_0 = \mu\ (b_{tp0}A_t + b_{fp0}A_f + b_{c0}A_c)$, $r_{\pm b} = \pm(b_{tp0}B_t + b_{c0}B_c)$,

$$z_1(t, y_{pt}^{(4)}, y_{pt}^{(3)}, y_{pt}^{(2)}) = -(m_{pt4}y_{pt}^{(4)}(t) + m_{pt3}y_{pt}^{(3)}(t) + m_{pt2}y_{pt}^{(2)}(t)) \pm r_{\pm b}$$

$$z_2(t, y_{pf}^{(4)}, y_{pf}^{(3)}, y_{pf}^{(2)}) = -(m_{pf4}y_{pf}^{(4)}(t) + m_{pf3}y_{pf}^{(3)}(t) + m_{pf2}y_{pf}^{(2)}(t)) \pm b_{fp0}B_f$$

$$e\ (t, F_{vt}^{(2)}, F_{vt}^{(1)}, F_{vf}^{(2)}, F_{vf}^{(1)}) = b_{tp2}F_{vt}^{(2)}(t) + b_{tp1}F_{vt}^{(1)}(t) + b_{fp2}F_{vf}^{(2)}(t) + b_{fp1}F_{vf}^{(1)}(t).$$

Remark A: The term $e\ (t, F_{vt}^{(2)}, F_{vt}^{(1)}, F_{vf}^{(2)}, F_{vf}^{(1)})$ is the lumped uncertain element in Eq. 7.1, its upper bound is assumed to be known, i.e., $\left\| e\ (t, F_{vt}^{(2)}, F_{vt}^{(1)}, F_{vf}^{(2)}, F_{vf}^{(1)}) \right\| \le \rho(t)$.

7.2.1 Dynamic Estimate of $z(t, y_p^{(4)}, y_p^{(3)}, y_p^{(2)})$

The value of disturbance $z_1(t, y_{pt}^{(4)}, y_{pt}^{(3)}, y_{pt}^{(2)})$ and $z_2(t, y_{pf}^{(4)}, y_{pf}^{(3)}, y_{pf}^{(2)})$ in Eq. 7.18 will be estimated dynamically. The detailed calculation can be referred to Appendix B. Based on Appendix B,

$$z_e(t) = \begin{pmatrix} z_{e1}(t) \\ z_{e2}(t) \end{pmatrix} = w_2(t) = \begin{pmatrix} w_{20}(t)b_1(\partial) \\ w_{21}(t)b_2(\partial) \end{pmatrix} \tag{7.19}$$

where $z_e(t)$ is the estimate of $z(t, y_p^{(4)}, y_p^{(3)}, y_p^{(2)})$; the $w_2(t)$, $b_1(\partial)$, $b_2(\partial)$ and ∂ refer to Appendix B.

7.2.2 Design Control Law

Define the switching surface $\sigma(t) \in R^{2\times 1}$ for the system as:

$$\sigma(t) = \begin{pmatrix} \sigma_1(t) \\ \sigma_2(t) \end{pmatrix} = S \cdot X(t) = \begin{pmatrix} s_{11}x_1(t) + s_{12}x_2(t) + s_{13}x_3(t) + s_{14}x_4(t) \\ s_{21}x_1(t) + s_{22}x_2(t) + s_{23}x_3(t) + s_{24}x_4(t) \end{pmatrix} = 0 \tag{7.20}$$

where $S \in R^{2\times 4}$, $X(t) \in R^{4\times 1}$; s_{11}, s_{12}, s_{13}, s_{14}, s_{21}, s_{22}, s_{23}, s_{24} are positive coefficients; $x_1(t)$, $x_2(t)$, $x_3(t)$, $x_4(t)$ are the state variable of the system in Eq. 7.1.

A tuning error σ_t is defined as following:

$$\sigma_{it}(t) = \sigma_i(t) - \varepsilon \cdot sat\ (\frac{\|\sigma_i(t)\|}{\varepsilon}),\ (\ i = 1,\ 2\ ) \tag{7.21}$$

where ε is an arbitrary positive constant; $sat(\cdot)$ is the saturation function; $\sigma(t)$ is the sliding surface.

Differentiating $\sigma(t)$ with respect to time t, one can obtain

$$\dot{\sigma}(t) = \frac{\partial \sigma(t)}{\partial x}\dot{x}(t) = \begin{pmatrix} s_{11} & s_{12} & s_{13} & s_{14} \\ s_{21} & s_{22} & s_{23} & s_{24} \end{pmatrix} \begin{pmatrix} \dot{x}_1(t) \\ \dot{x}_2(t) \\ \dot{x}_3(x) \\ \dot{x}_4(x) \end{pmatrix} \tag{7.22}$$

The above state variables are chosen as follows:

$x_1(t) = y(t),\ x_2(t) = \dot{x}_1(t),\ x_3(t) = \dot{x}_2(t),\ x_4(t) = \dot{x}_3(t)$. Therefore

$$\dot{\sigma}(t) = \frac{\partial \sigma(t)}{\partial x}\dot{x}(t) = \begin{pmatrix} s_{11} & s_{12} & s_{13} & s_{14} \\ s_{21} & s_{22} & s_{23} & s_{24} \end{pmatrix} \begin{pmatrix} y^{(1)}(t) \\ y^{(2)}(t) \\ y^{(3)}(t) \\ \Omega(x) \end{pmatrix} \tag{7.23}$$

where $Y_r(t) = r_2 y_r^{(2)}(t) + r_1 y_r^{(1)} + r_0 y_r(t)$; $e(t) = e(t, F_{pt}^{(2)}, F_{pt}^{(1)}, F_{pf}^{(2)}, F_{pf}^{(1)})$;

$$\Omega(x) = -\frac{\overline{a_0}}{a_4} y(t) - \frac{\overline{a_1}}{a_4} y^{(1)}(t) - \frac{\overline{a_2}}{a_4} y^{(2)}(t) - \frac{\overline{a_3}}{a_4} y^{(3)}(t) + \frac{b_{fp0}}{a_4} F_{pf}(t) + \frac{b_{tp0}}{a_4} F_{pt}(t) + \frac{1}{a_4}(Y_r(t) + e(t) + z_{e1}(t) + z_{e2}(t));$$

$z_{e1}(t)$ and $z_{e2}(t)$ are denoted as the estimates of $z_1(t, y_{pt}^{(4)}, y_{pt}^{(3)}, y_{pt}^{(2)})$ and $z_2(t, y_{pf}^{(4)}, y_{pf}^{(3)}, y_{pf}^{(2)})$.

Derivation of each element of the sliding surface $\sigma(t)$ is

$$\begin{aligned} \dot{\sigma}_1(t) = {} & (s_{11} - s_{14}\frac{\overline{a_1}}{a_4}) y^{(1)}(t) + (s_{12} - s_{14}\frac{\overline{a_2}}{a_4}) y^{(2)}(t) + (s_{13} - s_{14}\frac{\overline{a_3}}{a_4}) y^{(3)}(t) \\ & - s_{14}\frac{\overline{a_0}}{a_4} y(t) + \frac{s_{14}}{a_4}(Y_r(t) + e(t) + z_{e1}(t) + z_{e2}(t)) + s_{14}\frac{b_{tpo} p_t}{a_4} v_t(t) \\ & + s_{14}\frac{b_{tpo}}{a_4} g_t(v_t(t)) + s_{14}\frac{b_{fpo} p_f}{a_4} v_f(t) + s_{14}\frac{b_{fpo}}{a_4} g_f(v_f(t)) \end{aligned} \tag{7.24}$$

$$\begin{aligned} \dot{\sigma}_2(t) = {} & (s_{21} - s_{24}\frac{\overline{a_1}}{a_4}) y^{(1)}(t) + (s_{22} - s_{24}\frac{\overline{a_2}}{a_4}) y^{(2)}(t) + (s_{23} - s_{24}\frac{\overline{a_3}}{a_4}) y^{(3)}(t) \\ & - s_{24}\frac{\overline{a_0}}{a_4} y(t) + \frac{s_{24}}{a_4}(Y_r(t) + e(t) + z_{e1}(t) + z_{e2}(t)) + s_{24}\frac{b_{tpo} p_t}{a_4} v_t(t) \\ & + s_{24}\frac{b_{tpo}}{a_4} g_t(v_t(t)) + s_{24}\frac{b_{fpo} p_f}{a_4} v_f(t) + s_{24}\frac{b_{fpo}}{a_4} g_f(v_f(t)) \end{aligned} \tag{7.25}$$

where $b_{pto} = K_{pt} b_{pt0}$, $b_{pfo}(v) = K_{pf} b_{pf0}$, K_{pt} and K_{pf} are the stiffness of the each piezoactuator.

The Eqs. 7.24 and 7.25 can be transformed to the matrix forms:

$$\begin{pmatrix}\dot{\sigma}_1(t)\\ \dot{\sigma}_2(t)\end{pmatrix}=\begin{pmatrix}A_{11}\\ A_{21}\end{pmatrix}y^{(1)}(t)+\begin{pmatrix}A_{12}\\ A_{22}\end{pmatrix}y^{(2)}(t)+\begin{pmatrix}A_{13}\\ A_{23}\end{pmatrix}y^{(3)}(t)+\begin{pmatrix}A_{14}\\ A_{24}\end{pmatrix}y(t)+\begin{pmatrix}A_{15}\\ A_{25}\end{pmatrix}y_\tau^{(2)}(t)+\begin{pmatrix}A_{16}\\ A_{26}\end{pmatrix}y_\tau^{(1)}(t)+\begin{pmatrix}A_{17}\\ A_{27}\end{pmatrix}y_\tau(t)$$
$$+\begin{pmatrix}A_{18}\\ A_{28}\end{pmatrix}(e(t)+z_{e1}(t)+z_{e2}(t))+\begin{pmatrix}N_{11} & N_{12}\\ N_{21} & N_{22}\end{pmatrix}\begin{pmatrix}v_t(t)\\ v_f(t)\end{pmatrix}+\begin{pmatrix}M_{11} & M_{12}\\ M_{21} & M_{22}\end{pmatrix}\begin{pmatrix}g_t(v_t)\\ g_f(v_f)\end{pmatrix} \qquad (7.26)$$

where $A_{11}=s_{11}-s_{14}\frac{\bar{a}_1}{\bar{a}_4}$, $A_{21}=s_{21}-s_{24}\frac{\bar{a}_1}{\bar{a}_4}$, $A_{12}=s_{12}-s_{14}\frac{\bar{a}_2}{\bar{a}_4}$, $A_{22}=s_{22}-s_{24}\frac{\bar{a}_2}{\bar{a}_4}$,

$A_{13}=s_{13}-s_{14}\frac{\bar{a}_3}{\bar{a}_4}$, $A_{23}=s_{23}-s_{24}\frac{\bar{a}_3}{\bar{a}_4}$, $A_{14}=-s_{14}\frac{\bar{a}_0}{\bar{a}_4}$, $A_{24}=-s_{24}\frac{\bar{a}_0}{\bar{a}_4}$, $A_{15}=\frac{s_{14}r_2}{\bar{a}_4}$, $A_{25}=\frac{s_{24}r_2}{\bar{a}_4}$,

$A_{16}=\frac{s_{14}r_1}{\bar{a}_4}$, $A_{26}=\frac{s_{24}r_1}{\bar{a}_4}$, $A_{17}=\frac{s_{14}r_0}{\bar{a}_4}$, $A_{27}=\frac{s_{24}r_0}{\bar{a}_4}$, $A_{18}=\frac{s_{14}}{\bar{a}_4}$, $A_{28}=\frac{s_{24}}{\bar{a}_4}$,

$N_{11}=\frac{s_{14}b_{tpo}p_t}{\bar{a}_4}$, $N_{12}=\frac{s_{14}b_{fpo}p_f}{\bar{a}_4}$, $N_{21}=\frac{s_{24}b_{tpo}p_t}{\bar{a}_4}$, $N_{22}=\frac{s_{24}b_{fpo}p_f}{\bar{a}_4}$,

$M_{11}=\frac{s_{14}b_{tpo}}{\bar{a}_4}$, $M_{12}=\frac{s_{14}b_{fpo}}{\bar{a}_4}$, $M_{21}=\frac{s_{24}b_{tpo}}{\bar{a}_4}$, $M_{22}=\frac{s_{24}b_{fpo}}{\bar{a}_4}$.

We define:

$$\overline{A_1}=\begin{pmatrix}A_{11}\\ A_{21}\end{pmatrix},\ \overline{A_2}=\begin{pmatrix}A_{12}\\ A_{22}\end{pmatrix},\ \overline{A_3}=\begin{pmatrix}A_{13}\\ A_{23}\end{pmatrix},\ \overline{A_4}=\begin{pmatrix}A_{14}\\ A_{24}\end{pmatrix},\ \overline{A_5}=\begin{pmatrix}A_{15}\\ A_{25}\end{pmatrix},\ \overline{A_6}=\begin{pmatrix}A_{16}\\ A_{26}\end{pmatrix}\ \overline{A_7}=\begin{pmatrix}A_{17}\\ A_{27}\end{pmatrix}$$
$$\overline{A_8}=\begin{pmatrix}A_{18}\\ A_{28}\end{pmatrix},\ \overline{N}=\begin{pmatrix}N_{11} & N_{12}\\ N_{21} & N_{22}\end{pmatrix},\ \overline{M}=\begin{pmatrix}M_{11} & M_{12}\\ M_{21} & M_{22}\end{pmatrix},\ v(t)=\begin{pmatrix}v_t(t)\\ v_f(t)\end{pmatrix},\ g(v)=\begin{pmatrix}g_t(v_t)\\ g_f(v_f)\end{pmatrix}.$$

In terms of the above definitions, Eq. 7.26 can be rewritten

$$\dot{\sigma}(t)=\overline{A_1}y^{(1)}(t)+\overline{A_2}y^{(2)}(t)+\overline{A_3}y^{(3)}(t)+\overline{A_4}y(t)+\overline{A_5}y_\tau^{(2)}(t)+\overline{A_6}y_\tau^{(1)}(t)+\overline{A_7}y_\tau(t)$$
$$+\overline{A_8}(e(t)+z_1(t)+z_2(t))+\overline{N}v(t)+\overline{M}g(v)\ . \qquad (7.27)$$

Define $\theta_1=\overline{N}^{-1}\overline{A_1}$, $\theta_2=\overline{N}^{-1}\overline{A_2}$, $\theta_3=\overline{N}^{-1}\overline{A_3}$, $\theta_4=\overline{N}^{-1}\overline{A_4}$, $\theta_5=\overline{N}^{-1}\overline{A_5}$, $\theta_6=\overline{N}^{-1}\overline{A_6}$, $\theta_7=\overline{N}^{-1}\overline{A_7}$.

For the designs of the control law, the following assumptions concerning the system and hysteresis are required as following:

Assumption 1:

There exist positive scalars q_1, q_2, q_3, such that $\|y^{(2)}(t+\tau)\|\le q_1\|y^{(2)}(t)\|$, $\|y^{(1)}(t+\tau)\|\le q_2\|y^{(1)}(t)\|$ and $\|y(t+\tau)\|\le q_3\|y(t)\|$.

Assumption 2:

There exist known constants $b_{tp0\min}$ and $b_{tp0\max}$ such that the control gain b_{tp0} in Eq. 7.18 satisfies $b_{tp0} \in \lfloor b_{tp0\min}, b_{tp0\max} \rfloor$. There also exist known constants $b_{fp0\min}$ and $b_{fp0\max}$ such that the control gain b_{fp0} in Eq. 7.18 satisfies $b_{fp0} \in \lfloor b_{fp0\min}, b_{fp0\max} \rfloor$.

Assumption 3:

There exist known constants $p_{t\min}$ and $p_{t\max}$ such that the control gain p_t in Eq. 7.4 satisfies $p_t \in \lfloor p_{t\min}, p_{t\max} \rfloor$. There also exist known constants $p_{f\min}$ and $p_{f\max}$ such that the control gain p_f in Eq. 7.5 satisfies $p_f \in \lfloor p_{f\min}, p_{f\max} \rfloor$.

Assumption 4:

Define $\theta \in \Omega_\theta = \{\theta : \theta_{i\min} \le \theta_i \le \theta_{i\max}. \forall i \in \{1.r\}\}$, where $\theta_{i\min}$ and $\theta_{i\max}$ are known real numbers.

Assumption 5:

In Eq. 7.4 and 7.5, $g(v) = [g_t(v) \;\; g_f(v)]^T$ and $\| g(v) \| \le \rho_a$, ρ_a is constant.

With respect to the plant and hysteresis models subject to the assumptions, the following control laws and adaptation mechanisms are presented:

$$v(t) = -[k_r \sigma(t) + \hat{\theta}_1(t) y^{(1)}(t) + \hat{\theta}_2(t) y^{(2)}(t) + \hat{\theta}_3(t) y^{(3)}(t) + \hat{\theta}_4(t) y(t) + \hat{\theta}_5(t) \| y^{(2)}(t) \| + \hat{\theta}_6(t) \| y^{(1)}(t) \| + \hat{\theta}_7(t) \| y(t) \| + k^* sat(\frac{\sigma(t)}{\varepsilon})] \tag{7.28}$$

where k_r, k^* are constant positive gains; $\dot{\hat{\theta}}_i = proj(\hat{\theta}_i, -\gamma_i \omega_i)$, $proj(\cdot,\cdot)$ is a projection function defined as

$$proj(\hat{\theta}_i, -\gamma_i \omega_i) = \begin{cases} 0 & if\ (\hat{\theta}_i > \theta_{\max}\ and\ \gamma_i \omega_i < 0)\ or\ (\hat{\theta}_i < \theta_{\min}\ and\ \gamma_i \omega_i > 0) \\ -\gamma_i \omega_i & if\ (\theta_{\min} < \hat{\theta}_i < \theta_{\max})\ or\ (\hat{\theta}_i > \theta_{\max}\ and\ \gamma_i \omega_i \ge 0) \\ & \quad or\ \hat{\theta}_i < \theta_{\min}\ and\ \gamma_i \omega_i \le 0) \end{cases} \tag{7.29}$$

where $\omega_1(t)=\sigma_t(t)y^{(1)}(t)$, $\omega_2(t)=\sigma_t(t)y^{(2)}(t)$, $\omega_3(t)=\sigma_t(t)y^{(3)}(t)$, $\omega_4(t)=\sigma_t(t)y(t)$,

$\omega_5(t)=\sigma_t(t)\| y^{(2)}(t)\|$, $\omega_6(t)=\sigma_t(t)\| y^{(1)}(t)\|$, $\omega_7(t)=\sigma_t(t)\| y(t)\|$, $\varpi_i \in R^{2\times 1}$,

scalars γ_i $(i=1, 2, 3, 4, 5, 6, 7)$ are coefficients chosen by the designers.

7.2.3 Stability Analysis of the System

A Lyapunov function candidate for the system is defined as:

$$V(t)=\frac{1}{2}\{\sigma_t^T N\sigma_t(t)+\sum_{i=1}^{4}[\frac{1}{\gamma_i}(\hat{\theta}_i(t)-\theta_i)^T(\hat{\theta}_i(t)-\theta_i)]+\sum_{i=5}^{7}[\frac{1}{\gamma_i}(\hat{\theta}_i(t)-q_{i-4}\theta_i)^T(\hat{\theta}_i(t)-q_{i-4}\theta_i)]\} \qquad (7.30)$$

Case 1: when $\|\sigma(t)\| \le \varepsilon$, the derivative $\dot{V}(t)$ exists for all $\sigma(t)$, which is $\dot{V}(t)=0$.

Case 2: when $\|\sigma(t)\| > \varepsilon$, using Eq. 7.26 and the fact $\dot{\sigma} = \dot{\sigma}_t$, one can obtain

$$\begin{aligned}\dot{V}(t) &= \sigma_t^T \overline{N}^{-1}\dot{\sigma}+\sum_{i=1}^{4}[\frac{1}{\gamma_i}(\hat{\theta}_i(t)-\theta_i)^T\dot{\hat{\theta}}_i]+\sum_{i=5}^{7}[\frac{1}{\gamma_i}(\hat{\theta}_i(t)-q_{i-4}\theta_i)^T\dot{\hat{\theta}}_i] \\ &= \sum_{i=1}^{4}[\frac{1}{\gamma_i}(\hat{\theta}_i(t)-\theta_i)^T\dot{\hat{\theta}}_i]+\sum_{i=5}^{7}[\frac{1}{\gamma_i}(\hat{\theta}_i(t)-q_{i-4}\theta_i)^T\dot{\hat{\theta}}_i]+\sigma_t^T\overline{N}^{-1}(\overline{A}_1 y^{(1)}(t)+\overline{A}_2 y^{(2)}(t)+\overline{A}_3 y^{(3)}(t)+\overline{A}_4 y(t) \\ &+\overline{A}_5 y_\tau^{(2)}(t)+\overline{A}_6 y_\tau^{(1)}(t)+\overline{A}_7 y_\tau(t)+\overline{A}_8(e(t)+z_{e1}(t)+z_{e2}(t))+\overline{N}v(t)+\overline{M}g(v)) \qquad (7.31)\end{aligned}$$

As a projection function, it can obtain that $(\hat{\theta}_i-m_i\theta_i)proj(\hat{\theta}_i,r_i\varpi_i)\le(\hat{\theta}_i-m_i\theta_i)r_i\varpi_i$, m_i are positive scalars. Then,

$$\begin{aligned}\dot{V}(t) &\le \sigma_t^T(\theta_1 y^{(1)}+\theta_2 y^{(2)}+\theta_3 y^{(3)}+\theta_4 y+\theta_5 y_\tau^{(2)}+\theta_6 y_\tau^{(1)}+\theta_7 y_\tau+\overline{N}^{-1}\overline{A}_8(e(t)+z_{e1}(t)+z_{e2}(t))) \\ &+\sigma_t^T(v(t)+\overline{N}^{-1}\overline{M}g(v))+\sigma_t^T((\hat{\theta}_1-\theta_1)y^{(1)}+(\hat{\theta}_2-\theta_2)y^{(2)}+(\hat{\theta}_3-\theta_3)y^{(3)} \\ &+(\hat{\theta}_4-\theta_4)y+(\hat{\theta}_5-q_1\theta_5)\| y^{(2)}\|+(\hat{\theta}_6-q_2\theta_6)\| y^{(1)}\|+(\hat{\theta}_7-q_3\theta_7)\| y\|) \\ &\le \sigma_t^T(\theta_1 y^{(1)}+\theta_2 y^{(2)}+\theta_3 y^{(3)}+\theta_4 y+\theta_5 q_3\| y^{(2)}\|+\theta_6 q_2\| y^{(1)}\|+\theta_7 q_1\| y\|+\overline{N}^{-1}\overline{A}_8(e(t)+z_{e1}(t)+z_{e2}(t))) \\ &+\sigma_t^T(v(t)+\overline{N}^{-1}\overline{M}g(v))+\sigma_t^T((\hat{\theta}_1-\theta_1)y^{(1)}+(\hat{\theta}_2-\theta_2)y^{(2)}+(\hat{\theta}_3-\theta_3)y^{(3)} \\ &+(\hat{\theta}_4-\theta_4)y+(\hat{\theta}_5-q_1\theta_5)\| y^{(2)}\|+(\hat{\theta}_6-q_2\theta_6)\| y^{(1)}\|+(\hat{\theta}_7-q_3\theta_7)\| y\|) \\ &\le \sigma_t^T(\overline{N}^{-1}\overline{A}_8(e(t)+z_{e1}(t)+z_{e2}(t))+\overline{N}^{-1}\overline{M}g(v))-\sigma_t^T(k_r\sigma(t)+\hat{\theta}_1 y^{(1)}(t)+\hat{\theta}_2 y^{(2)}(t)\end{aligned}$$

$$+\hat{\theta}_3 y^{(3)}(t)+\hat{\theta}_4 y+\hat{\theta}_5 \| y^{(2)}(t)\| +\hat{\theta}_6 \| y^{(1)}(t)\| +\hat{\theta}_7 \| y(t)\| +k^* sat(\frac{\sigma}{\varepsilon}))$$

$$+\sigma_t^T(\hat{\theta}_1 y^{(1)}+\hat{\theta}_2 y^{(2)}+\hat{\theta}_3 y^{(3)}+\hat{\theta}_4 y+\hat{\theta}_5 \| y^{(2)}\| +\hat{\theta}_6 \| y^{(1)}\| +\hat{\theta}_7 \| y\|)$$

$$\le -\sigma_t^T k_r \sigma(t)-\sigma_t^T k^* sat(\frac{\sigma}{\varepsilon})+\sigma_t^T(\overline{N}^{-1}\overline{A}_8(e(t)+z_{e1}(t)+z_{e2}(t))+\overline{N}^{-1}\overline{M}g(v))$$

$$\le -\sigma_t^T k_r \sigma_t(t)-\sigma_t^T k^* sat(\frac{\sigma}{\varepsilon})+\sigma_t^T(\overline{N}^{-1}\overline{A}_8(e(t)+z_{e1}(t)+z_{e2}(t))+\overline{N}^{-1}\overline{M}g(v)) \qquad (7.32)$$

Based on the definition in Eq. 7.20, it leads to $\sigma_t^T k^* sat(\frac{\sigma}{\varepsilon}) = (|\sigma_1|+|\sigma_2|)\cdot k^* = \| \sigma_t \| \cdot k^*$ (7.33)

So Eq. 7.32 can be rewritten as:

$$\dot{V}(t) \le -k_r \| \sigma_t(t)\|^2 - \| \sigma_t^T \| k^* + \| \sigma_t^T \| \cdot \| \overline{N}^{-1} \| (\| \overline{A}_8 \| \cdot (\| e(t) \| + z_{e1}(t)+z_{e2}(t)) + \| \overline{M} \| \cdot \| g(v) \|) \qquad (7.34)$$

In the *Assumption 5* and the *Remark A*, $\| g(v)\| \le \rho_a$ and $\|e(t)\| \le \rho(t)$ are assumed. While defines $k^* = k^*_{\max} \ge \| \overline{N}^{-1} \| (\| \overline{A}_8 \| \cdot (\rho(t)+z_{e1}(t)+z_{e2}(t)) + \| \overline{M} \| \cdot \rho_a)$, one can obtain

$$\dot{V}(t) \le -k_r \| \sigma_t(t)\|^2 - \| \sigma_t^T \| \cdot k^*_{\max} + \| \sigma_t^T \| \cdot \| \overline{N}^{-1} \| (\| \overline{A}_8 \| \cdot (\| e(t) \| + z_{e1}(t)+z_{e2}(t)) + \| \overline{M} \| \cdot \| g(v) \|)$$

$$\le -k_r \| \sigma_t(t)\|^2 \qquad \forall \| \sigma(t)\| > \varepsilon \qquad (7.35)$$

Based on the above analyses and proof, the following theorem regarding the stability of the closed-loop system described by Eqs. (7.4), (7.5), (7.18) and (7.28) can be established.

Theorem: For the plant in Eq. (7.1) subject to *Assumptions 1-5* and *Remark A*, the robust adaptive controller specified by Eq. (7.28) ensures that all the closed-loop signals are bounded and the state variable $y(t)$ converges to zero for $\forall t \ge t_0$.

7.3 Simulation Results

In order to eliminate the chatter in the metal cutting processes, the adaptive controller in Eq. 7.28 is introduced into the system in Eq. 7.1. The parameters involved in all above equations in

simulation are given in Table D. Fig. 7.3 shows the dynamic response of the metal cutting system in Eq. 7.1 combined with the control law in Eq. 7.28; Fig. 7.4 illustrates the steady-state error between the desired value and actual response of the system in Eq. 7.1; Fig. 7.5 plots the dynamic response of the main cutting force $F_c(t)$ during the cutting process; Fig. 7.6 represents the dynamic response of the thrust force $F_t(t)$ during the cutting process; Fig. 7.7 plots the dynamic performance of the piezoactuator during the cutting process; Figs. 7.8 and 7.9 illustrate the performances of the two piezoactuatos in both the thrust-direction and the feed-direction during the cutting process.

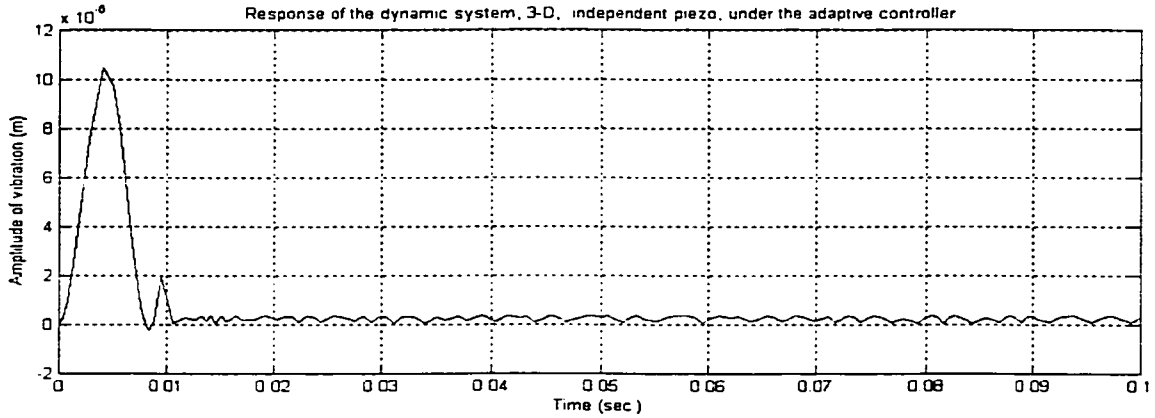

Figure 7.3 Response of dynamic system with the control law

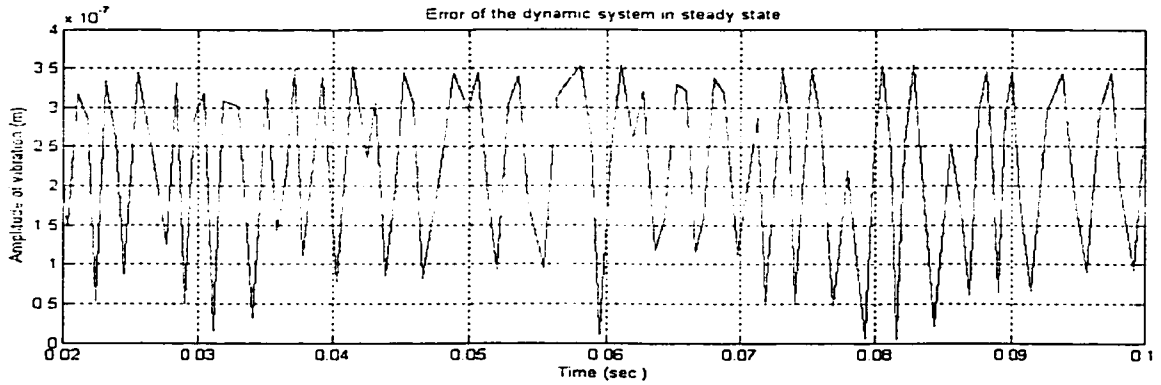

Figure 7.4 Steady-state error of the dynamic system with the control law

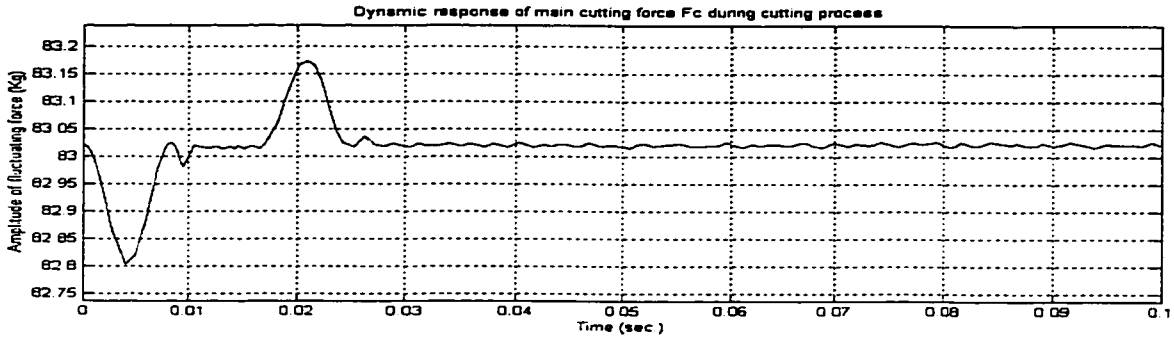

Figure 7.5 Response of main cutting force $F_c(t)$ during cutting process

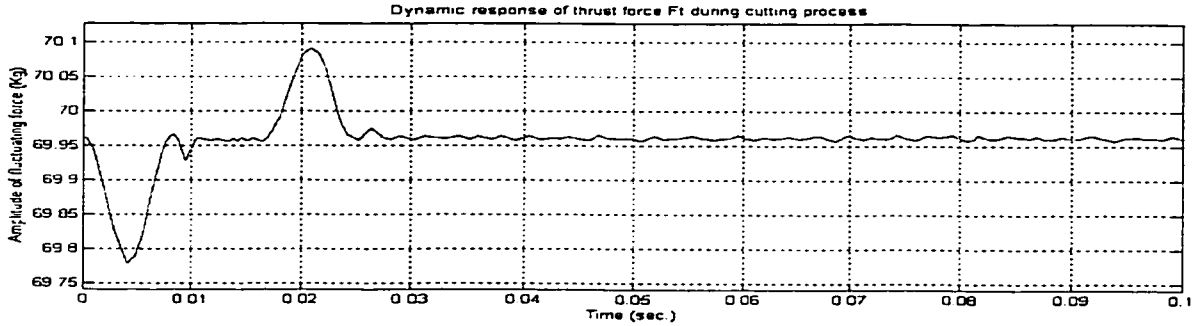

Figure 7.6 Response of thrust force $F_t(t)$ during cutting process

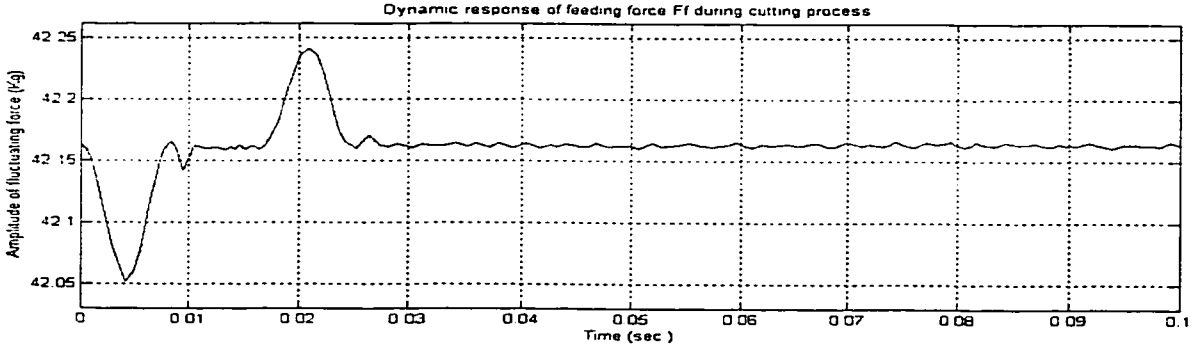

Figure 7.7 Response of thrust force $F_f(t)$ during cutting process

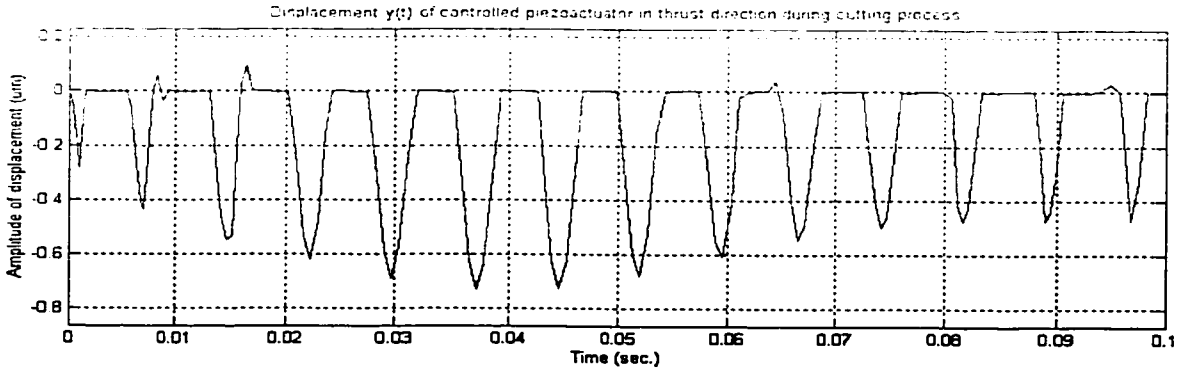

Figure 7.8 Displacement of the controlled piezoactuator in the thrust-direction

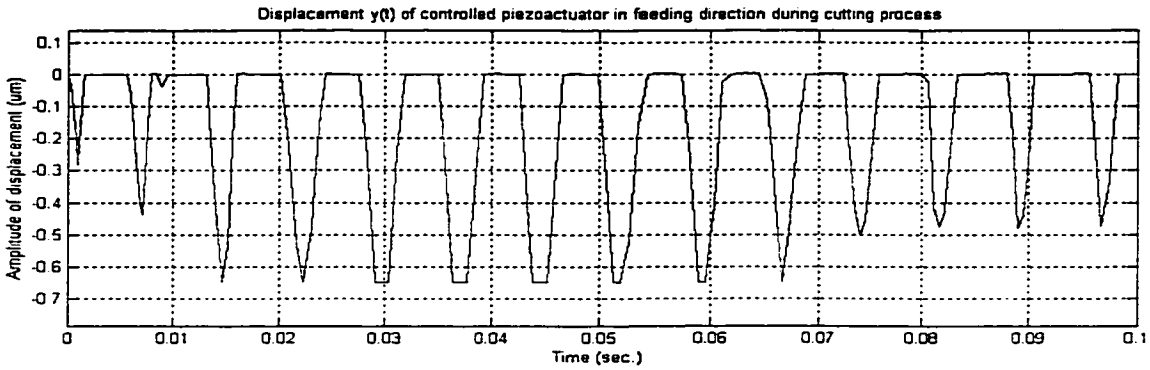

Figure 7.9 Displacement of the controlled piezoactuator in the feed-direction

From Fig. 7.3 through Fig. 7.9, the simulations of the dynamic performance of the system with the adaptive controllers show clearly that the proposed adaptive controllers can sigificantly suppress the chatter.

7.4 Summary

In order to suppress the chatter in metal cutting system with two degree-of-freedom and three-dimensional force models, two piezoactuators independent from the tool holder are introduced into the system with the hysteresis and time lag; two adaptive controllers for the system are presented; the simulation results show that the designed control law significantly eliminates the chatter effect in the metal cutting processes.

Chapter 8

Conclusions and Future Work

8.1 Conclusions

In this thesis, the work is focused on the self-exited vibrations, namely chatter, which is one of the main industrial problems in the metal cutting processes. The obvious characteristics of chatter are the small amplitudes and high frequencies, therefore, the active controllers providing the forces onto the cutting system to overcome the chatter effect are required. Recently, because of possessing many advantage properties, the piezoactuators are widely applied in the positioning control in the metal cutting systems. In order to suppress chatter in the metal cutting processes, particularly in turning, the robust adaptive controllers are designed by using the piezoactuators. Furthermore, it is necessary to investigate thoroughly over the turning structures, the dynamic cutting processes, and the relationships between the cutting forces and uncut chip thickness. The accurate and practical mathematical models concerning above physical processes are required so as to implement the system control for the purpose of the chatter suppression.

In this thesis, rather than using the commonly accepted linear models, the relations between the cutting forces and uncut chip thickness are treated as nonlinear hysteretic characteristic models, which have been proved to give a better description between the cutting forces and uncut chip thickness.

The machine structures are described as the classes of the uncertain systems with two degree-of-freedom, the hysteretic characteristics of relations between the cutting forces and uncut chip

thickness, and time delay output feedback. With respect to the different machining conditions, the metal cutting processes also are divided into two-dimensional force and three-dimensional force models.

The piezoactuators have been introduced in the metal cutting systems as the positioning control elements. The piezoactuators also display hysteretic behaviors of the relationship between the applied voltage and the deflection of the piezoactuator due to the voltage.

In generally, the work concentrates on the suppression of the type A of chatter in metal cutting processes in turning; construction of the four different dynamic structures of the metal cutting processes in terms of the cutting force models and piezoactuators' mechanical structures; building the nonlinear dynamic models of the piezoactuators; designing the robust adaptive control schemes with respect to the different dynamic structures of the metal cutting processes; theoretical proving the global stability of the controlled systems with the corresponding control laws; calculation and plot of the simulated dynamic performances of the metal cutting systems with proposed adaptive control laws.

8.2 Future Work

8.2.1 Phase Difference Effect on Chatter

The analyses on the stability of the metal cutting processes show that a phase difference between the vibration at an angular position of a workpiece's revolution and that at the same position of the previous revolution always occur for successive revolutions of the workpiece by the regenerative

effect [46]. However, so far, very few investigations, which describe the experimental characteristics of the phase difference in the metal cutting processes, have been published.

The phase difference has been considered to be directly related with the patterns of the chatter marks, which creating the different time delays relating to uncut chip thickness and likely varying from clockwise to counterclockwise along the feed. No systematic relation between the cutting conditions and the phase difference has been investigated currently. Nevertheless, some experiments show that the phase difference become constant at a value between 30 and 90 degrees following fluctuations after the excitation. The phase difference may increase or decrease during the fluctuation periods. What extent the effect of the phase difference on chatter and the reasons that the phase difference becomes a fixed quantity after sufficient growth of the amplitude of chatter are not obvious at present and will be studied in the future.

8.2.2 Damping Forces Acting on the Workpiece

In turning processes, not only there exists the nonlinearity caused by the cutting tool jumping and disengaging from the workpiece due to the vibrations between the cutting tool and workpiece, but also the other nonlinearity due to the cutting process damping caused by the interference of the tool flank with the machined surface (shown in Fig. 8.1).

It is seen that the clearance angle b between the tool flank and the machined surface varies when the cutting tool travels along the machined surface undulation. At position A (shown in Fig. 8.1), the clearance angle b is equal to the tool clearance b_0. However, the clearance angle b becomes smaller at position B and gets even smaller at position C when the cutting tool travels in the downward direction. With the decrease of the clearance angle b, the interference of the tool flank with the machined surface will generate the additional damping force in both degree-freedom

directions of Y and X. However, the interference of tool flank with the machined surface does not occur at position D, where the slope of machined surface is positive. As a result, the additional damping force will not be generated when the cutting tool travels in the upward direction.

Since the additional damping force as pointed out by Moriwaki and Iwata [47] is introduced into the dynamic systems, while the clearance angle b becomes smaller than the tool clearance angle, the equations of the dynamic systems supplied in preceding chapters would be updated. As a result, the clearance angle b becomes smaller so as to increase the process damping value. Due to the increase of damping at low cutting speeds, the system stability is greatly increased. Some experiments show that the additional damping force strongly influences the cutting stability at low cutting speeds. This phenomenon has been observed by Tlusty and Ismail [5]. However, it has to be pointed out that further investigations of the process damping is still required in order to model the process damping force more accurately.

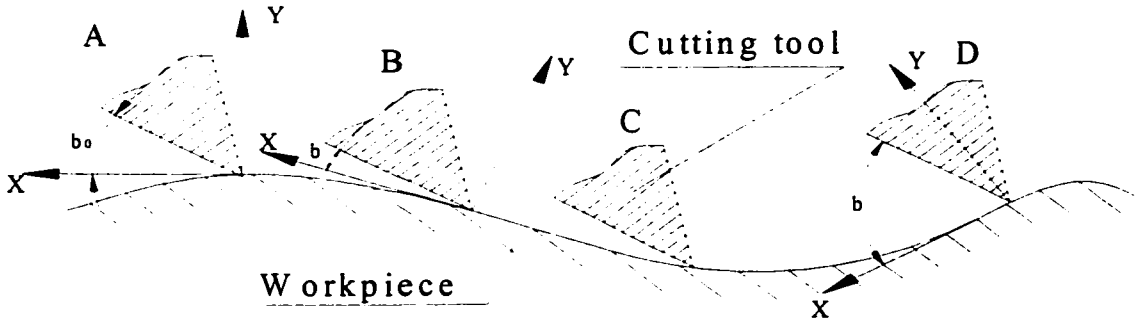

Figure 8.1 Variation of clearance angle b in the cutting process

8.2.3 Type *B* of Chatter

Referring to the Fig. 1.5, when relative stiffness in one direction *A* is small but in the direction *B* is large, Type *A* chatter occurs. The opposite relative stiffness conditions between cutting edge and workpiece result in Type *B* chatter

In some papers published presently, it has been commonly assumed that chatter can exist in either the direction *A* or the direction *B* referring to Fig. 1.5, but not in both at once. This means that two types of chatters are always distinguished depending on whether the chatter amplitudes fall in the direction of the tool shank or in the direction of the workpiece velocity. Accordingly, these will be named Typy *A* and Type *B* chatter respectively. Type *B* chatter is the more complicated form than Type *A* chatter and has been shown in [4] that the incremental thrust-component expression for Type *A* chatter is a special case of the equivalent expression for Type *B* chatter. In [4], there are a series of mathematical analyses concerning Type *B* chatter and the relation of Type *A* and Type *B* chatters under orthogonal cutting conditions.

To construct the dynamic models of the metal cutting processes and suppress the self-exited vibrations, the effect of Type *B* chatter on the finish of machined workpiece surfaces will be took into account along with Typy *A* chatter, and Type *B* will be also treated as one of the main aspects influencing uncut chip thickness.

Appendix A: The Estimate of Disturbance $z(t, y_p^{(4)}, y_p^{(3)}, y_p^{(2)})$ (scalar)

The uncertain system in Eq. 6.15 is as following:

$$\begin{aligned}
&\overline{a}_4 y^{(4)}(t) + \overline{a}_3 y^{(3)}(t) + \overline{a}_2 y^{(2)}(t) + \overline{a}_1 y^{(1)}(t) + \overline{a}_0 y(t) \\
&= r_2 y_r^{(2)}(t) + r_1 y_r^{(1)}(t) + r_0 y_r(t) + b_{ip0} F_v(t) + z(t, y_p^{(4)}, y_p^{(3)}, y_p^{(2)}) + e(t, F_v^{(1)}, F_v^{(2)}) \\
&= r_2 y_r^{(2)}(t) + r_1 y_r^{(1)}(t) + r_0 y_r(t) + b_{ip2} F_v^{(2)}(t) + b_{ip1} F_v^{(1)}(t) + b_{ip0} F_v(t) + z(t, y_p^{(4)}, y_p^{(3)}, y_p^{(2)}) \ .
\end{aligned} \tag{a.1}$$

where all coefficients in Eq. a.1 are defined in Eq. 6.15; the uncertain disturbance $z(t)$ will be estimated approximately.

Assumption: The disturbance $z(t)$ is bounded; its upper and lower bounds are unknown.

In terms of Eq. a.1, we define

$$\overline{a}(\partial) = \left(\overline{a}_4\partial^4 + \overline{a}_3\partial^3 + \overline{a}_2\partial^2 + \overline{a}_1\partial + \overline{a}_0 \quad - r_2\partial^2 - r_1\partial - r_0\right), \qquad b(\partial) = b_{ip2}\partial^2 + b_{ip1}\partial + b_{ip0}\ , \qquad v(t) = F_v(t),$$

$$\overline{z}(t) = \frac{z(t, y_p^{(4)}, y_p^{(3)}, y_p^{(2)})}{b(\partial)}, \qquad \overline{y}(t) = \left(y(t) \quad y_r(t)\right)^T, \qquad \overline{c} = \left(1 \quad 1\right).$$

where ∂ is the differential operator, $y(t)$ *and* $v(t)$ are the output and input respectively.

The uncertain system in Eq. a.1 can be rewritten as following:

$$\overline{a}(\partial)\overline{y}(t) = b(\partial)(v(t) + \overline{z}(t)) \tag{a.2}$$

where n is the order of $\overline{a}(\partial)$, m is the order of $b(\partial)$, thus $n = 4$; $m = 2$.

Motivated by the formulation of the state observer for a possibly unstable system, we introduce a monic second order Hurwitz polynomial $f(\partial)$

$$f(\partial) = \frac{b(\partial)(\partial + \psi)^2}{b_r} = \frac{(b_{ip2}\partial^2 + b_{ip1}\partial + b_{ip0})(\partial + \psi)^2}{b_r} \tag{a.3}$$

where ψ is a positive constant; $b_r = b_{ip2}$.

Now rewriting Eq. a.2 as

$$\overline{c}\ \overline{y}(t) = \frac{\overline{c}f(\partial) - \overline{a}(\partial)}{f(\partial)}\overline{y}(t) + \frac{b_r}{(\partial + \psi)^2}v(t) + \frac{b_r}{(\partial + \psi)^2}\overline{z}(t) \tag{a.4}$$

Multiplying both sides of Eq. a.4 with $(\partial+\psi)$ yields

$$\bar{c}\,\dot{\bar{y}}(t)+\bar{c}\,\psi\bar{y}(t)=b_r\frac{\bar{c}f(\partial)-\bar{a}(\partial)}{b(\partial)(\partial+\psi)}\bar{y}(t)+\frac{b_r}{(\partial+\psi)}v(t)+\frac{b_r}{(\partial+\psi)}\bar{z}(t) \tag{a.5}$$

The proposed formulation can be summarized in the following.

Step1: based on Eq. a.5, $\frac{1}{(\partial+\psi)^{r-1}}\bar{z}(t)$ is estimated.

Motivated by the formulation of the Luenberger-type state observer, consider the dynamical system described by

$$\bar{c}\,\dot{\hat{\bar{y}}}(t)+\bar{c}\,\psi\hat{\bar{y}}(t)=b_r\frac{\bar{c}f(\partial)-\bar{a}(\partial)}{b(\partial)(\partial+\psi)}\bar{y}(t)+\frac{b_r}{(\partial+\psi)}v(t)+b_r w_1(t) \tag{a.6}$$

$$\hat{\bar{y}}(t_0)=y(t_0)=0 \tag{a.7}$$

where $w_1(t)$ is a signal to be determined, $\hat{\bar{y}}(t)$ is the solution of the Eq. a.7.

Combining Eq. a.5 and a.7, yields

$$\bar{c}\,\dot{\Delta\bar{y}}(t)+\bar{c}\,\psi\Delta\bar{y}(t)=b_r\{\frac{1}{(\partial+\psi)}\bar{z}(t)-w_1(t)\} \tag{a.8}$$

where $\Delta\bar{y}=\bar{y}(t)-\hat{\bar{y}}(t)$, it can be seen that, If the signal $w_1(t)$ can be formulated such that $\dot{\Delta\bar{y}}(t)$ and $\Delta\bar{y}(t)$ are very small, then $w_1(t)$ can be regarded as the approximate estimate of $\frac{1}{(\partial+\psi)}\bar{z}(t)$.

In this research, the formulation of $w_1(t)$ is motivated by the variable structure method and the adaptive control technique. By adaptively updating the upper bound $C_{r-1}=C_1$ of $\left|\frac{1}{(\partial+\psi)^{r-1}}\bar{z}(t)\right|$, the signal $w_1(t)$ is considered as

$$w_1(t)=\hat{C}_1(t)\frac{b_r\bar{c}(\bar{y}(t)-\hat{\bar{y}}(t))}{\left\|b_r(\bar{y}(t)-\hat{\bar{y}}(t))\right\|+\delta_1}, \tag{a.9}$$

where $\delta_1(=2\times10^{-4\sim-5})$ is a small positive constant, $\hat{C}_1(t)$ is updated by the following adaptive mechanism

$$\dot{\hat{C}}_1(t)=\begin{cases}\chi_1\left\|\bar{y}(t)-\hat{\bar{y}}(t)\right\| & if\left\|\bar{y}(t)-\hat{\bar{y}}(t)\right\|>\sqrt{\dfrac{2\delta_1\hat{C}_1}{\psi}}\\ 0 & otherwise\end{cases} \tag{a.10}$$

where $\hat{C}_1(t_0)$ can be chosen as any small positive constant, χ_1 is a positive constant.

Thus, $w_1(t)$ is the approximate estimate of $\dfrac{1}{(\partial+\psi)}\bar{z}(t)$.

Step 2: $\dfrac{1}{(\partial+\psi)^{r-2}}\bar{z}(t)$ ($r=2$) is estimated by using $w_1(t)$ based on trivial Eq. a.11

$$\frac{d}{dt}\left(\frac{1}{(\partial+\psi)^{r-1}}\bar{z}(t)\right)+\frac{\psi}{(\partial+\psi)^{r-1}}\bar{z}(t)=\frac{1}{(\partial+\psi)^{r-2}}\bar{z}(t) \tag{a.11}$$

Corresponding to Eq. a.11, Eq. a.12 is considered

$$\dot{\bar{w}}_1(t)+\psi\bar{w}_1(t)=w_2(t) \tag{a.12}$$

where $w_2(t)$ is signal to be determined, $\bar{w}_1(t)$ is the solution of Eq. a.12, $\bar{w}_1(t_0)=0$.

By mimicking the formulation of the first step, $w_2(t)$ is chosen as

$$w_2(t)=\hat{C}_2(t)\frac{w_1(t)-\bar{w}_1(t)}{\left|w_1(t)-\bar{w}_1(t)\right|+\delta_2}, \tag{a.13}$$

where δ_2 is a small positive constant, $\hat{C}_2(t)$ is updated by the following adaptive mechanism

$$\dot{\hat{C}}_2(t)=\begin{cases}\chi_2\left|w_1(t)-\bar{w}_1(t)\right| & if\left|w_1(t)-\bar{w}_1(t)\right|>\sqrt{\dfrac{2\delta_2\hat{C}_2}{\psi}}\\ 0 & otherwise\end{cases} \tag{a.14}$$

where $\hat{C}_2(t_0)$ can be chosen as any small positive constant, χ_2 is a positive constant.

$w_2(t)$ is the approximate estimate of $\dfrac{1}{(\partial+\psi)^{r-r}}\bar{z}(t)$, i.e., $\bar{z}(t)=w_2(t)$.

Therefore $\bar{z}(t)b(\partial)=z(t,y_p^{(4)},y_p^{(3)},y_p^{(2)})$.

Appendix B: The Estimate of Disturbance $z(t, y_p^{(4)}, y_p^{(3)}, y_p^{(2)})$ (vector)

The uncertain system in Eq. 7.18 rewritten as following:

$$\begin{aligned}&\overline{a}_4 y^{(4)}(t) + \overline{a}_3 y^{(3)}(t) + \overline{a}_2 y^{(2)}(t) + \overline{a}_1 y^{(1)}(t) + \overline{a}_0 y(t)\\ &= r_2 y_r^{(2)}(t) + r_1 y_r^{(1)}(t) + r_0 y_r(t) + b_{fp2} F_{vt}^{(2)}(t) + b_{fp1} F_{vt}^{(1)}(t) + b_{fp0} F_{vt}(t)\\ &+ b_{fp2} F_{vf}^{(2)}(t) + b_{fp1} F_{vf}^{(1)}(t) + b_{fp0} F_{vf}(t) + z_1(t, y_{pt}^{(4)}, y_{pt}^{(3)}, y_{pt}^{(2)}) + z_2(t, y_{pf}^{(4)}, y_{pf}^{(3)}, y_{pf}^{(2)}) \quad .\end{aligned} \tag{b.1}$$

where the all coefficients in Eq. b.1 are defined in Eq. 7.18; and uncertain disturbance $z(t) = \left(z_1(t, y_{pt}^{(4)}, y_{pt}^{(3)}, y_{pt}^{(2)}) \quad z_2(t, y_{pf}^{(4)}, y_{pf}^{(3)}, y_{pf}^{(2)})\right)^T$ will be estimated online.

Assumption: the disturbance $z(t)$ is bounded; its upper and lower bounds are unknown.

In terms of Eq. b.1, we define

$$\overline{a}(\partial) = \left(\overline{a}_4\partial^4 + \overline{a}_3\partial^3 + \overline{a}_2\partial^2 + \overline{a}_1\partial + \overline{a}_0 \quad -r_2\partial^2 - r_1\partial - r_0\right),$$

$$b(\partial) = \left(b_1(\partial) \quad b_2(\partial)\right) = \left(b_{tp2}\partial^2 + b_{tp1}\partial + b_{tp0} \quad b_{fp2}\partial^2 + b_{fp1}\partial + b_{fp0}\right), \quad \overline{y}(t) = \left(y(t) \quad y_r(t)\right)^T,$$

$$v(t) = \left(v_1(t) \quad v_2(t)\right)^T = \left(F_{vt}(t) \quad F_{vf}(t)\right)^T, \quad \overline{z}(t) = \begin{pmatrix} \dfrac{1}{b_1(\partial)} & 0 \\ 0 & \dfrac{1}{b_2(\partial)} \end{pmatrix} z(t) \ , \quad \overline{c} = \begin{pmatrix} 1 & 1 \end{pmatrix} .$$

where ∂ is the differential operator, $y(t)$ *and* $v(t)$ are the output and input respectively.

For simplicity, the Eq. (b.1) can be written as follow,

$$\overline{a}(\partial)\overline{y}(t) = b(\partial)(v(t) + \overline{z}(t)) \tag{b.2}$$

where n is the order of $\overline{a}(\partial)$, m is the order of $b(\partial)$, thus $n = 4$; $m = 2$.

Motivated by the formulation of the state observer for a possibly unstable system, we introduce a monic second order Hurwitz polynomial $f(\partial)$

$$f(\partial) = \left(b_1(\partial) \quad b_2(\partial)\right)\begin{pmatrix} \dfrac{(\partial+\psi)^2}{b_{r1}} & \dfrac{(\partial+\psi)^2}{b_{r2}} \end{pmatrix}^T \tag{b.3}$$

where $b_r = \left(b_{r1} \quad b_{r2}\right)^T = \left(b_{tp2} \quad b_{fp2}\right)^T$, ψ is a positive constant.

Eq. b.2 is rewritten as: $\overline{c}\ \overline{y}(t) = \dfrac{\overline{c}f(\partial) - \overline{a}(\partial)}{f(\partial)}\overline{y}(t) + \begin{pmatrix} \dfrac{b_{r1}}{(\partial+\psi)^2} & \dfrac{b_{r2}}{(\partial+\psi)^2} \end{pmatrix}(v(t) + \overline{z}(t))$ (b.4)

Multiplying both sides of Eq. b.4 with $(\partial+\psi)$ yields

$$\bar{c}\dot{\bar{y}}(t)+\bar{c}\psi\bar{y}(t)=\frac{\bar{c}f(\partial)-\bar{a}(\partial)}{Z(\partial)(\partial+\psi)}\bar{y}(t)+(b_{r1}\quad b_{r2})(\frac{v(t)}{(\partial+\psi)}+\frac{\bar{z}(t)}{(\partial+\psi)}) \tag{b.5}$$

where $Z(\partial)=(b_1(\partial)\quad b_2(\partial))\cdot(1/b_{r1}\quad 1/b_{r2})^T$.

The proposed formulation can be summarized in the following.

Step1: based on the Eq. b.5, $\frac{1}{(\partial+\psi)^{r-1}}\bar{z}(t)$ is estimated.

Motivated by the formulation of the Luenberger-type state observer, consider the dynamical system described by

$$\bar{c}\dot{\hat{\bar{y}}}(t)+\bar{c}\psi\hat{\bar{y}}(t)=\frac{\bar{c}f(\partial)-\bar{a}(\partial)}{Z(\partial)(\partial+\psi)}\bar{y}(t)+(b_{r1}\quad b_{r2})(\frac{v(t)}{(\partial+\psi)}+w_1(t)) \tag{b.6}$$

$$\hat{\bar{y}}(t_0)=y(t_0) \tag{b.7}$$

where $w_1(t)=(w_{10}(t)\quad w_{11}(t))^T$ is a signal to be determined, $\hat{\bar{y}}(t)$ is the solution of Eq. b.6.

Combining Eq. b.5 and b.6, yields

$$\bar{c}\Delta\dot{\bar{y}}(t)+\bar{c}\psi\Delta\bar{y}(t)=(b_{r1}\quad b_{r2})\{\frac{1}{(\partial+\psi)}\bar{z}(t)-w_1(t)\} \tag{b.8}$$

where $\Delta\bar{y}=\bar{y}(t)-\hat{\bar{y}}(t)$, it can be seen that, If the signal $w_1(t)$ can be formulated such that $\dot{\Delta\bar{y}}(t)$ and $\Delta\bar{y}(t)$ are very small, then $w_{1j}(t)$ can be regarded as the approximate estimate of $\frac{\bar{z}_j(t)}{(\partial+\psi)}$, ($j=0$,1), because $\bar{z}(t)\in R^{2x1}$.

The formulation of $w_1(t)$ is motivated by the variable structure method and the adaptive control technique. By adaptively updating the upper bound $C_{r-1}=C_1$ of $\left\|\frac{\bar{z}(t)}{(\partial+\psi)^{r-1}}\right\|$, the signal $w_1(t)$ is considered as:

$$w_1(t)=\begin{pmatrix}w_{10}(t)\\ w_{11}(t)\end{pmatrix}=\frac{\hat{C}_1(t)\bar{c}(\bar{y}(t)-\hat{\bar{y}}(t))b_r}{\left\|b_r(\bar{y}(t)-\hat{\bar{y}}(t))\right\|+\delta_1}=\frac{\hat{C}_1(t)\bar{c}(\bar{y}(t)-\hat{\bar{y}}(t))}{\left\|b_r(\bar{y}(t)-\hat{\bar{y}}(t))\right\|+\delta_1}\begin{pmatrix}b_{r1}\\ b_{r2}\end{pmatrix}, \tag{b.9}$$

where $\delta_1(=2\times10^{-4\sim-5})$ is a small positive constant, $\hat{C}_1(t)$ is updated by the following adaptive law

$$\dot{\hat{C}}_1(t)=\begin{cases}\chi_1\left\|\bar{y}(t)-\hat{\bar{y}}(t)\right\| & if\left\|\bar{y}(t)-\hat{\bar{y}}(t)\right\|>\sqrt{\dfrac{2\delta_1\hat{C}_1}{\psi}}\\ 0 & otherwise\end{cases} \tag{b.10}$$

where $\hat{C}_1(t_0)$ can be chosen as any small positive constant, χ_1 is a positive constant.

Thus, $w_{1i}(t)$ is the approximate estimate of $\dfrac{1}{(\partial+\psi)^{r-1}}\bar{z}_j(t)$ ($j=0,\ 1$).

Step 2: $\dfrac{1}{(\partial+\psi)^{r-i}}\bar{z}(t)$ ($i=2$) is estimated by using $w_1(t)$ based on Eq. b.11:

$$\frac{d}{dt}\left(\frac{1}{(\partial+\psi)^{r-1}}\bar{z}(t)\right)+\frac{\psi}{(\partial+\psi)^{r-1}}\bar{z}(t)=\frac{1}{(\partial+\psi)^{r-2}}\bar{z}(t). \tag{b.11}$$

Corresponding to Equation above, Eq. b.12 is considered

$$\dot{\tilde{w}}_{i-1}(t)+\psi\tilde{w}_{i-1}(t)=w_i(t) \tag{b.12}$$

where $w_i(t)=\left(w_{i0}(t)\quad w_{i1}(t)\right)^T$ is the signal to be determined, $\tilde{w}_{i-1}(t)=\left(\tilde{w}_{(i-1)0}(t)\quad \tilde{w}_{(i-1)1}(t)\right)^T$ is the solution of Eq. b.12, $\tilde{w}_{i-1}(t_0)=0$.

By mimicking the formulation of the first step, $w_2(t)$ is chosen as

$$w_2(t)=\frac{(w_1(t)-\tilde{w}_1(t))\hat{C}_2(t)}{\left\|w_1(t)-\tilde{w}_1(t)\right\|+\delta_1}, \tag{b.13}$$

where δ_2 is a small positive constant, $\hat{C}_2(t)$ is updated by the following adaptive mechanism

$$\dot{\hat{C}}_2(t)=\begin{cases}\chi_2\left\|w_1(t)-\tilde{w}_1(t)\right\| & if\left\|w_1(t)-\tilde{w}_1(t)\right\|>\sqrt{\dfrac{2\delta_2\hat{C}_2}{\psi}}\\ 0 & otherwise\end{cases} \tag{b.14}$$

where $\hat{C}_i(t_0)$ can be chosen as any small positive constant, χ_2 is a positive constant.

$w_2(t)$ will be the approximate estimate of $\dfrac{1}{(\partial+\psi)^{r-r}}\bar{z}(t)$, i.e., $w_{2_j}(t)=\bar{z}_j(t)$, $(j=0,\ 1)$.

Therefore, $z_1(t,y_{pr}^{(4)},y_{pr}^{(3)},y_{pr}^{(2)})=b_1(\partial)\bar{z}_0$; $z_2(t,y_{pf}^{(4)},y_{pf}^{(3)},y_{pf}^{(2)})=b_2(\partial)\bar{z}_1$.

Appendix C: Sliding Surface Design for the Dynamic System with Two-Dimensional Forces

The equivalent system in Eq. 4.14 is as follow

$$\begin{pmatrix} \dot{x}_1(t) \\ \dot{x}_2(t) \\ \dot{x}_3(t) \\ \dot{x}_4(t) \end{pmatrix} = \begin{pmatrix} 0 & 1 & 0 & 0 \\ 0 & 0 & 1 & 0 \\ 0 & 0 & 0 & 1 \\ -\frac{\overline{a_0}}{\overline{\overline{a_4}}} & -\frac{\overline{a_1}}{\overline{\overline{a_4}}} & -\frac{\overline{a_2}}{\overline{\overline{a_4}}} & -\frac{\overline{a_3}}{\overline{\overline{a_4}}} \end{pmatrix} \cdot \begin{pmatrix} x_1(t) \\ x_2(t) \\ x_3(t) \\ x_4(t) \end{pmatrix} + \begin{pmatrix} 0 \\ 0 \\ 0 \\ \frac{b_{tp0}}{\overline{\overline{a_4}}} \end{pmatrix} \cdot u(t) = Ax(t) + Bu(t). \qquad \text{(c.1)}$$

where $u(t) = F_p(t)$.

We concentrate on the case of linear sliding surface, $\sigma(x(t)) = Sx(t)$, where $S = (s_1 \quad s_2 \quad s_3 \quad s_4)$, and $x(t) = (x_1(t) \quad x_2(t) \quad x_3(t) \quad x_4(t))^T$.

The method of the quivalent control produces the following system further

$$\dot{x}(t) = (I - B(SB)^{-1}S)Ax(t) \qquad \text{(c.2)}$$

Provided $\sigma(x(t_0)) = 0$ for some t_0

In terms of Eq. c.1 and c.2, $SB = \frac{s_4 b_{tp0}}{\overline{\overline{a_4}}}$, $\quad SB^{-1} = \frac{\overline{a_4}}{s_4 b_{tp0}}$,

Then Eq. c.2 can be rewritten as following

$$\dot{x}(t) = \left[I - \frac{\overline{a_4}}{s_4 b_{tp0}} \begin{pmatrix} 0 \\ 0 \\ 0 \\ \frac{b_{tp0}}{\overline{\overline{a_4}}} \end{pmatrix} (s_1 \quad s_2 \quad s_3 \quad s_4) \right] \cdot \begin{pmatrix} 0 & 1 & 0 & 0 \\ 0 & 0 & 1 & 0 \\ 0 & 0 & 0 & 1 \\ -\frac{\overline{a_0}}{\overline{\overline{a_4}}} & -\frac{\overline{a_1}}{\overline{\overline{a_4}}} & -\frac{\overline{a_2}}{\overline{\overline{a_4}}} & -\frac{\overline{a_3}}{\overline{\overline{a_4}}} \end{pmatrix} \cdot \begin{pmatrix} x_1(t) \\ x_2(t) \\ x_3(t) \\ x_4(t) \end{pmatrix} = \begin{pmatrix} 0 & 1 & 0 & 0 \\ 0 & 0 & 1 & 0 \\ 0 & 0 & 0 & 1 \\ 0 & -\frac{s_1}{s_4} & -\frac{s_2}{s_4} & -\frac{s_3}{s_4} \end{pmatrix} \cdot x(t) \qquad \text{(c.3)}$$

Subject to $\sigma(x) = 0$, solving for $x_4(t)$ yields

$$x_4(t) = -\frac{1}{s_4}(s_1 x_1(t) + s_2 x_2(t) + s_3 x_3(t)). \qquad \text{(c.4)}$$

The reduced order equivalent linear time-invariant system.

$$\begin{pmatrix} \dot{x}_1(t) \\ \dot{x}_2(t) \\ \dot{x}_3(t) \end{pmatrix} = \begin{pmatrix} 0 & 1 & 0 \\ 0 & 0 & 1 \\ -\frac{s_1}{s_4} & -\frac{s_2}{s_4} & -\frac{s_3}{s_4} \end{pmatrix} \cdot \begin{pmatrix} x_1(t) \\ x_2(t) \\ x_3(t) \end{pmatrix} = \bar{A} \cdot \bar{x}(t) \tag{c.5}$$

To see how control design might be accomplished, supposed one of the design constraint requires the spectrum of the equivalent system be $\{ -100, -100, -100 \}$; the desired characteristic polynomial is

$$\Pi_A(\lambda) = \lambda^3 + 3\times 10^2 \lambda^2 + 3\times 10^4 \lambda + 10^6 \tag{c.6}$$

The characteristic polynomial of the equivalent reduced order system given in Eq. c.5 is

$$\Pi_A(\lambda) = \det(\lambda I - \bar{A}) = \lambda^3 + \frac{s_3}{s_4}\lambda^2 + \frac{s_2}{s_4}\lambda + \frac{s_1}{s_4} \tag{c.7}$$

Without loss of generality, define $s_4 = 1$. Then oefficients of like powers of λ, produces the set of

$$S = \{1\times 10^6 \quad 3\times 10^4 \quad 3\times 10^2 \quad 1\}.$$

Hence the sliding surface of the equivalent system is as following:

$$\sigma(x(t)) = \begin{pmatrix} 1\times 10^6 & 3\times 10^4 & 3\times 10^2 & 1 \end{pmatrix} \cdot \begin{pmatrix} x_1(t) \\ x_2(t) \\ x_3(t) \\ x_4(t) \end{pmatrix}. \tag{c.8}$$

Appendix D: Sliding Surface Design for the Dynamic System with Three-Dimensional Forces

The equivalent system in Eq. 5.16 is as follow

$$\begin{pmatrix} \dot{x}_1(t) \\ \dot{x}_2(t) \\ \dot{x}_3(t) \\ \dot{x}_4(t) \end{pmatrix} = \begin{pmatrix} 0 & 1 & 0 & 0 \\ 0 & 0 & 1 & 0 \\ 0 & 0 & 0 & 1 \\ -\frac{a_0}{a_4} & -\frac{a_1}{a_4} & -\frac{a_2}{a_4} & -\frac{a_3}{a_4} \end{pmatrix} \cdot \begin{pmatrix} x_1(t) \\ x_2(t) \\ x_3(t) \\ x_4(t) \end{pmatrix} + \begin{pmatrix} 0 & 0 \\ 0 & 0 \\ \frac{b_{tp0}}{a_3} & 0 \\ 0 & \frac{b_{fp0}}{a_4} \end{pmatrix} \cdot u(t) = Ax(t) + Bu(t). \tag{d.1}$$

where $u(t) = \begin{pmatrix} u_1(t) \\ u_2(t) \end{pmatrix} = \begin{pmatrix} F_{tt}(t) \\ F_{tn}(t) \end{pmatrix}$.

We concentrate on the case of linear 3-dimensional sliding surface, $\sigma(x(t)) = Sx(t)$, where

$S = \begin{pmatrix} s_{11} & s_{12} & s_{13} & s_{14} \\ s_{21} & s_{22} & s_{23} & s_{24} \end{pmatrix}$, and $x(t) = \begin{pmatrix} x_1(t) & x_2(t) & x_3(t) & x_4(t) \end{pmatrix}^T$.

The method of equivalent control produces the following equivalent system further

$$\dot{x}(t) = (I - B(SB)^{-1}S)Ax(t) \tag{d.2}$$

Provided $\sigma(x(t_0)) = 0$ for some t_0

In terms of Eq. d.1 and d.2, Then

$$SB = \begin{pmatrix} s_{13}b_1 & s_{14}b_2 \\ s_{23}b_1 & s_{24}b_2 \end{pmatrix}, \qquad SB^{-1} = \begin{pmatrix} \frac{s_{24}}{\Delta s \cdot b_1} & -\frac{s_{14}}{\Delta s \cdot b_1} \\ -\frac{s_{23}}{\Delta s \cdot b_2} & \frac{s_{13}}{\Delta s \cdot b_2} \end{pmatrix},$$

where $b_1 = \frac{b_{tp0}}{a_3}$, $b_2 = \frac{b_{fp0}}{a_4}$, $\Delta s = s_{13}s_{24} - s_{14}s_{23}$.

$$\text{Hence } \dot{x}(t) = \begin{pmatrix} 0 & 1 & 0 & 0 \\ 0 & 0 & 1 & 0 \\ 0 & \frac{s_{14}s_{21} - s_{11}s_{24}}{\Delta s} & \frac{s_{14}s_{22} - s_{12}s_{24}}{\Delta s} & 0 \\ 0 & \frac{s_{11}s_{23} - s_{13}s_{21}}{\Delta s} & \frac{s_{12}s_{23} - s_{13}s_{22}}{\Delta s} & 0 \end{pmatrix} \cdot x(t) \tag{d.3}$$

Subject to $\sigma(x) = 0$, solving for $x_3(t)$ *and* $x_4(t)$ yields

$$\begin{pmatrix} s_{13} & s_{14} \\ s_{23} & s_{24} \end{pmatrix} \cdot \begin{pmatrix} x_3(t) \\ x_4(t) \end{pmatrix} = -\begin{pmatrix} s_{11} & s_{12} \\ s_{21} & s_{22} \end{pmatrix} \cdot \begin{pmatrix} x_1(t) \\ x_2(t) \end{pmatrix} \tag{d.4}$$

$$\text{i.e., } \begin{pmatrix} x_3(t) \\ x_4(t) \end{pmatrix} = -\frac{1}{\Delta s}\begin{pmatrix} s_{11}s_{24} - s_{14}s_{21} & s_{12}s_{24} - s_{14}s_{22} \\ s_{13}s_{21} - s_{11}s_{23} & s_{13}s_{22} - s_{12}s_{23} \end{pmatrix} \cdot \begin{pmatrix} x_1(t) \\ x_2(t) \end{pmatrix} \tag{d.5}$$

The reduced order equivalent linear time-invariant system.

$$\begin{pmatrix} \dot{x}_1(t) \\ \dot{x}_2(t) \end{pmatrix} = \begin{pmatrix} 0 & 1 \\ \frac{s_{14}s_{21} - s_{11}s_{24}}{\Delta s} & \frac{s_{14}s_{22} - s_{12}s_{24}}{\Delta s} \end{pmatrix} \begin{pmatrix} x_1(t) \\ x_2(t) \end{pmatrix} = \bar{A} \cdot \bar{x}(t) \cdot \tag{d.6}$$

For simplicity, let us choose $\Delta s = s_{13}s_{24} - s_{14}s_{23} = 1$. Specifically, choose $s_{13} = 2$,

$s_{14} = s_{23} = s_{24} = 1$. Then $\dot{\bar{x}}(t) = \begin{pmatrix} 0 & 1 \\ s_{21} - s_{11} & s_{22} - s_{12} \end{pmatrix} \cdot \bar{x}(t) = \bar{A} \cdot \bar{x}(t)$. (d.7)

To see how control design might be accomplished, supposed one of the design constraint requires the spectrum of the equivalent system be $\{-100, -200\}$; the desired characteristic polynomial is

$$\Pi_A(\lambda) = \lambda^2 + 300\lambda + 20000 \tag{d.8}$$

The characteristic polynomial of the equivalent reduced order system given in Eq. d.8 is

$$\Pi_A(\lambda) = \det(\lambda I - \bar{A}) = \lambda^2 + (s_{12} - s_{22})\lambda + s_{11} - s_{21}\,. \tag{d.9}$$

Then coefficients of like powers of λ, produces the set of s

$$\begin{pmatrix} 0 & 1 & 0 & -1 \\ 1 & 0 & -1 & 0 \end{pmatrix} \cdot \begin{pmatrix} s_{11} \\ s_{12} \\ s_{21} \\ s_{22} \end{pmatrix} = \begin{pmatrix} 300 \\ 20000 \end{pmatrix}\,. \tag{d.10}$$

One solution of Eq. d.10 is $s_{11} = 100$, $s_{12} = 10$, $s_{21} = -100$, $s_{22} = -20$.

Hence the sliding surface of the equivalent system is as following:

$$\sigma(x(t)) = \begin{pmatrix} 30000 & 500 & 2 & 1 \\ 10000 & 200 & 1 & 1 \end{pmatrix} \cdot \begin{pmatrix} x_1(t) \\ x_2(t) \\ x_3(t) \\ x_4(t) \end{pmatrix}\,. \tag{d.11}$$

Table A: Parameters of the Controlled System with 2-Dimensional Forces and Dependent Piezoactuator

(Unit system: kg, Ns/m, N/m)			
Identifiers	Values	Units	Remarks
Cutting speed	80	M/min	Working condition
Spindle speed	600	rpm	
Cutting width	3.0	mm	
Work material	S45C		
m1	100.00	Kg	Equivalent mass
c1	6320.00	Ns/m	Damping ratio
k1	4.00E+07	N/m	Spring stiffness
c2	7480.00	Ns/m	Damping ratio
k2	5.60E+07	N/m	Spring stiffness
α_1	0.52	Radian	Angle between axis Y and degree 1
α_2	1.05	Radian	Angle between axis Y and degree 2
At	4.5e(+6)	N/m	Slope of backlash for thrust force
Bt	25.00	N	Distance in axis X for thrust force
Ac	3e(+6)	N/m	Slope of backlash for main cutting force
Bc	15.00	N	Distance in axis X for main cutting force
T	2e(-3)	Sec	Time delay effect on uncut chip thickness
μ	0.88		Overlapping factor
$\rho(\|\|e\|\|)$	1.0472		Up bounded of $\|\|e\|\|$
ε	1.35e(-3)	mm	Desirable error
$p(\|\|g(v)\|\|)$	1.2013-3.0450		The bound of g(u)
p	3.5e(+4)~5.5e(+4)	N/m	The slope of piezo's deflection due to volatge
Bp	1.652e(+5)		
k_τ	2.5e(-5)		The constant of the controller
k*	by calculation		
θ_{1min}	-7.8e(-5)		The minimal value of parameters θ_1
θ_{1max}	-2.5e(-5)		The maximal value of parameters θ_1
θ_{2min}	-4.5e(-5)		The minimal value of parameters θ_2
θ_{2max}	-0.5e(-5)		The maximal value of parameters θ_2
θ_{3min}	-3.5e(-5)		The minimal value of parameters θ_3
θ_{3max}	-1e(-5)		The maximal value of parameters θ_3
θ_{4min}	-5e(-4)		The minimal value of parameters θ_4
θ_{4max}	-1.5e(-4)		The maximal value of parameters θ_4
θ_{5min}	-6.55e(-5)		The minimal value of parameters θ_5
θ_{5max}	1.5e(-5)		The maximal value of parameters θ_5
θ_{6min}	-4.05e(-5)		The minimal value of parameters θ_6
θ_{6max}	-0.79e(-5)		The maximal value of parameters θ_6
θ_{7min}	-0.5e(-4)		The minimal value of parameters θ_7
θ_{7max}	1.02e(-4)		The maximal value of parameters θ_7

K_p	-1.429e(+4)	Lb/μm	The ratio of the force and deflection in the piezo, referring to TS-H5-104
u_0	0.15	mm/rev	Average or steady state uncut chip thickness
$q_{i=1,2,3}$	1.0		The coefficient of time delay in the *assumption 1*
$\gamma_{l=1,2,3,4,5,6,7}$	1.17		The coefficient of proj functions

Table B: Parameters of the Controlled System with 3-Dimensioanl Forces and Dependent Piezoactuators

(Unit system: kg, Ns/m, N/m)			
Identifiers	Values	Units	Remarks
Cutting speed	80	m/min	Working condition
Spindle speed	600	rpm	
Cutting width	3.0	mm	
Work material	S45C		
m1	100.00	Kg	Equivalent mass
c1	6320.00	Ns/m	Damping ratio
k1	4.00E+07	N/m	Spring stiffness
c2	7480.00	Ns/m	Damping ratio
k2	5.60E+07	N/m	Spring stiffness
α_1	0.52	Radian	Angle between axis Y and degree 1
α_2	1.05	Radian	Angle between axis Y and degree 2
At	4.5e(+6)	N/m	Slope of backlash for thrust force
Bt	25.00	N	Distance in axis X for thrust force
Ac	3e(+6)	N/m	Slope of backlash for main cutting force
Bc	20.00	N	Distance in axis X for main cutting force
Af	3.5e(+6)	N/m	Slope of backlash for feeding force
Bf	15.00	N	Distance in axis X for feeding force
β	0.3489	Radian	Angle between the direction along main axis of turning and the direction normal to machining surface in Fig 5.1
Time delay(T)	2e(-3)	Sec	Time delay effect on uncut chip thickness
μ	0.88		Overlap factor
$\rho(\|\|e\|\|)$	2.0200		Up bounded of $\|\|e\|\|$
ε	1.5e(-3)	mm	Desirable error
$p(\|\|g_t(v)\|\|)$	1.2013 – 3.045		The bound of $g_t(u)$
$p(\|\|g_f(v)\|\|)$	1.2013 – 3.045		The bound of $g_f(u)$
Pt	3.5e(+6)~5.5e(+6)	N/m	The slope of piezo's deflection due to voltage in the thrust force direction
B_{pt}	1.652e(+5)		
Pf	3.5e(+6)~5.5e(+6)	N/m	The slope of piezo's deflection due to voltage in the feeding force direction
B_{pf}	1.652e(+5)		
k_τ	2.5e(-5)		The constant of the controller
K*	by calculation		
θ_{1min}	[-7.8e(-5), -7.8e(-5)]'	R^{2x1}	The minimal value of parameters θ_1
θ_{1max}	[-2.5e(-5), -2.5e(-5)]'		The maximal value of parameters θ_1
θ_{2min}	[-4.5e(-5), -4.5e(-5)]'		The minimal value of parameters θ_2
θ_{2max}	[-0.5e(-5), -0.5e(-5)]'		The maximal value of parameters θ_2
θ_{3min}	[-3.5e(-5), -3.5e(-5)]'		The minimal value of parameters θ_3
θ_{3max}	[-1e(-5), -1e(-5)]'		The maximal value of parameters θ_3
θ_{4min}	[-5e(-4), -5e(-4)]'		The minimal value of parameters θ_4

θ_{4max}	[-1.5e(-4), -1.5e(-4)]'		The maximal value of parameters θ_4
θ_{5min}	[-6.5e(-5), -6.5e(-5)]'		The minimal value of parameters θ_5
θ_{5max}	[-1.2e(-5), -1.2e(-5)]'		The maximal value of parameters θ_5
θ_{6min}	[-3.08e(-5), -3.08e(-5)]'		The minimal value of parameters θ_6
θ_{6max}	[-0.79e(-5), -0.79e(-5)]'		The maximal value of parameters θ_6
θ_{7min}	[-0.5e(-4), -0.5e(-4)]'		The minimal value of parameters θ_7
θ_{7max}	[-1.341e(-4), -1.341e(-4)]'		The maximal value of parameters θ_7
$K_{\rho=t,f}$	-1.429e(+4), -1.429e(+4)	Lb/μm	The ratio of the force and deflection in the piezo, referring to TS-H5-104
u_0	0.15	mm/rev	Average or steady state uncut chip thickness
$q_{i=1,2,3}$	1.0		The coefficient of time delay in the *assumption 1*
$\gamma_{i=1,2,3,4,5,6,7}$	1.17		The coefficient of proj functions

Table C: Parameters of the Controlled System with 2-Dimensional Forces and Independent Piezoactuator

(Unit system: kg, Ns/m, N/m)			
Identifiers	Values	Units	Remarks
Cutting speed	80	M/min	Working condition
Spindle speed	600	Rpm	
Cutting width	3.0	mm	
Work material	S45c		
m1	100.00	Kg	Equivalent mass of structure
c1	6320.00	Ns/m	Damping ratio
k1	4.00E+07	N/m	Spring stiffness
c2	7480.00	Ns/m	Damping ratio
k2	5.60E+07	N/m	Spring stiffness
α_1	0.52	Radian	Angle between axis Y and degree 1
α_2	1.05	Radian	Angle between axis Y and degree 2
At	4.5e(+6)	N/m	Slope of backlash for thrust force
Bt	25.00	N	Distance in axis X for thrust force
Ac	3e(+6)	N/m	Slope of backlash for main cutting force
Bc	20.00	N	Distance in axis X for main cutting force
m_p	140	Gram	Mass of the piezoelectric actuator
Time delay(T)	2e(-3)	Sec	Time delay effect on uncut chip thickness
μ	0.88		Overlapping factor
$\rho(\|\|e\|\|)$	5.0~17.0		Up bounded of $\|\|e\|\|$
$p(\|\|g(v)\|\|)$	1.2013-3.0450		The bound of g(u)
ε	1.5e(-3)	mm	Desirable error
P	3.5e(+6)~5.5e(+6)	N/m	The slope of piezo's deflection due to voltage
B_p	1.652e(+5)		
$k\tau$	2.5e(-5)		The constant of controller
k*	by calculation		
θ_{1min}	-7.8e(-4)		The minimal value of parameters θ_1
θ_{1max}	-2.5e(-4)		The maximal value of parameters θ_1
θ_{2min}	-4.5e(-4)		The minimal value of parameters θ_2
θ_{2max}	-0.5e(-4)		The maximal value of parameters θ_2
θ_{3min}	-3.5e(-4)		The minimal value of parameters θ_3
θ_{3max}	-1e(-4)		The maximal value of parameters θ_3
θ_{4min}	-5e(-3)		The minimal value of parameters θ_4
θ_{4max}	-1.5e(-3)		The maximal value of parameters θ_4
θ_{5min}	-6.45e(-5)		The minimal value of parameters θ_5
θ_{5max}	1.5e(-5)		The maximal value of parameters θ_5
θ_{6min}	-4.05e(-5)		The minimal value of parameters θ_6
θ_{6max}	-0.79e(-5)		The maximal value of parameters θ_6
θ_{7min}	-0.5e(-4)		The minimal value of parameters θ_7

θ_{7max}	1.02e(-4)		The maximal value of parameters θ_7
K_p	-1.429e(+4)	Lb/μm	The ratio of the force and deflection in the piezo, referring to TS-H5-104
u_0	0.15	Mm/rev	Average or steady state uncut chip thickness
$q_{i=1,2,3}$	1.0		The coefficient of time delay in the *assumption 1*
$\gamma_{l=1,2,3,4,5,6,7}$	1.17		The coefficient of proj functions
b_r	1		The parameters in appendix A
ψ	3~10		>0, determines the estimating speed
δ_1	$2.2x10^{-4}$		>0, determines the estimating precision
δ_2	$2.2x10^{-4}$		
χ_1	50.0		>0, Chosen large enough to adjust the estimated upper bounds rapidly
χ_2	50.0		

Table D: Parameters of the Controlled System with 3-Dimensional Forces and Independent Piezoactuators

(Unit system: kg, Ns/m, N/m)			
Identifiers	Values	Units	Remarks
Cutting speed	80	M/min	Working condition
Spindle speed	600	Rpm	
Cutting width	3.0	mm	
Work material	S45c		
m1	100.00	Kg	Equivalent mass of structure
c1	6320.00	Ns/m	Damping ratio
k1	4.00E+07	N/m	Spring stiffness
c2	7480.00		Damping ratio
k2	5.60E+07		Spring stiffness
α_1	0.52	Radian	Angle between axis Y and degree 1
α_2	1.05	Radian	Angle between axis Y and degree 2
At	4.5e(+6)	N/m	Slope of backlash for thrust force
Bt	25.00	N	Distance in axis X for thrust force
Ac	3e(+6)	N/m	Slope of backlash for main cutting force
Bc	20.00	N	Distance in axis X for main cutting force
Af	3.5e(+6)	N/m	Slope of backlash for feeding force
Bf	15.0	N	Distance in axis X for feeding force
m_p	140	Gram	Mass of the piezoelectric actuator
β	0.3489	Radian	Angle between the direction along main axis of turning and the direction normal to machining surface in Fig 7.1
Time delay (T)	2e(-3)	Sec	Time delay effect on uncut chip thickness
μ	0.65		Overlapping factor
$\rho(\|\|e\|\|)$	2.0200		Up bounded of $\|\|e\|\|$
ε	1.5e(-3)	mm	Desirable error
$p(\|\|g_t(v)\|\|)$	1.2013 – 3.045		The bound of $g_t(u)$
$p(\|\|g_f(v)\|\|)$	1.2013 – 3.045		The bound of $g_f(u)$
Pt	3.5e(+6)~5.5e(+6)	N/m	The slope of piezo's deflection due to voltage in the thrust force direction
B_{pt}	1.652e(+5)		
Pf	3.5e(+6)~5.5e(+6)	N/m	The slope of piezo's deflection due to voltage in the feeding force direction
B_{pf}	1.652e(+5)		
$k\tau$	2.5e(-5)		The constant of the controller
k*	by calculation		
θ_{1min}	[-7.8e(-4), -7.8e(-4)]'	R^{2x1}	The minimal value of parameters θ_1
θ_{1max}	[-2.5e(-4), -2.5e(-4)]'		The maximal value of parameters θ_1
θ_{2min}	[-4.5e(-4), -4.5e(-4)]'		The minimal value of parameters θ_2
θ_{2max}	[-0.5e(-4), -0.5e(-4)]'		The maximal value of parameters θ_2
θ_{3min}	[-3.5e(-4), -3.5e(-4)]'		The minimal value of parameters θ_3
θ_{3max}	[-1e(-4), -1e(-4)]'		The maximal value of parameters θ_3

θ_{4min}	[-5e(-3), -5e(-3)]'		The minimal value of parameters θ_4
θ_{4max}	[-1.5e(-3), -1.5e(-3)]'		The maximal value of parameters θ_4
θ_{5min}	[-6.5e(-5), -6.5e(-5)]'		The minimal value of parameters θ_5
θ_{5max}	[-1.2e(-5), -1.2e(-5)]'		The maximal value of parameters θ_5
θ_{6min}	[-3.08e(-5), -3.08e(-5)]'		The minimal value of parameters θ_6
θ_{6max}	[-0.79e(-5), -0.79e(-5)]'		The maximal value of parameters θ_6
θ_{7min}	[-0.5e(-4), -0.5e(-4)]'		The minimal value of parameters θ_7
θ_{7max}	[-1.341e(-4), -1.341e(-4)]'		The maximal value of parameters θ_7
$K_{\rho=t,f}$	-1.429e(+4), -1.429e(+4)	Lb/μm	The ratio of the force and deflection in the piezo, referring to TS-H5-104
u_0	0.15	mm/rev	Average or steady state uncut chip thickness
$q_{i=1,2,3}$	1.0		The coefficient of time delay in the *assumption 1*
$\gamma_{i=1,2,3,4,5,6,7}$	1.17		The coefficient of proj functions
b_r	[1, 1]'		The parameters in appendix A
ψ	3~10		>0, determines the estimating speed
δ_1	$2.2x10^{-4}$		>0, determines the estimating precision
δ_2	$2.2x10^{-4}$		
χ_1	50.0		>0, Chosen large enough to adjust the estimated upper bounds rapidly
χ_2	50.0		

References

1. S. Kato, E. Marui, "On the Cause of Regenerative Chatter Due to Workpiece Deflection", 1974, Journal of Engineering for Industry, pp 179-186.

2. J. C. Pan, "Modeling and Robust Adaptive Control of Metal Cutting via Application of Piezoactuator", 2001, the Department of Mechanical Engineering, Concordia.

3. H. E. Merritt, "Theory of Self-Excited Machine-Tool Chatter: Contribution to Machine-Tool Chatter", 1965, Journal of Engineering for Industry, pp 447-454.

4. S. A. Tobias, W. Fishwick, "The Chatter of Lathe Tools Under Orthogonal Cutting Conditions", July 1958, Transaction of the ASME, pp 1079-1088.

5. J. Tlusty, F. Ismail, "Basic Non-linearity in Machining Chatter", 1981, McMaster University, Hamilton, Ontario/Canada, CIRP, pp 299-304.

6. N. H. Hanna, S. A. Tobias, "A Theory of Nonlinear Regenerative Chatter", 1974, Journal of Engineering for Industry, pp 247-255.

7. G. W. Long, J. R. Lemon, "Structural Dynamics in Machine-Tool Chatter: Contribution to Machine-Tool Chatter", 1965, Journal of Engineering for Industry, pp 455-461.

8. J. R. Lemon, P. C. Ackermann, "Application of Self-Excited Machine-Tool Chatter Theory: Contribution to Machine-Tool Chatter", 1965, Journal of Engineering for Industry, pp 471-479.

9. S. Doi, S. Kato, "Chatter Vibration of Lathe Tools", 1956, NAGOYA, Japan, pp 1127-1131.

10. C. L. Nachtigal, N. H. Cook, "Active Control of Machine – Tool Chatter", 1970, Journal of Engineering for Industry, pp 238-244.

11. I. Minis, A. Tembo, "Experiment Verification of a Stability Theory for Periodic Cutting Operations", 1993, Journal of Engineering for Industry, pp 9-14.

12. J. D. Cumming, S. Kobayashi, "A New Analysis of the Forces in Orthogonal Metal Cutting", 1965, Journal of Engineering for Industry, pp 480-485.

13. J. F. Sarnicola, G. Boothroyd, "Machine Tool Chatter: Effect of Surface Slope on Machining Forces During Wave Removing", 1974, Journal of Engineering for Industry, pp 1202-1206.

14. E. Aslie, A. Achen, "Self-Excited Vibrations of Systems With Two Degrees of Freedom", 1956, Transaction of the ASME, pp 737-748.

15. J. Delio, J.Tlusty, "Use of Audio Signals for Chatter Detection and Control", 1992, Journal of Engineering for Industry, pp 146-157.

16. S. Taylor, S. Tobias, "A Lumped Constants Method for the Prediction of the Vibration Characteristics of Machine Tool Structures", *proc. 5th INT M. T. D. R. conf.*, Pergamon, 1964.

17. H. Ota, K. Kono, "On Chatter Vibrations of Machine Tool or Work Due to Regenerative Effect and Time Lag", November 1974, Journal of Engineering for Industry, pp 1337-1346.

18. T. Kaneko, H. Sato, "Self-Excited Chatter and its Marks in Turning", Journal of Engineering for Industry, pp 222-228

19. P. Albrecht, "Dynamics of the Metal-Cutting Process", 1965, Journal of Engineering for Industry, pp 429-441.

20. R. L. Kegg, "Cutting Dynamics in Machine-Tool Chatter: Contribution to Machine-Tool Chatter", 1965, Journal of Engineering for Industry, pp 464-470.

21. E. Marui, S. Kato, "The Mechanism of Chatter Vibration in a Spindle-Workpiece System: Part 1- Properties of Self-Excited Chatter Vibration in Spindle-Workpiece System", 1988, Journal of Engineering for Industry, pp 236-241.

22. E. Marui, S. Ema, "Chatter Vibration of Lathe Tools. Part 1; General Characteristic of Chatter Vibration", 1983, Journal of Engineering for Industry, pp 100-106.

23. L. K. Lauderbaugh, A. G. Ulsoy, "Model Reference Adaptive Force Control in Milling", 1989, Journal of Engineering for Industry, pp 13-21.

24. S. Doi, "On the Chatter Vibrations of Lathe Tools", September 1953, Memoirs of the Faculty of Engineering, Nagoya Unviersity, pp 205-211.

25. R. A. Thompson, "Chatter Growth – Tests to Evaluate the Theory", 1988, Transaction of the ASME, pp 344-350.

26. R. Nair, K. Danai, "Turning Process Identification Through Force Transients", 1992, Journal of Engineering for Industry, pp 1-7.

27. N. Saravanja-fabris, A. F. D'souza, "Nonlinear Stability Analysis of Chatter in Metal Cutting", 1974, Journal of Engineering for Industry, pp 670-675.

28. D. M. Alter, Tsu-Chin, Tsao, "Stability of Turning Processes with Actively Controlled Linear Motor Feed Drives", 1994, Journal of Engineering for Industry, pp 298-307.

29. F. Koenigsberger, J. Tlusty, " Machine Tool Structure", volume 1, 1970, Pergamon Press.

30. K. Srinivasan, C. L. Nachtigal, "Investigation of the Cutting Process Dynamics in Turning Operations", 1978, Journal of Engineering for Industry, pp 323-331.

31. R. A. Thompson, "A General Theory for Regenerative Stability", 1980, North American Manufacturing Research Conference (*NAMRC*), pp 377-387.

32. E. M. Trent, "Metal Cutting", Third Edition, 1991, Butterworth-Heinemann Ltd.

33. E. Marui, S. Ema, "Chatter Vibration of Lathe Tools. Part 2; On the Mechanism of Exciting Energy Supply", 1983, Journal of Engineering for Industry, pp 107-113.

34. C. Y. Su, Y. Stepanenko, "Robust Adaptive Control of a Class of Nonlinear Systems with Unknown Backlash-like Hysteresis", IEEE Transactions on Automatic Control, pp 2427-2432.

35. Y. S. Tarng, H. T. Young, "An Analytical Model of Chatter Vibration in Metal Cutting", 1992, Int. J. Mach. Tools. Manufact, pp 183-197.

36. E. Marui, S. Kato, "The Mechanism of Chatter Vibration in a Spindle-Workpiece System: Part 2- Characteristics of Dynamic Cutting Force and Vibration Energy", 1988, Journal of Engineering for Industry, pp 242-47.

37. J. D. Rasmussen, "Dynamic Variable Depth of Cut Machining Using Piezoelectric Actuators", 1994, Int. J. Mach. Tools Manufact, pp 379-392.

38. R. F. Recht, "A Dynamic Analysis of High-Speed Machining", 1985, Journal of Engineering for Industry, pp 309-315.

39. X. Chen, C. Y. Su, " Robust Output Tracking Control for the System with Uncertainties", 2002, International Journal of System Science, pp 247-257.

40. X. G. Yang, K. F. Eman, "Analysis of Three-Dimensional", 1985, Journal of Engineering for Industry, pp 336-341.

41. M. S. Mahmoud, N. F. Al-Muthairi, "Design of Robust Controller for Time-delay Systems", 1994, IEEE Transactions on Automatic Control, pp 995-999.

42. Piezo Systems. Inc, "History of Piezoelectricity", http://www.piezo.com/transel.htm.

43. Physik Instrumente (PI) GmbH & Co. KG, "Theory and Applications of Piezo Actuators and PZT Nanopositioning Systems", http://www.physikinstrumente.com//tutorial/index.html

44. D. W. Wu, C. R. Liu, "An Analytical Model of Cutting Dynamics, Part 1: Model Building", 1985, Journal of Engineering for Industry, pp 107-111.

45. D. W. Wu, C. R. Liu, "An Analytical Model of Cutting Dynamics, Part 2: Verfication", 1985, Journal of Engineering for Industry, pp 112-118.

46. O. Masory, "Real-Time Estimation of Cutting Process Parameters in Turning", 1984, Journal of Engineering for Industry, pp 218-221.

47. T. Moriwaki, K. Iwata, "In-Process Analysis of Machine Tool Structure Dynamics and Prediction of Machining Chatter", 1976, Journal of Engineering for Industry, pp 301-305.

48. I. E. Minis, E. B. Magrab, "Improved Methods for the Prediction of Chatter in Turning, Part 1: Determination of Structural Response Parameters", 1990, Journal of Engineering for Industry, pp 12-20.

49. I. E. Minis, E. B. Magrab, "Improved Methods for the Prediction of Chatter in Turning, Part 2: Determination of Cutting Process Parameters", 1990, Journal of Engineering for Industry, pp 21-27.

50. I. E. Minis, E. B. Magrab, "Improved Methods for the Prediction of Chatter in Turning, Part 3: A Generalized Linear Theory", 1990, Journal of Engineering for Industry, pp 28-35.

51. S. M. Pandit, S. M. Wu, "Modeling Machine Tool Chatter by Time Series", 1975, Journal of Engineering for Industry, pp 211-214.

52. J. L. Stein, K. Huh, "Monitoring Cutting Forces In Turning: A Model-Based Approach", 2002, Journal of Manufacturing Science and Engineering, pp 26-31.

53. R. A. Decarlo, S. H. Zak, "Variable Structure Control of Nonlinear Multivariable System: A Tutorial"(invited paper), 1987, IEEE, (IEEE Log Number 8719082).

54. M. J. Corless, G. Leitmann, "Continuous State Feedback Guaranteeing Uniform Ultimate Boundedness for Uncertain Dynamic Systems", 1981, IEEE Transactions on Automatic Control, pp 1139-1144.

55. K. S. Narendra, A. M. Annaswamy, "Stable Adaptive Systems", Perntice-Hall International, Inc, ISBN: 0-13-640034-2.

56. J. P. Den Hartog, "Mechanical Vibrations", second edition, 1940, McGraw-Hill Book Company, INC.